

# **NCHRP**

## **REPORT 445**

### **Debris Forces on Highway Bridges**

**TRANSPORTATION RESEARCH BOARD**

REPRODUCED BY: **NTIS**  
U.S. Department of Commerce  
National Technical Information Service  
Springfield, Virginia 22161

PB2001-105355



**NATIONAL  
COOPERATIVE  
HIGHWAY  
RESEARCH  
PROGRAM**

**NATIONAL RESEARCH COUNCIL**

## TRANSPORTATION RESEARCH BOARD EXECUTIVE COMMITTEE 2000

### OFFICERS

**Chair:** *Martin Wachs, Director, Institute of Transportation Studies, University of California at Berkeley*

**Vice Chair:** *John M. Samuels, Senior Vice President-Operations Planning & Support, Norfolk Southern Corporation, Norfolk, VA*

**Executive Director:** *Robert E. Skinner, Jr., Transportation Research Board*

### MEMBERS

THOMAS F. BARRY, JR., *Secretary of Transportation, Florida DOT*

JACK E. BUFFINGTON, *Associate Director and Research Professor, Mack-Blackwell National Rural Transportation Study Center, University of Arkansas*

SARAH C. CAMPBELL, *President, TransManagement, Inc., Washington, DC*

ANNE P. CANBY, *Secretary of Transportation, Delaware DOT*

E. DEAN CARLSON, *Secretary of Transportation, Kansas DOT*

JOANNE F. CASEY, *President, Intermodal Association of North America*

JOHN L. CRAIG, *Director, Nebraska Department of Roads*

ROBERT A. FROSCHE, *Senior Research Fellow, John F. Kennedy School of Government, Harvard University*

GORMAN GILBERT, *Director, Institute for Transportation Research and Education, North Carolina State University*

GENEVIEVE GIULIANO, *Professor, School of Policy, Planning, and Development, University of Southern California, Los Angeles*

LESTER A. HOEL, L. A. *Lacy Distinguished Professor, Department of Civil Engineering, University of Virginia*

H. THOMAS KORNEGAY, *Executive Director, Port of Houston Authority*

THOMAS F. LARWIN, *General Manager, San Diego Metropolitan Transit Development Board*

BRADLEY L. MALLORY, *Secretary of Transportation, Pennsylvania DOT*

JEFFREY R. MORELAND, *Senior Vice President-Law and Chief of Staff, Burlington Northern Santa Fe Corporation, Fort Worth, TX*

SID MORRISON, *Secretary of Transportation, Washington State DOT*

JOHN P. POORMAN, *Staff Director, Capital District Transportation Committee, Albany, NY*

WAYNE SHACKELFORD, *Senior VP, Gresham Smith & Partners, Alpharetta, GA*

MICHAEL S. TOWNES, *Executive Director, Transportation District Commission of Hampton Roads, Hampton, VA*

THOMAS R. WARNE, *Executive Director, Utah DOT*

ARNOLD F. WELLMAN, JR., *Vice President, Corporate Public Affairs, United Parcel Service, Washington, DC*

JAMES A. WILDING, *President and CEO, Metropolitan Washington Airports Authority*

M. GORDON WOLMAN, *Professor of Geography and Environmental Engineering, The Johns Hopkins University*

DAVID N. WORMLEY, *Dean of Engineering, Pennsylvania State University*

MIKE ACOTT, *President, National Asphalt Pavement Association (ex officio)*

SUE BAILEY, *National Highway Traffic Safety Administrator, U.S.DOT (ex officio)*

KELLEY S. COYNER, *Research and Special Programs Administrator, U.S.DOT (ex officio)*

MORTIMER L. DOWNEY, *Deputy Secretary of Transportation, U.S.DOT (ex officio)*

NURIA I. FERNANDEZ, *Acting Administrator, Federal Transit Administration, U.S.DOT (ex officio)*

RUSSELL L. FUHRMAN (Maj. Gen., U.S. Army), *Acting Commander, U.S. Army Corps of Engineers (ex officio)*

JANE F. GARVEY, *Federal Aviation Administrator, U.S.DOT (ex officio)*

JOHN GRAYKOWSKI, *Acting Administrator, Maritime Administration, U.S.DOT (ex officio)*

EDWARD R. HAMBERGER, *President and CEO, Association of American Railroads (ex officio)*

CLYDE J. HART, JR., *Acting Deputy Administrator, Federal Motor Carrier Safety Administration, U.S.DOT (ex officio)*

JOHN C. HORSLEY, *Executive Director, American Association of State Highway and Transportation Officials (ex officio)*

JAMES M. LOY (Adm., U.S. Coast Guard), *Commandant, U.S. Coast Guard (ex officio)*

WILLIAM W. MILLAR, *President, American Public Transportation Association (ex officio)*

JOLENE M. MOLITORIS, *Federal Railroad Administrator, U.S.DOT (ex officio)*

MARGO OGE, *Director, Office of Transportation and Air Quality, U.S. Environmental Protection Agency (ex officio)*

VALENTIN J. RIVA, *President and CEO, American Concrete Pavement Association (ex officio)*

ASHISH K. SEN, *Director, Bureau of Transportation Statistics, U.S.DOT (ex officio)*

KENNETH R. WYKLE, *Federal Highway Administrator, U.S.DOT (ex officio)*

### NATIONAL COOPERATIVE HIGHWAY RESEARCH PROGRAM

*Transportation Research Board Executive Committee Subcommittee for NCHRP*

MARTIN WACHS, *Institute of Transportation Studies, University of California at Berkeley (Chair)*

LESTER A. HOEL, *University of Virginia*

JOHN C. HORSLEY, *American Association of State Highway and Transportation Officials*

JOHN M. SAMUELS, *Norfolk Southern Corporation, Norfolk, VA*

WAYNE SHACKELFORD, *Gresham Smith & Partners, Alpharetta, GA*

ROBERT E. SKINNER, JR., *Transportation Research Board*

KENNETH R. WYKLE, *Federal Highway Administration*

*Project Panel C12-39 Field of Design Area of Bridges*

RICHARD BARKER, *Virginia Polytechnic Institute and State University*

REBECCA S. BURNS, *Pennsylvania DOT*

TIMOTHY DIEHL, *U.S. Geological Survey*

JOHN F. HARTKERN, *New York State DOT*

DONALD HAYNES, *Hancock, MI*

WILLIAM J. KROUSE, *Ohio DOT*

A. MAINARD WACKER, *Cheyenne, WY*

STEVEN B. CHASE, *FHWA*

BILL DEARASAUGH, *TRB Liaison Representative*

*Program Staff*

ROBERT J. REILLY, *Director, Cooperative Research Programs*

CRAWFORD F. JENCKS, *Manager, NCHRP*

DAVID B. BEAL, *Senior Program Officer*

LLOYD R. CROWTHER, *Senior Program Officer*

B. RAY DERR, *Senior Program Officer*

AMIR N. HANNA, *Senior Program Officer*

EDWARD T. HARRIGAN, *Senior Program Officer*

CHRISTOPHER HEDGES, *Senior Program Officer*

TIMOTHY G. HESS, *Senior Program Officer*

RONALD D. MCCREADY, *Senior Program Officer*

CHARLES W. NIESSNER, *Senior Program Officer*

EILEEN P. DELANEY, *Managing Editor*

JAMIE FEAR, *Associate Editor*

HILARY FREER, *Associate Editor*

ANDREA BRIERE, *Assistant Editor*

BETH HATCH, *Editorial Assistant*

NATIONAL COOPERATIVE HIGHWAY RESEARCH PROGRAM

---

**NCHRP REPORT 445**

---

**Debris Forces on  
Highway Bridges**

**ARTHUR C. PAROLA**  
University of Louisville  
Louisville, KY

and

**COLIN J. APELT**  
**MARK A. JEMPSON**  
University of Queensland  
Queensland, Australia

**SUBJECT AREAS**

Bridges, Other Structures, and Hydraulics and Hydrology

---

Research Sponsored by the American Association of State Highway and Transportation Officials  
in Cooperation with the Federal Highway Administration

---

**TRANSPORTATION RESEARCH BOARD — NATIONAL RESEARCH COUNCIL**

NATIONAL ACADEMY PRESS  
WASHINGTON, D.C. — 2000



NATIONAL COOPERATIVE HIGHWAY RESEARCH PROGRAM

---

**NCHRP REPORT 445**

---

**Debris Forces on  
Highway Bridges**

**ARTHUR C. PAROLA**  
University of Louisville  
Louisville, KY

**SUBJECT AREAS**

Bridges, Other Structures, and Hydraulics and Hydrology

---

Research Sponsored by the American Association of State Highway and Transportation Officials  
in Cooperation with the Federal Highway Administration

---

**TRANSPORTATION RESEARCH BOARD — NATIONAL RESEARCH COUNCIL**

NATIONAL ACADEMY PRESS  
WASHINGTON, D.C. — 2000

## **NATIONAL COOPERATIVE HIGHWAY RESEARCH PROGRAM**

Systematic, well-designed research provides the most effective approach to the solution of many problems facing highway administrators and engineers. Often, highway problems are of local interest and can best be studied by highway departments individually or in cooperation with their state universities and others. However, the accelerating growth of highway transportation develops increasingly complex problems of wide interest to highway authorities. These problems are best studied through a coordinated program of cooperative research.

In recognition of these needs, the highway administrators of the American Association of State Highway and Transportation Officials initiated in 1962 an objective national highway research program employing modern scientific techniques. This program is supported on a continuing basis by funds from participating member states of the Association and it receives the full cooperation and support of the Federal Highway Administration, United States Department of Transportation.

The Transportation Research Board of the National Research Council was requested by the Association to administer the research program because of the Board's recognized objectivity and understanding of modern research practices. The Board is uniquely suited for this purpose as it maintains an extensive committee structure from which authorities on any highway transportation subject may be drawn; it possesses avenues of communications and cooperation with federal, state and local governmental agencies, universities, and industry; its relationship to the National Research Council is an insurance of objectivity; it maintains a full-time research correlation staff of specialists in highway transportation matters to bring the findings of research directly to those who are in a position to use them.

The program is developed on the basis of research needs identified by chief administrators of the highway and transportation departments and by committees of AASHTO. Each year, specific areas of research needs to be included in the program are proposed to the National Research Council and the Board by the American Association of State Highway and Transportation Officials. Research projects to fulfill these needs are defined by the Board, and qualified research agencies are selected from those that have submitted proposals. Administration and surveillance of research contracts are the responsibilities of the National Research Council and the Transportation Research Board.

The needs for highway research are many, and the National Cooperative Highway Research Program can make significant contributions to the solution of highway transportation problems of mutual concern to many responsible groups. The program, however, is intended to complement rather than to substitute for or duplicate other highway research programs.

---

Note: The Transportation Research Board, the National Research Council, the Federal Highway Administration, the American Association of State Highway and Transportation Officials, and the individual states participating in the National Cooperative Highway Research Program do not endorse products or manufacturers. Trade or manufacturers' names appear herein solely because they are considered essential to the object of this report.

## **NCHRP REPORT 445**

Project 12-39 FY'93

ISSN 0077-5614

ISBN 0-309-06661-1

Library of Congress Control Number 00-134734

© 2000 Transportation Research Board

*NTIS is authorized to reproduce and sell this report. Permission for further reproduction must be obtained from the copyright owner.*

### **NOTICE**

The project that is the subject of this report was a part of the National Cooperative Highway Research Program conducted by the Transportation Research Board with the approval of the Governing Board of the National Research Council. Such approval reflects the Governing Board's judgment that the program concerned is of national importance and appropriate with respect to both the purposes and resources of the National Research Council.

The members of the technical committee selected to monitor this project and to review this report were chosen for recognized scholarly competence and with due consideration for the balance of disciplines appropriate to the project. The opinions and conclusions expressed or implied are those of the research agency that performed the research, and, while they have been accepted as appropriate by the technical committee, they are not necessarily those of the Transportation Research Board, the National Research Council, the American Association of State Highway and Transportation Officials, or the Federal Highway Administration, U.S. Department of Transportation.

Each report is reviewed and accepted for publication by the technical committee according to procedures established and monitored by the Transportation Research Board Executive Committee and the Governing Board of the National Research Council.

Published reports of the

### **NATIONAL COOPERATIVE HIGHWAY RESEARCH PROGRAM**

are available from:

Transportation Research Board  
National Research Council  
2101 Constitution Avenue, N.W.  
Washington, D.C. 20418

and can be ordered through the Internet at:

<http://www4.nationalacademies.org/trb/homepage.nsf>

Printed in the United States of America

## **FOREWORD**

*By Staff  
Transportation Research  
Board*

This report contains the findings of a study undertaken to develop practical methods for determining drag and hydrostatic forces, on bridge piers and on superstructures, due to waterborne debris. The report includes recommended specifications for assessing these forces. The material in this report will be of immediate interest to bridge designers.

---

The accumulation of debris on bridge piers and on superstructures can create significant forces. Bridge designers must have reliable procedures to estimate the magnitude of these forces to ensure that the structure is properly sized. Under NCHRP Project 12-39, the University of Louisville developed equations for predicting the maximum debris forces. The equations were validated through small-scale laboratory tests at the University of Louisville, the University of Queensland (Australia), and the U.S. Army Corps of Engineers Riprap Test Facility. In addition, information collected at bridges that had been damaged by debris forces was included in the research.

The report is organized into four chapters and an appendix. The first chapter provides background information and discusses the objectives, tasks, and scope of the study. The second chapter summarizes the state of knowledge on the effect of debris on bridges. The chapter also discusses experimental studies conducted to determine a method for predicting debris forces on piers and on superstructures. The third chapter both introduces the recommended specification and commentary on debris forces and applies the debris-loading specification to three examples. The final chapter draws conclusions from the research and recommends areas for further research. A five-part appendix is also included, which provides a more detailed account of the procedures and outcomes of this research project.



# CONTENTS

- 1 SUMMARY**
- 2 CHAPTER 1 Introduction and Research Approach**
  - Introduction, 2
  - Background and Problem Statement, 2
  - Objectives, 4
  - Research Tasks, 4
  - Scope of Study, 5
- 6 CHAPTER 2 Findings**
  - Summary of State-of-Knowledge Account, 6
  - Experimental Investigations, 9
  - Results, 10
- 13 CHAPTER 3 Application: Draft Specification and Examples**
  - Draft Debris-Loading Specification and Commentary, 13
  - Example Applications of Debris-Loading Specification, 14
- 31 CHAPTER 4 Conclusions and Recommended Research**
  - Conclusions, 31
  - Recommendations, 32
- 34 REFERENCES**
- 35 APPENDIX A Supporting Information**

#### **AUTHOR ACKNOWLEDGMENTS**

The research reported herein was performed under NCHRP Project 12-39 by the University of Louisville Research Foundation, Department of Civil and Environmental Engineering, University of Louisville; and by the Department of Civil Engineering, University of Queensland, Australia. The University of Louisville Research Foundation was the contractor for this study. The work undertaken at the University of Queensland was under subcontract with the University of Louisville.

Arthur C. Parola Jr., Professor of Civil and Environmental Engineering, University of Louisville, was the principal investigator. The work done at the University of Queensland was completed

under the supervision of Professor Colin J. Apelt with the assistance of Research Assistant Mark A. Jempson. The work done at the University of Louisville was completed under the supervision of Professor Parola with the help of Research Assistants Anthony McClellan, Charles D. McCormick, Charles J. Melhart, Prasad Gattu, Sridhar Kamojjala, Shahriyar Mojahed, and Douglas S. Schlickman. Mary E. Parola and Professor D. Joseph Hagerty's editorial review of this document is gratefully acknowledged.

Steven T. Maynard and Douglas White of the U.S. Army Corp of Engineers are acknowledged for their assistance with completing the experimental testing at the Riprap Test Facility at the Waterways Experiment Station in Vicksburg, Mississippi.

# DEBRIS FORCES ON HIGHWAY BRIDGES

## SUMMARY

In 1989, during a flood event, a bridge collapsed over the Great Miami River in Ohio. Two people died as a result. A National Transportation Safety Board (NTSB) report that summarizes an investigation of the collapse attributes the most probable cause of the collapse to forces associated with a debris accumulation on one of the bridge-pile bents. In its report, the NTSB states the need for more effective guidance in the AASHTO specifications and recommends the development of improved specifications for debris loading on bridges.

The purpose of NCHRP Project 12-39 was to develop a rational debris-loading prediction methodology on which a reliable and practical debris-loading specification could be based. The objectives of the project were accomplished through calibration of analytical hydrodynamic force models with data obtained from three model test studies of debris on model piers and superstructures. Small-scale laboratory model testing at the University of Queensland Bridge Flood Force Testing Facility and the University of Louisville Hydraulics Laboratory, as well as medium-scale model testing at the U.S. Army Corps of Engineers Riprap Test Facility, provided the data necessary to develop the force-prediction methodology.

A draft specification for and commentary on maximum debris loading on piers and superstructures was written in the format of specifications provided in the *AASHTO LRFD Bridge Design Specifications*, second edition (1998). The applicability of the specification was demonstrated in three examples, where debris loads were determined on a single pier, on multiple piers, and on a superstructure. The examples demonstrated the use of Hydraulic Engineering Center River Analysis Software (HEC-RAS) to evaluate the reaction of the flow to debris accumulations and to provide the parameters necessary for predicting debris loading on piers and superstructures.

The practicality of the specification was greatly enhanced by information obtained from field investigation on sites where debris accumulation had caused the damage or collapse of bridges. An extension to NCHRP Project 12-39, Task 7 (which was sponsored by FHWA), provided an opportunity for the researchers to obtain critical site information. This information altered the approach of the researchers. A critical factor that was determined from the site examinations was the influence of flow blockage produced by debris accumulation. The development of the debris-loading methodology is based on the influence of a flow-blockage ratio.

---

## CHAPTER 1

# INTRODUCTION AND RESEARCH APPROACH

### INTRODUCTION

Submerged bridge components are subjected to the forces of flowing water during flood events. These forces may be increased substantially where debris lodge and accumulate on bridge piers and superstructures. The debris not only increase the effective area of substructure components, but also reduce the flow area and cause backwater upstream and increased velocities through the bridge opening.

Complete collapse of bridge spans during flood events has been attributed to debris loads. In 1989, during a flood event, a bridge collapsed over the Great Miami River in Ohio. Two people died as a result. A National Transportation Safety Board (NTSB) report (1) summarizing an investigation of the collapse attributes the collapse to forces associated with a debris accumulation on one of the bridge-pile bents. In its report, the NTSB states the need for more effective guidance in AASHTO specifications and recommends the development of improved specifications for debris loading on bridges.

Section 3.18 of the AASHTO *Standard Specifications for Highway Bridges*, thirteenth edition (2) (which was the most recent edition at the time of the Harrison Road bridge collapse) states, "All piers and other portions of structures that are subjected to the force of flowing water, floating ice, or drift shall be designed to resist the maximum stresses induced thereby." Unfortunately, this statement is the limit of the guidance provided in the specifications to the bridge designer for determining debris (drift) forces. Subsequent specifications in the *AASHTO LRFD Bridge Design Specifications*, first edition (3) and second edition (4) provide a brief commentary; however, information based on documented debris-loading conditions or analytical procedures has not been available. A method for ascertaining the loads caused by debris accumulation was needed.

The purpose of NCHRP Project 12-39 was to provide sufficient information to be able to quantify drag and hydrostatic forces that result from debris loads and to develop rational design specifications. This report addresses only the hydrostatic and drag force components of this study.

The report is organized into four chapters and an appendix. This first chapter provides background information and discusses the objectives, tasks, and scope of the study. The second chapter summarizes a state-of-knowledge account, compiled by the project researchers, on the effect of debris

on bridges. The chapter also discusses the experimental investigations, and results, of studies conducted to determine a method for predicting debris forces on piers and on superstructures. The third chapter both (a) introduces the draft specification for and commentary on debris accumulation forces and (b) applies the debris-loading specification to three examples. The last chapter, Chapter 4, draws conclusions from the research and recommends areas for further research. A five-part appendix is also included, which provides a more detailed account of the procedures and outcomes of this research project.

The investigation of impact forces was published separately as *NCHRP Report 417*, "Highway Infrastructure Damage Caused by the 1993 Upper Mississippi River Basin Flooding" (5).

### BACKGROUND AND PROBLEM STATEMENT

Debris principally consist of brush, grass, and woody remains of trees that have lost soil support around their roots as a result of streambank erosion. Household items, such as refrigerators, water heaters, furniture, and carpeting, and even structural parts from homes destroyed by floodwaters, may also make up debris. Debris can also include mobile homes, automobiles, propane tanks, and campers that have been washed into a stream. During flood events, debris in the floodway will be transported into the waterway as the flow depth increases. Debris transport depends heavily on secondary currents. Debris will remain in transport until secondary currents transport them into floodplain vegetation or slackwater areas, they are caught on an obstacle such as a bridge, they are lodged against other vegetation along streambanks, or they are beached as a result of a local change in flow depth or recession of the floodwaters.

Debris that are transported in rivers during flood events accumulate on bridge piers and submerged superstructures (6). The transport of such debris has been found to occur along the thalweg (the main thread of high-flow velocity in rivers), although the debris transport is not limited to this region of flow. Piers and superstructure components in high-transport zones may be supplied with large quantities of debris. Debris accumulations that rotate off piers or other locations in river systems may be transported as large mats. Figure 1



Figure 1. Floating debris mat colliding with existing debris accumulation.

shows a small debris mat colliding with an existing debris accumulation on a pier located in the thalweg. Such a debris mat was reported to have collided with the Harrison Road bridge. Secondary currents in some channels concentrate floating debris to form “debris ribbons.” Piers and submerged superstructures that obstruct the flow of debris may accumulate debris rapidly.

Debris accumulations can block large portions of bridge-waterway openings. Figures 2 and 3 show the bridge that collapsed over Florida Creek near Skidmore, Missouri (5). The large blockage of flow area in the main channel causes backwater upstream of the bridge that increases floodwater elevations, high-flow velocity through the bridge opening, and erosion of the streambed and banks.

A solid model was created to show the simulation of flow in an area of the Brazos River in Texas where a large debris accumulation was formed on one of several piers (7, 8). Figure 4 shows this model. Although the river is more than 120 m wide at this location, the debris accumulation affects flow across the channel. A two-dimensional flow simulation (see



Figure 2. Missouri Highway 113 bridge over Florida Creek near Skidmore, Missouri, hours after collapse. (5)



Figure 3. Missouri Highway 113 bridge over Florida Creek near Skidmore, Missouri, following flood recession. (5)

Figure 5) shows that the debris-encumbered pier was located along the highest-velocity flow region of the main channel (7). The debris accumulation deflected flow, causing relatively high velocity and skewed flow at adjacent piers. In addition to increasing the loads to the structure, the local-flow acceleration and general contraction of flow caused deep scour across most of the channel and around the pier and debris. Although this accumulation did not cause the pier to fail, the situation illustrates several factors that decrease the stability of structures encumbered by debris:

- Additional flow-obstruction area and increased hydrodynamic loading transferred to structure,
- Increased upstream water surface elevations,
- Decreased effective-flow area through the bridge opening,
- Increased local and general scour, and
- Deflection of flow to adjacent piers and abutments.

Highway bridges partially or fully submerged during a flood event are subjected to hydrodynamic forces, impact forces

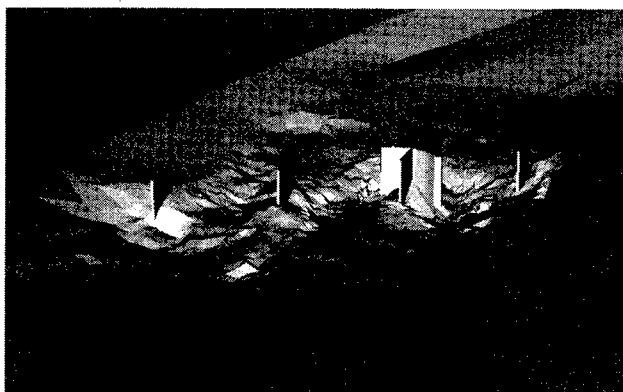


Figure 4. Solid model of piers, debris, streambed, and banks at a bridge crossing over the Brazos River, Texas. (7)

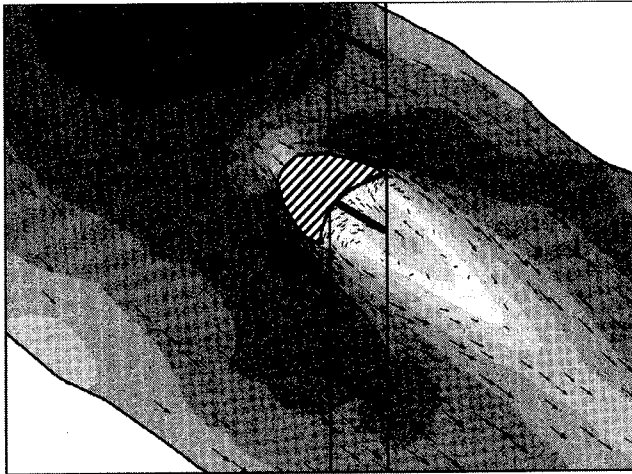


Figure 5. Two-dimensional simulation of flow around a debris accumulation on a pier in the Brazos River, Texas (arrows show flow direction and magnitude; contours show depth-averaged velocity magnitude, with the darkest contour shade representing the highest velocity magnitude). (7)

caused by colliding debris, and forces associated with floating debris that accumulate on the bridges. The total force system, excluding impact, consists of hydrodynamic drag and side forces, hydrostatic forces, buoyant forces, and hydrodynamic lift forces. Hydrodynamic drag forces act parallel to the flow direction and result from the reaction of the water as it flows around an obstacle. Side forces are similar to drag forces, but act perpendicular to the flow direction. The hydrostatic forces on bridge elements are caused principally by the effect of flow constriction (that is, either by blockage of waterway openings because of debris or by embankment encroachment). The buoyant forces result from the displacement of water by the bridge or by the debris lodged under the bridge. Hydrodynamic-lift forces are the component of the total dynamic pressure force acting perpendicular to the flow direction and side force. These forces, along with debris impact, may contribute to bridge collapse by causing buckling of bridge substructures, shearing of roadway deck supports, and overturning of bridge structures.

AASHTO has stated that the hydrostatic, buoyant, and hydrodynamic-lift forces must be considered in bridge analysis and design. Although the AASHTO *Standard Specifications for Highway Bridges*, fifteenth edition (9), provides recommendations regarding debris loads for the design of bridges, reliable guidance for design is not available. This study was undertaken to formulate analytical procedures to evaluate debris forces.

## OBJECTIVES

The overarching goal of this research was to develop practical design specifications for and supporting commentary on

determining the amount of drag and hydrostatic forces, on bridge piers and superstructures, that are due to debris. The specific objectives of the project were to

- Develop analytical models to estimate hydrodynamic drag and hydrostatic forces,
- Calibrate and verify the analytical models to provide practical and reliable design equations,
- Develop a draft specification and supporting commentary, and
- Apply the developed design methodology and specification to design examples.

The objectives of this research were accomplished using theoretical, experimental, and practical information developed in this study through the following tasks.

## RESEARCH TASKS

The research conducted under Project 12-39 included the following sequence of tasks:

1. Collect and review relevant domestic and foreign literature, research findings, and current practices related to design for hydrodynamic and debris-induced forces on bridges.
2. Develop analytical methods to quantify drag and hydrostatic forces, on bridge piers and superstructures, that are due to debris. Compile and integrate these methods into a procedure that can be used as the basis for specifications to calculate significant debris forces on bridges. Although the procedure developed considered debris size, type, and accumulation characteristics, information was provided by an FHWA- and U.S. Geological Survey (USGS)-sponsored study (10) to provide maximum definitions for design purposes.
3. Present the findings of Tasks 1 and 2 in an interim report that includes a detailed research plan.
4. Conduct laboratory studies in accordance with the detailed research plan from Task 3. The purpose of these experiments is to calibrate and validate the analytical methods developed in Task 2.
5. Revise the analytical methods as required using the experimental results. Develop bridge-design specifications for and supporting commentary on debris forces in a format suitable for consideration by AASHTO. Demonstrate the use of the proposed specifications with practical examples.
6. Prepare and submit a final report containing the research findings, the proposed specifications and commentary, and recommendations for further research.

An additional task (Task 7) was sponsored by FHWA to conduct field surveys and to evaluate flood-related damage and damage processes to highway bridges, approaches, and

culverts that resulted from the 1993 floods in the Mississippi River Basin. Through this additional task, two bridges that failed as a result of debris loading were investigated. A series of documents detailing important practical information on site conditions was made available for use in Tasks 1–6 through this investigation. The results of Task 7 are provided in *NCHRP Report 417*, “Highway Infrastructure Damage Caused by the 1993 Upper Mississippi River Basin Flooding” (5).

#### **SCOPE OF STUDY**

The scope of this study was limited to (1) developing a practical methodology, using a predetermined amount of debris and debris characteristics, for predicting maximum

loads as limited by accumulation of debris on bridge piers and on superstructures; and (2) developing design criteria. Information on debris geometry became available through the Task 7 report (5) and through the site investigations of the FHWA/USGS-sponsored research conducted by Diehl (10). This information on debris geometry was considered, and the model-debris accumulations were altered to match observed field configurations. Recommendations for debris geometry to determine debris loads in the specification were obtained from Diehl (10).

This study focused on aligned-bridge crossings, including piers aligned with subcritical approaching flow and superstructures aligned with flow. Scour, flow-alignment variation, river bends, and debris other than woody debris were not investigated in this study.

---

## CHAPTER 2

# FINDINGS

### SUMMARY OF STATE-OF-KNOWLEDGE ACCOUNT

Historically, bridge damage by debris has been considered an important factor in bridge design (11, 6); however, only a single study on debris forces on bridges has been reported in the literature that was reviewed for this project (12). As stated in the introduction of this report, only recently has any information regarding the determination of design debris loads been provided in the AASHTO guidelines and specifications. Because ice forces appear similar in nature to debris forces, it may first seem reasonable to develop force-prediction methodologies for debris loading similar to those for ice forces. Examination of the *AASHTO LRFD Bridge Design Specifications*, first edition (3), section on ice forces shows that the maximum size of ice forces is associated with the strength of the ice (13). The maximum size of debris accumulations, which are composed mainly of woody debris, is primarily a function of the debris accumulation geometry, although the strength of the debris within the accumulation is certainly a factor in the formation of debris accumulations (10).

Relevant available information for developing analytical models for debris loading was examined and summarized in the following categories:

- Mean hydrodynamic forces on submerged objects,
- Hydrodynamic forces on bridge piers and on superstructures,
- Hydrodynamic forces on debris accumulations,
- Geometry of debris accumulations on bridges, and
- Conditions at bridge failures where debris contributed to damage.

A brief summary highlighting the most important information of each category is provided in this section. A more complete state-of-knowledge account is provided in Appendix A, Part 1.

#### Mean Hydrodynamic Forces on Submerged Objects

Well-established, practical methods for relating fluid mean hydrodynamic forces to the flow around submerged objects have been developed using an empirical drag equa-

tion. The general form of the drag equation that was developed from dimensional analysis is

$$F_D = C_D \rho A_r \frac{(V_r)^2}{2} \quad (1)$$

where

- $F_D$  = drag force, N;
- $C_D$  = coefficient of drag;
- $\rho$  = fluid density, Kg/m<sup>3</sup>;
- $A_r$  = reference area, m<sup>2</sup>; and
- $V_r$  = reference velocity, m/s.

The equation is consistent dimensionally and, therefore, can be used with any consistent unit system. The drag coefficients ( $C_D$ ) for objects submerged in flow fields that are not severely contracted by the object range from approximately 2.0, for a square plate oriented perpendicular to the flow, to 0.01, for air foils. The profile area of the obstacle perpendicular to the flow direction and the unobstructed-flow velocity are typically used as the reference area and reference velocity in Equation 1. The coefficient of drag is a function of several geometric and flow factors, including Reynolds number, angle of flow attack, surface waves, shape of obstacle, and turbulence intensity (14).

#### Hydrodynamic Forces on Bridge Piers and Superstructures

Information on the mean hydrodynamic forces on bridge piers and superstructures has been obtained from laboratory studies by Apelt (15, 16, 17), Apelt and Issac (18), Denson (19), Jempson and Apelt (12), Naudascher and Medlarz (20), and Wellwood and Fenwick (21). The most extensive research has been conducted at the Bridge Testing Facility at the University of Queensland, Australia, by Apelt and several collaborators. The drag coefficients for piers and pier superstructures, as related in Equation 1, vary widely, from about 0.6 to 3.5, depending on many factors.

One reason for the large variation in drag coefficient is the inconsistency in definition of reference velocities and reference areas. A second reason for the large variation in drag coefficient is the lack of consideration for overall flow contraction

caused by the relatively large blockages. As the flow obstruction contracts the overall flow area, the upstream-flow velocity is reduced while the upstream depth and pressure increase. Hydrodynamic forces can increase significantly as flow blockage approaches about 30 percent of the total flow area. Typically, tests on piers skewed to the flow direction and superstructures block 10–40 percent of the flow area.

To account for the variation of flow depth and pressure through bridge openings, Koch et al. (22) recommend a model for partitioning the total hydrodynamic force on the obstruction into a hydrostatic component associated with streamwise variation of flow depth and into a dynamic component associated with flow velocity. The total streamwise force can be defined as

$$F_s = F_D + (F_{hu} - F_{hd}) \quad (2)$$

where

$F_s$  = streamwise force, N;

$F_D$  = drag force, N;

$F_{hu}$  = hydrostatic force on the upstream side of the obstruction, N; and

$F_{hd}$  = hydrostatic force on the downstream side of the obstruction, N.

The total hydrostatic component of force on the upstream was computed as

$$F_{hu} = wh_{cou} A_{ou} \quad (3)$$

where

$F_{hu}$  = hydrostatic force on the upstream side of the obstruction, N;

$w$  = specific weight of water (9,810 N/m<sup>3</sup>);

$h_{cou}$  = vertical distance from the water surface to the centroid of area  $A_{ou}$ , m; and

$A_{ou}$  = projected area of an obstruction normal to the flow direction and below the upstream water surface, m<sup>2</sup>.

Likewise, the total hydrostatic component of force on the downstream side was computed as

$$F_{hd} = wh_{cod} A_{od} \quad (4)$$

where

$F_{hd}$  = hydrostatic force on the downstream side of the obstruction, N;

$w$  = specific weight of water (9,810 N/m<sup>3</sup>);

$h_{cod}$  = vertical distance from the water surface to the centroid of area  $A_{od}$ , m; and

$A_{od}$  = projected area of an obstruction normal to the flow direction and below the downstream water surface, m<sup>2</sup>.

## Hydrodynamic Forces on Debris Accumulations

Apelt (17) used a rectangular prism with drilled holes, narrow planks, and cylindrical logs arranged to simulate idealized debris mats to evaluate the drag forces experienced by debris mats. Apelt showed that drag forces depend on the internal geometry of the mat and on the open-area percentage. The preliminary research conducted by Apelt (17) on idealized debris mats shows that the drag coefficient for idealized debris accumulations varies from 1.0 to 2.0, with a corresponding variation in percentage of area openings of 10–30 percent. In these experiments, debris mats were studied in the absence of bridge pier or superstructure models. Investigations of debris accumulation on bridge elements have not been reported.

Wellwood and Fenwick (21) proposed a method for computing debris forces on bridge superstructures. The method considers an idealized debris accumulation geometry. The drag force is computed using the drag equation (Equation 1). Wellwood and Fenwick (21) developed a method of predicting drag forces on superstructures with a debris mat that extended below the superstructure. A drag coefficient of 1.04 was recommended, with the reference velocity being the velocity that occurred at the midheight of the debris mat or the restricted-flow velocity beneath the superstructure.

## Geometry of Debris Accumulations on Bridges

Perhaps the most complex aspect of debris-force prediction is the determination of debris-accumulation size and characteristics. The dimensions of debris accumulation on bridge piers and superstructures not only influence the value of the terms that represent area in the drag equation (Equation 1), but they also may influence the entire flow field through the bridge opening. Prediction of the effective blockage size of debris accumulation and its overall effect on flow velocities and depths may be the most important factor in the prediction of debris forces. Despite the importance of determining debris geometry and its influence on flow at bridges, very little information is available on which to base prediction of debris accumulation geometry for design.

Wellwood and Fenwick (21) provide suggestions for the dimensions of debris on piers and superstructures. They recommend that the width of the debris accumulation on a pier be equal to the average of adjacent-span lengths up to a maximum of 20 m, with a minimum assumed-vertical accumulation depth of 1.2 m. Wellwood and Fenwick (21) recommend that the accumulation extend the entire length of the superstructure, with a vertical extent equal to the width of the superstructure plus 1.2 m (the width of the superstructure is the difference between the highest elevation of the railing system and the lowest elevation of the girder). The maximum vertical extent should be limited to 3 m unless site evidence warrants a larger extent.

Diehl (10) provides information developed from documented field observations. This FHWA/USGS-sponsored study provides information on maximum debris accumulation geometric characteristics. Diehl (10) developed criteria for design debris blockages using evaluation of over 2,577 reported accumulations and 144 field investigations of drift accumulations. Using the field observations as a base, Diehl developed suggested guidelines for assessing drift potential, including a description of three phases to estimate the potential for (1) drift delivery to the bridge, (2) drift delivery to each bridge element, and (3) maximum accumulation geometry. The methodology for predicting maximum debris-accumulation size uses a design log that is based on a sturdy log length that can transfer hydrodynamic loads to the superstructure and piers. The length of the design log was determined by field observations of debris accumulations.

Because of the difficulties of observing debris accumulations on superstructures, Diehl (10) could not provide a basis for developing a means to predict the size of accumulations on superstructures in deep-flow conditions. Consequently, he recommends following the suggestions provided by Wellwood and Fenwick (21) for deep-flow conditions. A detailed description of Diehl's method is provided in Appendix A, Part 1.

#### Conditions at Bridge Failures Where Debris Contributed to Damage

Several studies have provided information about the conditions of bridge sites where debris accumulations have caused damage at bridges (11, 6, 1, 10). In addition, information gathered during the field investigations that were conducted under Task 7 of this project (5) provides site conditions where debris accumulations have caused bridge collapse.

Descriptions of site conditions frequently addressed the effects of flow contraction in the bridge openings where debris accumulations caused damage. Although attempts were made to minimize the effects of general-flow contraction around the bridge component in most laboratory flume studies of forces on bridges, examination of bridges where debris forces have caused collapse shows that debris blockages typically cause a moderate to severe contraction of the flow in the main channel through the bridge openings. Figures 2, 3 and 6 illustrate sites where the effects of debris dominate flow through the bridge opening. The large flow blockages in the main channel require the water surface elevation of the upstream flow to rise and generate the energy necessary to pass flow around the accumulation and to accelerate flow through the contracted bridge opening. The force required to change the flow pattern, increase upstream water surface elevations, and accelerate flow through the bridge opening is primarily the result of the debris that are supported by the bridge.

Fine debris, such as leaves, tree branches, grasses, and other plant material, tend to block a core region of woody-

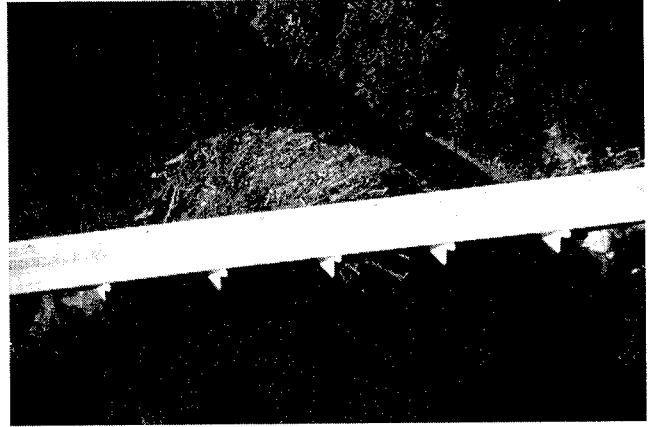


Figure 6. Large debris accumulation that causes severe flow contraction.

debris support matrix (5). Parola's experience in examining debris accumulations in the midwestern and eastern United States has shown that this type of blockage of the woody-debris matrix is typical (5), as illustrated in Figures 3 and 7.

Stream bends, backwater effects, and interaction between the floodplain and main channel cause highly nonuniform flows that make characterizing representative velocity in the approach to the bridge (equivalent to the reference velocity) highly uncertain and subjective.

Although debris accumulations are often considered to be floating rafts, they have been observed to develop from the surface of the water to the streambed at piers (10, 5). When trees are longer than the height of the superstructure above the streambed, debris accumulations can span the gap between the superstructure and streambed. If trees longer than bridge spans are transported to a bridge, then severe blockages are possible in the bridge opening, as shown in Figure 8.



Figure 7. Woody-debris matrix with fine debris blockage.



Figure 8. Severe debris blockage where bridge spans are shorter than the lengths of trees that can be transported to the bridge site.

## EXPERIMENTAL INVESTIGATIONS

A series of three experimental investigations was conducted to develop a methodology for predicting drag forces, as defined by Equation 1, and hydrostatic forces, as defined by Equation 2, that are caused by debris accumulations on piers and superstructures. The experimental investigations included the University of Queensland Idealized-Model Debris Investigation; the WES Medium-Scale, Woody-Debris Model Data Investigation; and the University of Louisville Vertical-Plate; Flow-Blockage Investigation.

Appendix A, Part 2, provides a detailed description of the experimental apparatus, procedures, and data for each investigation. The following sections provide a general description of each investigation.

### University of Queensland Idealized-Model Debris Investigation

A series of small-scale tests was conducted in the Bridge Force Testing Facility at the University of Queensland, Brisbane, Australia. These tests were completed at a scale of 1:25. The objective of the small-scale tests was to obtain data on idealized model debris on typical pier and superstructure bridges. The piers that were tested included a typical two-column pier with a rectangular pier cap; a typical solid, rectangular pier with a rectangular pier cap; and a four-steel H-pile bent pier with the dimensions of the Harrison Road bridge pile bent. The models included typical two-lane, concrete-deck superstructures with New Jersey-type guardrails. The four superstructures had different beam configurations: prestressed concrete I-beam girder, steel girder, spread box beam, and adjacent box beam. Debris models included vertical plates and roughened cones on piers, as well as vertical plates and roughened wedges on superstructures.

### WES Medium-Scale, Woody-Debris Model Data Investigation

The second series of tests was completed at the Riprap Testing Facility of the U.S. Army Corps of Engineers Waterways Experiment Station in Vicksburg, Mississippi. These tests were completed at a scale of about 1:16. The objective of these tests was to obtain data at the largest scale feasible, using model debris elements to form accumulations on a pier and on a superstructure. The model superstructure was a typical steel-girder superstructure. The model pier was a two-column pier. Both models resembled those tested under the University of Queensland investigation. Figures 9 and 10 show different views of a typical model debris accumulation that formed on a model pier. Figure 11 shows a typical model debris accumulation floating upstream of a model superstructure. Figure 12 shows a model debris accumulation that had plunged under and was then pinned under the model superstructure, where it was at least partially supported by the streambed.

### University of Louisville Vertical-Plate, Flow-Blockage Investigation

The third series of tests was completed at the University of Louisville Hydraulics Laboratory. The objective of the University of Louisville tests was to obtain force data over the complete range of possible flow-blockage ratios. The researchers used vertical plates to examine the effects of flow blockage. Although these tests were conducted on simple plate models, they provided a framework for evaluating the other study data.

Data that were collected in each of these studies included approach-flow velocity, water surface elevation both upstream and downstream of the debris on piers or superstructures,

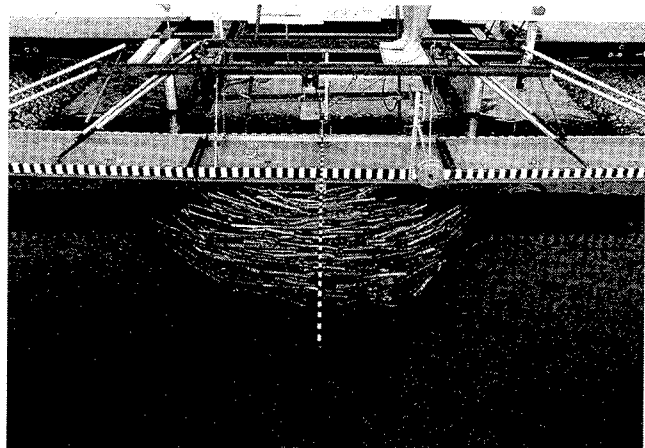


Figure 9. Typical model debris accumulation on a pier, front view.

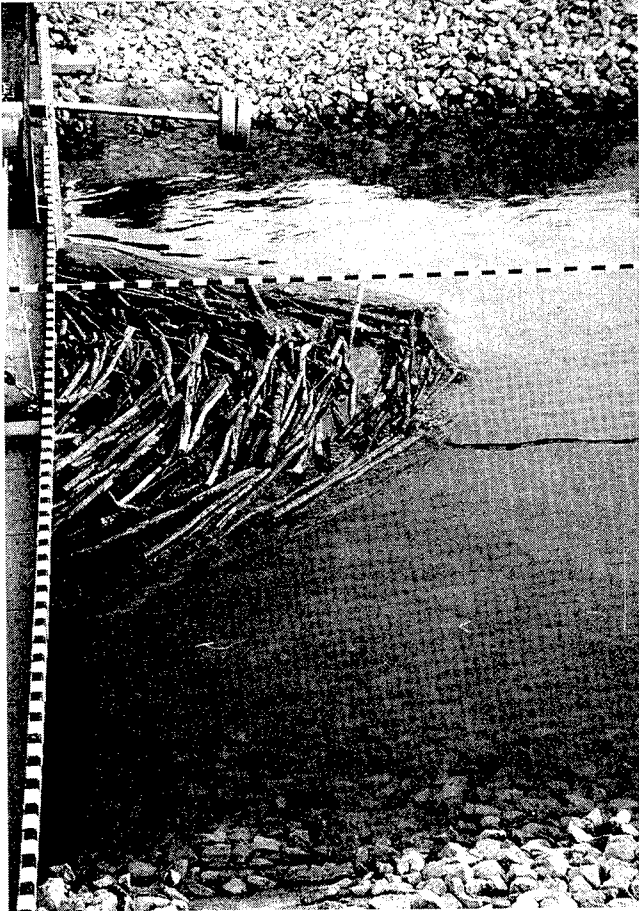


Figure 10. Typical model debris accumulation on a pier, side view.

and total streamwise force on the model debris and bridge component. Contracted-flow velocity and depth were computed from these data sets. Appendix A, Part 2, presents the data sets for each test series.

## RESULTS

Analysis of the data was conducted to establish the most reliable parameters for determining drag and hydrostatic forces. The large amount of data available from the University of Louisville plate-blockage tests spanned the entire range of flow blockage (5–90 percent) and a wide range of subcritical Froude numbers. Therefore, analysis of the University of Louisville blockage data was used to determine both the appropriate reference velocity for the drag equation and the effectiveness of partitioning the total horizontal-streamwise force into drag and hydrostatic components. The analysis focused on the variation of drag coefficient as a function primarily of flow-blockage ratio:

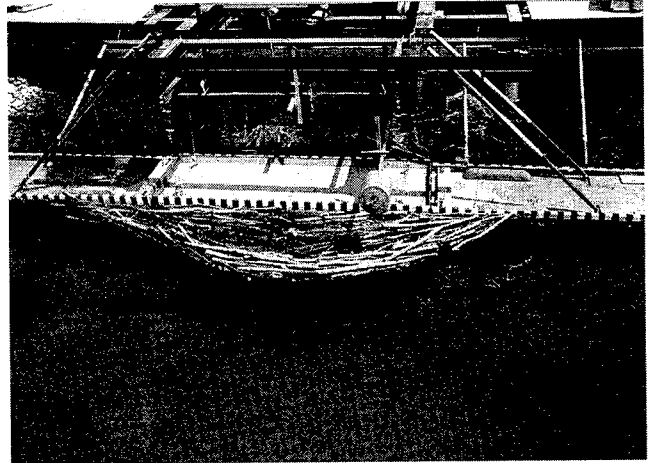


Figure 11. Floating debris accumulation on a superstructure.

$$B = \frac{A_b}{A_b + A_c} \quad (5)$$

where

$B$  = flow-blockage ratio;

$A_b$  = flow area blocked by debris in the contracted bridge section,  $m^2$ ; and

$A_c$  = unobstructed cross-sectional flow area in the contracted section,  $m^2$ .

The influence of Froude number and Reynolds number are also considered.

After appropriate reference velocities and the method for partitioning the drag and hydrostatic forces were established, drag coefficients from the University of Queensland small-

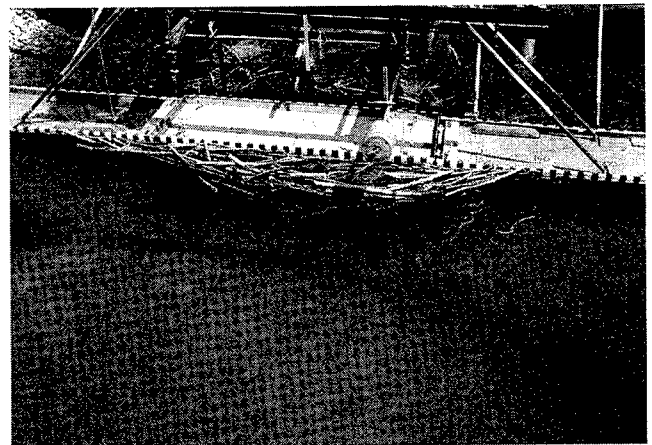


Figure 12. Debris accumulation caught between the superstructure and the streambed.

scale idealized debris data and from the WES medium-scale data were developed and compared with the plate data. The University of Queensland and WES data sets essentially served to verify the relation established through analysis of the simplified plate-blockage data.

The analysis of the results of the three investigations shows that the partitioning of total streamwise force into drag and hydrostatic components, as related in Equation 2, and the use of contracted-flow velocity ( $V_c$ ) in Equation 1 provide a consistent variation of drag coefficient over the complete range of flow-blockage ratios. Figures 13 and 14 show the variation of drag coefficient for debris on piers and superstructures, as well as the full-depth plate data.

The contracted-flow Froude number ( $Fr_c$ ) describes variation of drag coefficient through a range of specific flow and blockage-ratio conditions. The contracted-flow Froude number is defined as

$$Fr_c = \frac{V_c}{\sqrt{gY_c}} \quad (6)$$

where

$Fr_c$  = contracted-flow Froude number;

$V_c$  = contracted-flow velocity, m/s;

$g$  = gravitational acceleration constant ( $9.81 \text{ m/s}^2$ ); and

$Y_c$  = average flow depth in the flow contraction, m.

For blockage ratios ( $B$ ) less than 0.36 and for Froude numbers ( $Fr$ ) between 0.4 and 0.8, coefficient of drag ( $C_D$ ) decreases when Froude number increases. The trend may continue for higher Froude numbers; however, the data in this study were limited to Froude numbers lower than 0.8 and blockage ratios lower than 0.36.

Conservative envelope relations for variation of drag coefficient with blockage ratio and Froude number were developed for debris on both piers and superstructures. These envelope relations are provided in Tables 1 and 2 and described in the following sections.

### Debris on Piers

The data collected from the medium-scale model conditions for piers and from the idealized debris tests for piers fall within or slightly below the range of flat-plate data, as shown

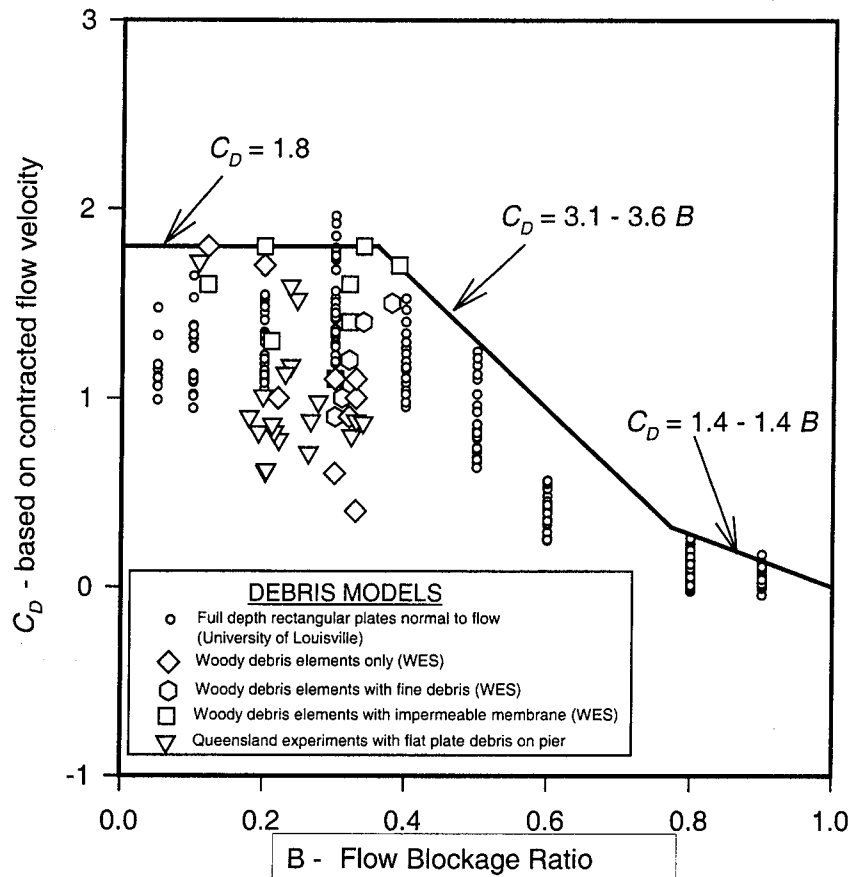


Figure 13. Method 3 variation of drag coefficient with blockage ratio for vertical plates, simulated debris, and idealized debris on piers.

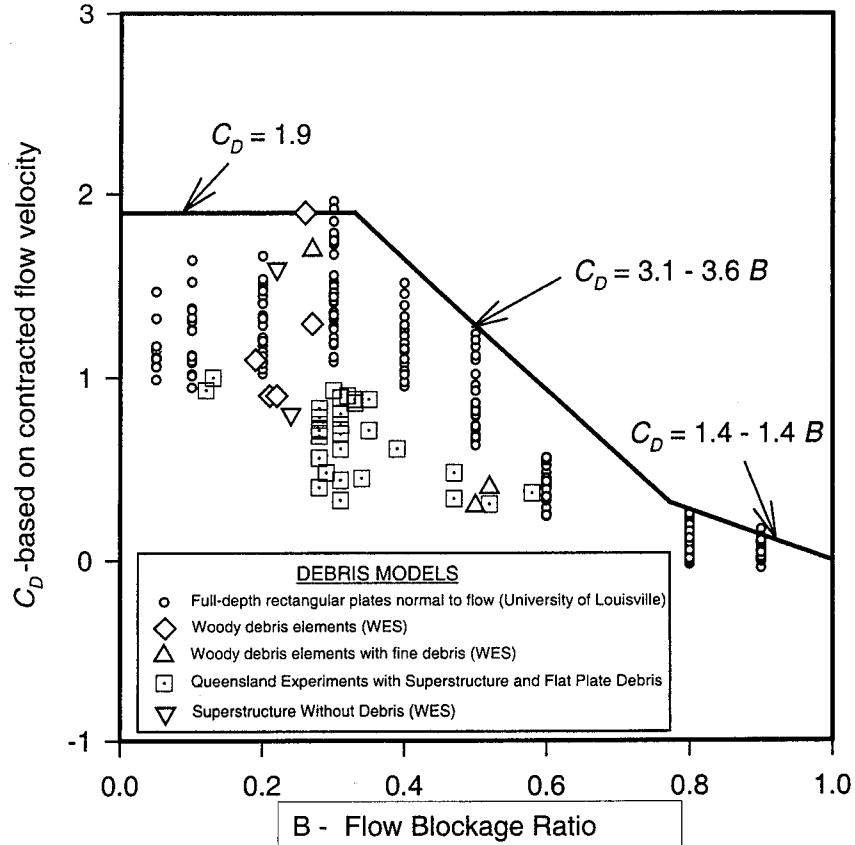


Figure 14. Method 3 variation of drag coefficient with blockage ratio for vertical plates, simulated debris, and idealized debris on superstructures.

TABLE 1 Envelope line segments for drag coefficients for debris on piers

B - Range	Fr - Range	$C_D$
$B < 0.36$	$Fr < 0.4$	$C_D = 1.8$
$B < 0.36$	$0.4 < Fr < 0.8$	$C_D = 2.6 - 2.0 Fr$
$0.36 < B < 0.77$	$Fr < 1$	$C_D = 3.1 - 3.6 B$
$B > 0.77$	$Fr < 1$	$C_D = 1.4 - 1.4 B$

TABLE 2 Envelope line segments for drag coefficients for debris on superstructures

B - Range	Fr - Range	$C_D$
$B < 0.33$	$Fr < 0.4$	$C_D = 1.9$
$B < 0.33$	$0.4 < Fr < 0.8$	$C_D = 2.8 - 2.25 Fr$
$0.33 < B < 0.77$	$Fr < 1$	$C_D = 3.1 - 3.6 B$
$B > 0.77$	$Fr < 1$	$C_D = 1.4 - 1.4 B$

in Figure 13. Table 1 provides a conservative design set of relations for drag coefficients for debris on piers.

#### Debris on Superstructures

Drag coefficients computed from the WES model debris on superstructures are in the range computed for blockage ratios lower than 0.3 in the plate experiments, as shown in Figure 14. Drag coefficients that were computed from the University of Queensland's idealized debris experiments provide lower drag coefficients. The WES data and the University of Queensland data cover different ranges of flow blockage, with the exception of four overlapping data points. Given the discrepancy between data sets, a conservative envelope line with a maximum drag coefficient of 1.9, as shown in Figure 14, is recommended for design. As with piers, an adjustment is provided for Froude numbers in the range of 0.4–0.8 (see Table 2).

## CHAPTER 3

### APPLICATION: DRAFT SPECIFICATION AND EXAMPLES

The first part of this chapter introduces the draft specification for and commentary on debris accumulation forces. The second part of the chapter applies the debris-loading specification to three examples in which debris accumulate on piers and superstructures. The first example applies the specification to a bridge on which a single pier is encumbered with debris. The second example applies the specification to two adjacent piers with a single large debris accumulation that blocks flow between the piers. The third example applies the specification to a debris-encumbered superstructure. Detailed explanation is provided for one-dimensional hydraulic modeling using the U.S. Army Corps of Engineers HEC-RAS, version 2.2, program (23); and guidance is provided to help establish a framework for estimating debris forces.

#### DRAFT DEBRIS-LOADING SPECIFICATION AND COMMENTARY

A draft specification for estimating drag and hydrostatic forces that are caused by debris accumulations on piers and superstructures was written in the style of the *AASHTO LRFD Bridge Design Specifications*, second edition (4), using the International System of Units (SI) base units. The specification includes subsections for determining drag and hydrostatic pressures. Commentary was written to provide both guidelines for the application of the specification and references that form the basis of the specification.

In the commentary on the specification, the following procedure for computing debris forces is given:

1. Estimate the geometry of debris accumulation on the structure;
2. Compute flow hydraulics for situations in which debris are in the flow; and
3. Compute hydrodynamic loads, using the flow as it is altered by the presence of debris.

The researchers of this project considered the recommendations and suggestions for estimating the geometry of debris accumulation that were provided by Diehl (10) and Wellwood and Fenwick (21) to be guidelines; therefore, they included the recommendations and suggestions in the commentary rather than in the specification. Neither the specification nor the commentary provide detailed procedures for obtaining

hydraulic parameters, as methods for computing flow hydraulic parameters are widely available in one-dimensional and multi-dimensional flow models. However, some recommendations are provided for selecting the locations to determine reference water surface elevations.

The formula provided for computing drag pressures is

$$p_D = C_D w \frac{(V_r)^2}{2g} \quad (7)$$

where

$p_D$  = component of average stream pressure on debris due to stream flow, N/m<sup>2</sup>;

$C_D$  = drag coefficient;

$w$  = specific weight of water (9,810 N/m<sup>3</sup>);

$V_r$  = reference velocity, m/s; and

$g$  = gravitational acceleration constant (9.81 m/s<sup>2</sup>).

The drag coefficient for piers is provided in Table 3 and for superstructures in Table 4.

Blockage ratio is defined as

$$B = \frac{A_b}{A_b + A_c} \quad (8)$$

where

$B$  = blockage ratio;

$A_b$  = cross-sectional flow area blocked by debris in the contracted bridge section, m<sup>2</sup>; and

$A_c$  = unobstructed cross-sectional flow area in the contracted section, m<sup>2</sup>.

The Froude number in Tables 3 and 4 is defined as

$$Fr = \frac{V_r}{\sqrt{gY_c}} \quad (9)$$

where

$Fr$  = Froude number;

$V_r$  = reference velocity, m/s;

$g$  = gravitational acceleration constant (9.81 m/s<sup>2</sup>); and

$Y_c$  = average flow depth in the flow contraction, m.

**TABLE 3 Drag pressure coefficient for debris on piers as a function of blockage ratio and Froude number**

B - Range	Fr - Range	C <sub>D</sub>
B < 0.36	Fr < 0.4	C <sub>D</sub> = 1.8
B < 0.36	0.4 < Fr < 0.8	C <sub>D</sub> = 2.6 - 2.0 Fr
0.36 < B < 0.77	Fr < 1	C <sub>D</sub> = 3.1 - 3.6 B
B > 0.77	Fr < 1	C <sub>D</sub> = 1.4 - 1.4 B

The following procedure for evaluating the reference velocity ( $V_r$ ) is also provided:

- If the reduction in area of the waterway opening by debris and bridge components is anticipated to be greater than 30 percent of the entire wetted cross-sectional flow area in the bridge opening, then the reference velocity is taken as the average velocity in the contracted section of the bridge opening.
- If the reduction in area of the waterway opening by debris and bridge components is anticipated to be less than 30 percent of the entire cross-sectional flow area in the bridge opening, then the reference velocity for piers and for full-depth blockages on superstructures is taken as the maximum local average velocity in the area just outside the influence of the pier and associated debris. For floating debris accumulations on superstructures, the restricted-flow velocity under the superstructure should be used as the reference velocity.

The equation for computing the resultant drag load is given in the commentary as

$$F_D = C_D w A_D \frac{(V_r)^2}{2g} \quad (10)$$

where

$F_D$  = drag force, N;

$C_D$  = drag coefficient (see Table 3 for piers and Table 4 for superstructures);

$w$  = specific weight of water (9,810 N/m<sup>3</sup>);

$A_D$  = area of wetted debris based on the upstream water surface elevation projected normal to flow direction, m<sup>2</sup>;

**TABLE 4 Drag pressure coefficient for debris on superstructures as a function of blockage ratio and Froude number**

B - Range	Fr - Range	C <sub>D</sub>
B < 0.33	Fr < 0.4	C <sub>D</sub> = 1.9
B < 0.33	0.4 < Fr < 0.8	C <sub>D</sub> = 2.8 - 2.25 Fr
0.33 < B < 0.77	Fr < 1	C <sub>D</sub> = 3.1 - 3.6 B
B > 0.77	Fr < 1	C <sub>D</sub> = 1.4 - 1.4 B

$V_r$  = reference velocity (see the procedure that follows Equation 9) m/s; and

$g$  = gravitational acceleration constant (9.81 m/s<sup>2</sup>).

The formula for computing hydrostatic pressure is provided in the specification as

$$p_h = wh \quad (11)$$

where

$p_h$  = hydrostatic pressure, N/m<sup>2</sup>;

$w$  = specific weight of water (9,810 N/m<sup>3</sup>); and

$h$  = distance from the water surface elevation to the point of pressure computation, m.

The commentary describes the locations and methods for computing the resultant hydrostatic force.

The total force on the structure that is caused by the hydrostatic pressure difference is approximated as

$$F_h = w(h_{cu}A_{hu} - h_{cd}A_{hd}) \quad (12)$$

where

$F_h$  = horizontal hydrostatic force on area  $A_h$ , N;

$w$  = specific weight of water (9,810 N/m<sup>3</sup>);

$h_{cu}$  = vertical distance from the upstream water surface to the centroid of area  $A_{hu}$ , m;

$A_{hu}$  = area of the vertically projected, submerged portion of the debris accumulation below the upstream water surface, m<sup>2</sup>;

$h_{cd}$  = vertical distance from the downstream water surface to the centroid of area  $A_{hd}$ , m; and

$A_{hd}$  = area of the vertically projected, submerged portion of the debris accumulation below the downstream water surface elevation, m<sup>2</sup>.

The examples in the following section demonstrate applications of the specification.

## EXAMPLE APPLICATIONS OF DEBRIS-LOADING SPECIFICATION

Three examples were developed to apply the debris-loading specification and commentary. The three examples were based partly on stream channel data that were available from a crossing of the Miami River in southern Ohio (1). The dimensions of the channel and bridge, the flow rates, and the boundary roughness were altered from one example to the next to provide variation of channel and flow conditions as well as of bridge geometries. In each of the examples, HEC-RAS, version 2.2 (23), was used to compute the flow hydraulics.

### Example 1: Debris on a Single Pier in a Wide Channel

#### Site Information

The bridge shown in Figure 15 was constructed over a small river in the eastern United States. The river has a history of chronic debris problems at other bridges upstream and downstream from the site examined. Mature stands of trees on the floodplains and streambanks exist upstream of the bridge. The tree-lined banks are eroded severely throughout the watershed, and the banks are eroded severely for approximately 50 mi upstream. The piers are composed of concrete pile bents. The potential for debris transport to the bridge is high; however, mature trees in the floodplain and along the channel banks shelter all of the pile bents except Pile Bent 2. Pile Bent 2 is located along the main channel bank. The flow runs essentially straight into the bridge opening. The design flow rate for analysis of the debris loads was  $800 \text{ m}^3/\text{s}$ .

#### Debris Delivery Potential and Maximum Debris Accumulation Geometry

The potential for delivering debris to the bridge was estimated to be high because of a history of chronic debris accumulation problems at other bridges in the watershed. The banks are lined with mature riparian trees.

Although the width of the main channel at the bridge is about 40 m, the cross-stream clear width of the upstream channel between tree-lined banks was estimated to be 30 m; therefore, the length of the design log was limited by the size of trees transported to the site. The maximum length of the

design log was estimated from Figure 16 as 16.5 m. Thus, the length of the design debris accumulation was 16.5 m.

The bridge superstructure does not become submerged. Pile Bent 2 is not sheltered by upstream trees and is located on the edge of the main channel. The potential for debris accumulation was estimated to be low for this bridge except for Pile Bent 2, where it was estimated to be high.

The maximum debris accumulation area for Pile Bent 2 was estimated as 16.5 m wide (the width of the design log length), with a depth equal to that of the flow. Although the depth of this accumulation may seem to be excessive, information is not available to allow a reduction of the maximum vertical extent. (Additional site history information may be available in other cases to provide a basis for reducing the depth of the accumulation.)

#### Modeling Debris on a Single Pier

Debris on Pile Bent 2 were modeled by increasing the width of the bent to the design log length (Figure 17) and by removing flow area from cross sections located downstream of the bridge. The flow-area reductions were necessary to conform to the ineffective-flow-area recommendations for large obstructions (23) as Figure 18 illustrates. The regions in Figure 18 represent stagnation zones upstream of the debris and wake zones downstream of the debris. In this example, the cross section upstream of the bridge was located sufficiently far upstream that consideration of ineffective-flow areas was unnecessary. The remaining model development was typical for bridges that have piers aligned with flow and that do not have roadway-approach embankments that encroach on flow.

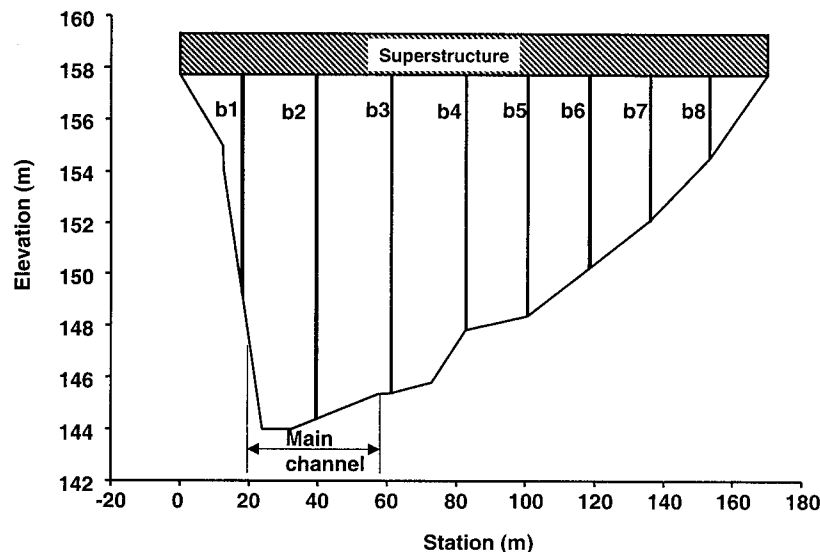


Figure 15. Example 1 upstream bridge cross section.

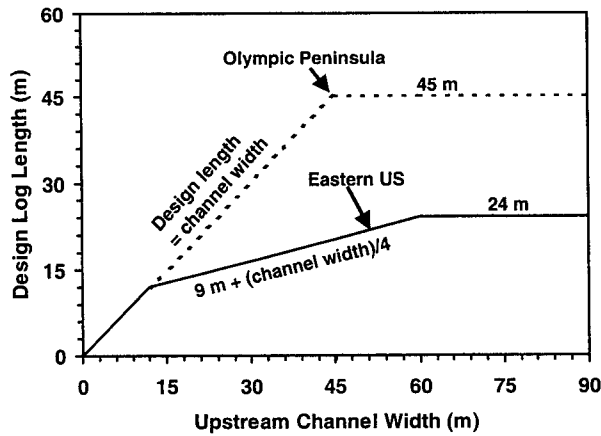


Figure 16. Design log length as a function of channel width, modified from Diehl. (10)

*Energy-Loss Coefficients*

The Manning roughness coefficients that were used in this model were 0.03, for the main channel, and 0.1, for the heavily wooded floodplains. The flow blockage of this example caused flow first to contract and then to expand within a relatively short distance between River Station 159 m and River Station 76 m; therefore, the contraction coefficients and expansion coefficients were set at 0.3 and 0.5, respectively, over the same distance. In this example, bridge embankments or other obstacles were not present.

*Hydraulic-Model Results*

Figure 19 shows the water surface profile and the relatively minor changes in flow depth associated with the design block-

age from River Station 0 m to River Station 296 m. A profile plot of water surface elevation at a highly exaggerated vertical scale (see Figure 20) was developed to clearly identify the locations where upstream and downstream water surface elevations could be selected for determining hydrostatic forces. Table 5, obtained directly from an output table generated by HEC-RAS, provides the corresponding numerical data. These data show that water surface elevation rises slightly in response to the increase in flow depth and the decrease in flow velocity as flow approaches the bridge area. The water surface elevation then drops as flow enters the bridge opening, which is contracted mainly by the debris on Pile Bent 2. Flow velocities increase slightly, and the water surface elevation drops in the bridge opening. The water surface elevation recovers from this drop by increasing downstream of the bridge in response to the flow expansion.

*Water Surface Elevation and Hydrostatic Pressure Variation*

Table 6 outlines the data requirements and calculations necessary for computing hydrostatic and drag forces on the debris accumulation. The hydrostatic force on the debris and bridge is estimated from the average drop in water surface elevation through the bridge contraction. Water surface elevations upstream and downstream of the bridge are necessary for computing hydrostatic force. The water surface elevations that are used to compute hydrostatic forces on the upstream side of the bridge should be selected at locations sufficiently far upstream that flow has not accelerated in response to the debris. Likewise, the water surface elevations necessary to compute hydrostatic forces on the downstream side of the

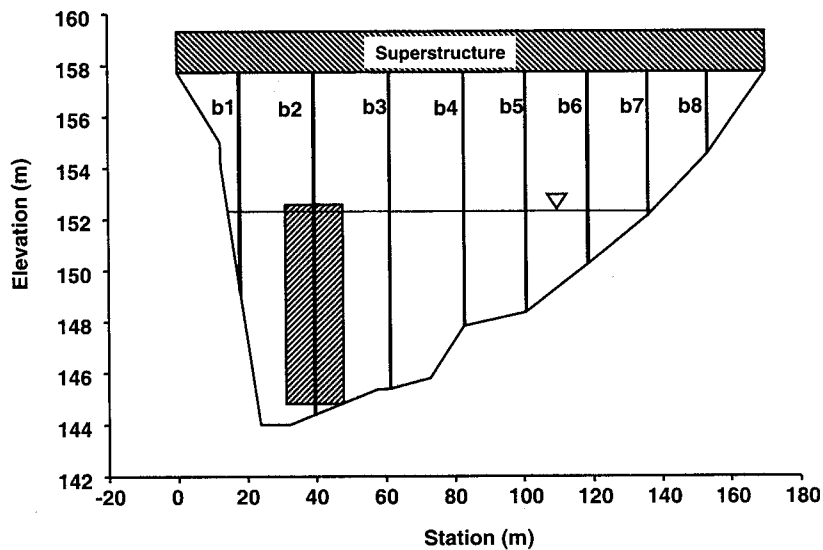


Figure 17. Example 1 upstream bridge cross section, computed water surface elevation, and model debris on Pile Bent 2.

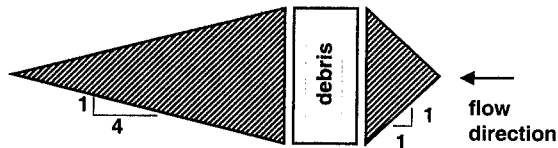


Figure 18. Ineffective-flow areas for debris on a pier.

debris should be obtained sufficiently far downstream from the bridge that the flow velocity and elevation are not in the wake flow of the debris. For this example, the water surface elevations were obtained at the limits of the ineffective areas associated with the debris, as shown in Figures 18 and 20. River Stations 159 m and 76 m correspond to the limits of the ineffective-flow areas and to the locations for obtaining water surface elevations and computing hydrostatic pressures in this example. The design debris-accumulation area and the distances to the centroid of that area for computing hydrostatic forces on the upstream and downstream sides of the debris were computed from the water surface elevations at River Stations 159 m and 76 m, respectively. Table 6 provides the data for these computations. The debris accumulation in this example was rectangular; therefore, the area for any hydrostatic pressure computation was equal to the product of the depth (measured from the water surface to the bottom of the debris) and the width of the design debris accumulation. For each computation, the centroidal distance was computed as one-half of the debris accumulation depth below the appropriate water surface.

The upstream water surface elevation that was used to compute the area for hydrostatic forces was used also to determine

the area for computing drag. Use of two-dimensional or three-dimensional flow models may provide more accurate predictions of flow-separation regions (that is, of ineffective-flow areas) and hydrostatic pressure variations than the flow-separation regions and hydrostatic pressure variations assumed in this one-dimensional analysis.

Under some conditions, the water surface elevation downstream from the flow contraction may not recover (that is, rise in elevation). High rates of energy dissipation (that is, high friction-loss rates), large channel slope, or large changes in channel geometry may prevent increases in water surface elevation downstream from the debris. Under these conditions, the water surface elevation downstream from the debris may be lower than that in the contraction around the debris. In such cases, the water surface elevation in the contraction should be used to compute downstream hydrostatic forces. The downstream water surface elevation that is used to compute hydrostatic forces should not be lower than the elevation of flow in the contraction around the debris.

#### Hydrostatic Pressure and Force

Computation of hydrostatic pressure distribution on the debris accumulation may be useful for distributing loads; however, the total load in this example was transferred as a point load to the pier, and so only the total hydrostatic loads on the upstream and downstream sides of the debris were computed. Item 14 of Table 6 provides the total hydrostatic force on the debris as determined by Equation 12. Items 1–5 of the same table provide input data necessary to compute the total hydrostatic force. Items 7–13 provide the computations necessary to determine areas, centroidal distances of the

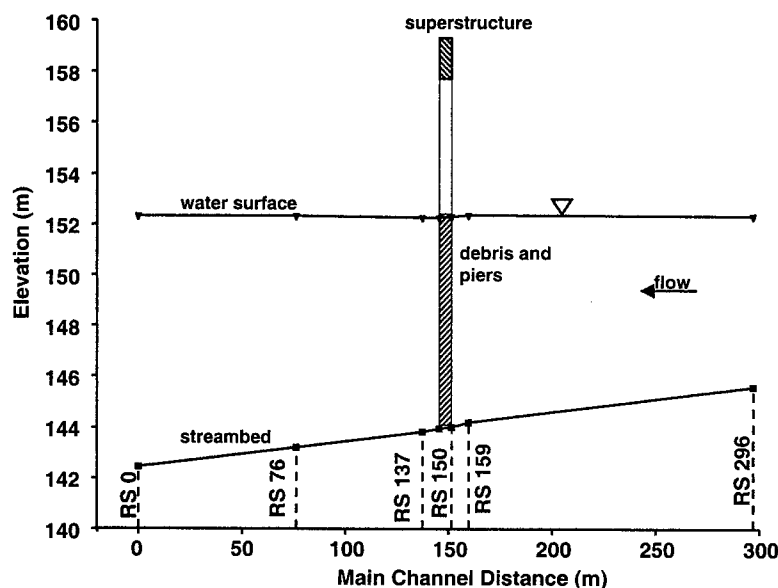


Figure 19. Example 1 computed water surface profile and stream thalweg elevation.

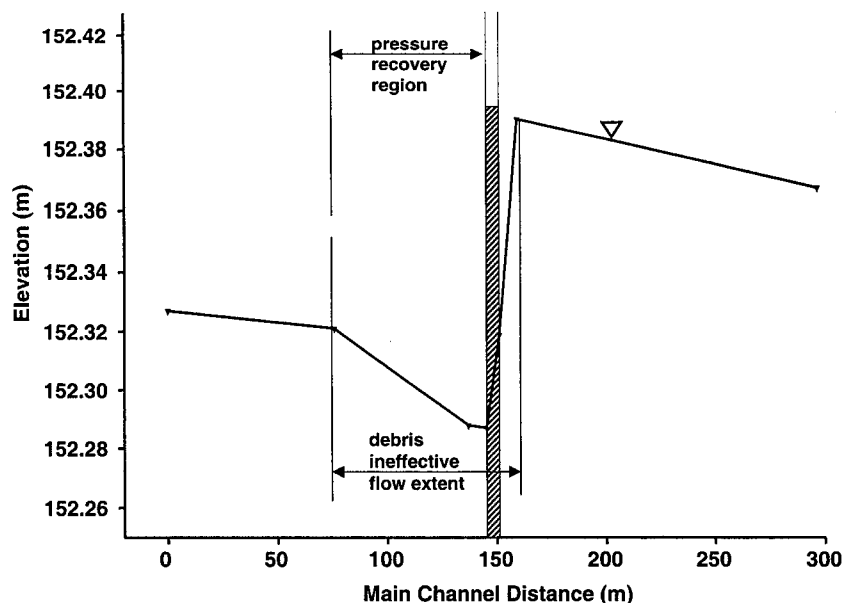


Figure 20. Example 1 computed water surface profile variation, with pressure-recovery regions and ineffective-flow extents.

areas, and hydrostatic forces on the upstream and downstream sides of the accumulation. For a detailed description of each variable, refer to Equation 12.

#### Computation of the Blockage Ratio

Drag coefficient and reference-velocity selection depend on the degree to which debris block the waterway opening. The blockage ratio was computed using Equation 8. The area of debris blockage ( $A_b$ ) is represented adequately at this station by Item 8, the area of upstream-hydrostatic pressure. The contracted-flow area ( $A_c$ ) was measured at the most contracted area in the bridge opening. The smallest flow area and highest cross-sectional velocity were found at River Station 150 m at the downstream face of the bridge. The value of  $A_c$  was taken as 479 m<sup>2</sup>. The value of  $B$  was computed as 0.21.

#### Selection of Reference Velocity and Area for Drag Computations

The value of  $B$  was less than 0.30; therefore, the maximum local average velocity outside the influence of the pier and the debris was used as the reference velocity. The main obstruction was the debris on the bridge pier located in the main channel. Although the debris blocked only 21 percent of the total flow area, they blocked approximately 38 percent of the main-channel flow area (the main-channel flow area was 329 m<sup>2</sup>). The reference velocity for computing debris drag force was approximated as the main channel contracted-flow velocity in the bridge opening. The maximum contracted-flow velocity in the main channel was computed by HEC-RAS at River Station 150 m (which is on the downstream face of the bridge) as 2.12 m/s.

The reference area for drag was estimated from the water surface elevation at Station 159 m and is provided in Table 6 as Item 8, although it is repeated in Item 16 for clarity.

TABLE 5 Example 1 HEC-RAS results

River Station (m)	Water Surface Elevation (m)	Flow Area (m <sup>2</sup> )	Main Channel Velocity (m/s)	Cross Section Average Velocity (m/s)
296	152.37	438	2.15	1.83
159	152.39	598	1.67	1.34
150 BR U	152.32	480	2.05	1.67
150 BR D	152.29	479	2.12	1.67
137	152.29	529	2.01	1.51
76	152.32	711	1.45	1.12
0	152.33	812	1.30	0.98

#### Drag Pressure and Force

The pressure difference on the submerged-profile area of the debris perpendicular to the flow direction was computed using Equation 7. The blockage ratio ( $B$ ) that was arrived at in the section on computing blockage ratio was 0.21; therefore, the drag coefficient from Table 3 was 1.8. The reference velocity was considered to be the main channel contracted-flow velocity (2.12 m/s), as described in the previous section. Item 20 of Table 6 computed the total drag pressure. Appli-

**TABLE 6 Example 1 summary of hydrostatic and drag force computations**

Item No.	Parameter	Value*	Computation and Reference*
1	WSE Upstream (m)	152.39	Table 5 HEC-RAS Output
2	WSE Downstream (m)	152.32	Table 5 HEC-RAS Output
3	Bottom Elevation of Debris Segment (m)	144.80	HEC-RAS Input
4	Left Station of Segment (m)	31.3	HEC-RAS Input
5	Right Station of Segment (m)	47.8	HEC-RAS Input
6	WSE change (m)	0.07	(1) – (2)
7	W (m)	16.5	(5) – (4)
8	$A_{hu}$ (m <sup>2</sup> )	125.2	[(1) – (3)] x (7)
9	$A_{hd}$ (m <sup>2</sup> )	124.0	[(2) – (3)] x (7)
10	$h_{cu}$ for $A_{hu}$ (m)	3.79	[(1) – (3)] / 2
11	$h_{cd}$ for $A_{hd}$ (m)	3.76	[(2) – (3)] / 2
12	$F_{hu}$ (kN)	4660	9.81 x (8) x (10)
13	$F_{hd}$ (kN)	4574	9.81 x (9) x (11)
14	$F_h$ (kN)	86	(12) – (13)
15	$V_c$ (m/s)	2.12	Table 5 HEC-RAS Output
16	$A_D$ (m <sup>2</sup> )	125.2	(8)
17	$A_C$ (m <sup>2</sup> )	479	Table 5 HEC-RAS Output
18	B	0.21	(8) / [(17) + (8)]
19	$C_D$	1.80	Table 3
20	$P_D$ (kN/m <sup>2</sup> )	4.04	[(19) x (15) <sup>2</sup> ] / 2
21	$F_D$ (kN)	506	(16) x (20)
22	Total Segment Force (kN)	592	(14) + (21)
23	Station of Hydrostatic Force (m)	39.6	[(4) + (5)] / 2
24	Elevation of Hydrostatic Force (m)	148.6	See Below **
25	Station of Drag Force (m)	39.6	[(4) + (5)] / 2
26	Elevation of Drag Force (m)	148.6	[(1) + (3)] / 2
27	Station of Resultant Force (m)	39.6	[(4) + (5)] / 2
28	Elevation of Resultant Force (m)	148.6	See Below ***

\*Computed table values were calculated to four-decimal precision and then rounded to the precision shown.

\* The computations provided include the referenced item number in parentheses. For example, "(20)" refers to Item 20.

$$\text{**Item 24 Computation: } (24) = (3) + \frac{(12) \times \left[ \frac{(1) - (3)}{3} \right] - (13) \times \left[ \frac{(2) - (3)}{3} \right]}{(14)}$$

$$\text{***Item 28 Computation: } (28) = \frac{(21) \times (26) + (24) \times (14)}{(22)}$$

cation of the drag pressure to the appropriate area in Item 16 provided the pressure force, as indicated in Item 21.

#### Location of the Resultant Force

The vertical location of the resultant hydrostatic and drag forces and that of the total force were computed by adding the moments about convenient axes. Items 24, 26, and 28 of Table 6 provide the computation of each force. The lateral location of the resultant force in this example was the center of the symmetrical debris accumulation; however, for more complex debris configurations, the horizontal position of the

resultant force could be located by adding the moments about a convenient vertical axis.

#### Transfer of Hydrodynamic Loads to the Structure

The loads computed for this example correspond to the pressure forces of the water on the debris. Transfer of the load from the debris to the structure depends on many factors, including the characteristics of the debris accumulation and the degree to which streambed and banks support the debris accumulation. A few large debris elements may transfer large portions of the load to a few points on the structure

or to points on the streambed or banks. The recommendation for this example is that the resultant force be applied at the vertical location as computed in Table 6 as a point load. Less conservative distribution of the load to the structure may be warranted where there is more information available on the debris configuration and structural susceptibility.

### Example 2: Debris on Two Adjacent Piers

#### Site Information

The bridge in Figure 21 was constructed over a river in the eastern United States. The stream has a history of chronic debris problems at other bridges both upstream and downstream. Mature stands of trees on the floodplains and stream banks exist upstream of the bridge. The tree-lined banks are severely eroded throughout the watershed. Concrete pile bents make up the piers. Pile Bents 2 and 3 are within the main channel, Pile Bent 4 is on the bank of the main channel, and Pile Bents 1 and 5 are on the floodplain. Flow at high discharge was taken to be aligned with the bridge opening; however, an embankment on the right floodplain encroaches on the potential-flow cross section at high stage, thus causing flow to contract into the bridge opening. The design flow rate for analysis of the debris loads was  $800 \text{ m}^3/\text{s}$ . The upstream clear width of the main channel between the tree-lined banks was 65 m.

#### Debris-Delivery Potential and Maximum Debris Accumulation Geometry

The potential for delivering debris to the bridge was estimated to be high because of a history of chronic debris-accumulation problems at other bridges upstream. The source

of the debris is riparian trees lining the stream banks. Severely eroded banks are present for approximately 50 mi upstream.

The width of the main channel at the bridge is about 70 m. The cross-stream clear width of the upstream channel between tree-lined banks was estimated to be 65 m; therefore, the length of the design log was limited by the sturdy length. The design log length was taken from Figure 16 as 24 m.

The potential for debris transport to the bridge is high; however, mature trees in the floodplain and along the channel banks shelter all of the pile bents except Pile Bents 2 and 3. The bridge superstructure does not become submerged. Pile Bents 2 and 3 are on the edge of the main channel. The potential for debris accumulation is low for this bridge except for Pile Bents 2 and 3. The potential for accumulation on these bents is considered high.

The distance between Pile Bents 2 and 3 was 22.2 m. This distance was less than the 24-m length of the design log; therefore, this horizontal gap was considered blocked. The design overhang on each side of Pile Bents 2 and 3 away from the central blockage was 12 m (half of the design log length). The total blockage width was 46.2 m.

The depth of the accumulation was considered to be the full-flow depth. Although the depth of this accumulation may seem excessive, information is not available to suggest a lower maximum vertical extent. Additional site history information may be available in other cases to provide a basis for reducing the estimated depth of the debris accumulation.

#### Modeling Debris Blockage

The effect of debris on Pile Bents 2 and 3 was modeled by increasing the width of the bents and by modeling the width of the accumulation (see Figure 22). To account for the loss of flow area in upstream stagnation zones and in downstream wake zones, ineffective-flow area was modeled

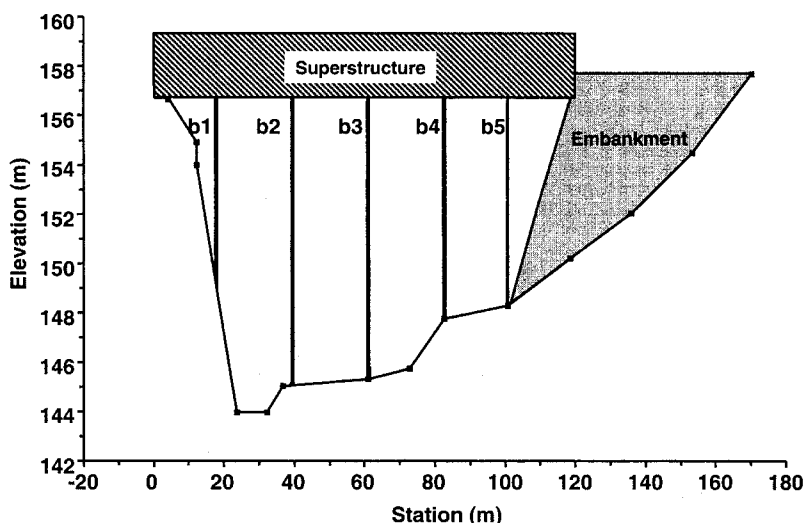


Figure 21. Example 2 upstream bridge cross section.

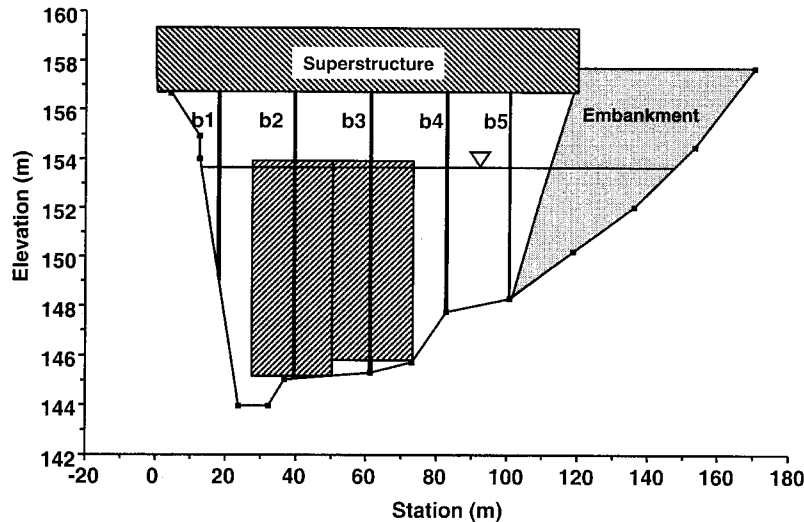


Figure 22. Example 2 upstream bridge cross section, computed water surface elevation, and model debris on Pile Bents 2 and 3.

using Figure 18 as a guide. Model ineffective-flow areas were removed from model cross sections that included the debris accumulation as well as from model cross sections that included the embankment. For the design debris accumulation, the ineffective-flow areas did not extend beyond 23 m (that is, beyond a 1:1 contraction rate) upstream from the accumulation and beyond 92 m (that is, beyond a 4:1 expansion rate) downstream. Ineffective-flow areas were also included for the embankment using the same figure as a guide. Ineffective-flow areas for the debris and embankment extended from River Station 76 m to River Station 173 m. The remaining model development was typical for bridges that are aligned with flow and that have roadway-approach embankments that encroach on flow.

#### Energy-Loss Coefficients

The Manning roughness coefficients used in this model were 0.03 for the main channel and 0.1 for the heavily wooded floodplains. The severe-flow blockage of this example required expansion and contraction coefficients for a moderately contracted bridge opening. The coefficients of contraction and expansion were estimated to be 0.6 and 0.8, respectively, for when the Manning roughness coefficients were 0.03 for the main channel and 0.1 for the heavily wooded floodplains. The coefficients were applied appropriately in the zone from River Station 76 m to River Station 250 m.

#### Hydraulic-Model Results

Figure 23 shows the water surface profile and the relatively minor changes in flow depth from River Station 0 m to River Station 387 m. A profile plot of water surface elevation

at a highly exaggerated vertical scale (see Figure 24) was developed to clearly identify the locations where upstream and downstream water surface elevations could be selected for determination of hydrostatic forces. Table 7, obtained from output tables generated by HEC-RAS, provides the corresponding numerical data.

#### Water Surface Elevation and Hydrostatic-Pressure Force

Figure 24 shows that most of the drop in water surface elevation occurs between River Stations 250 m and 213 m. The reference water surface elevations for computing hydrostatic forces were selected at sections upstream of the bridge where the flow did not yet accelerate in response to the debris and at sections sufficiently far downstream from the bridge that the flow velocity and elevation were not affected by the wake flow of the debris. These sections were taken at the limits of the ineffective-flow areas that were associated with the debris, as shown in Figure 24. River Stations 250 m and 76 m correspond to locations for computing hydrostatic pressures in this example.

#### Load Distribution Between Piers

In the case of two piers separated by a distance shorter than the length of the design log, the transfer of the water-pressure loads to the structure depends on the deformation of the debris accumulation, which, in turn, depends on the material properties of the accumulation. The load transfer also depends on the interaction between the debris and the streambed and banks. Even if no interaction occurs between the debris and the streambed and banks, at least the following three scenarios are possible:

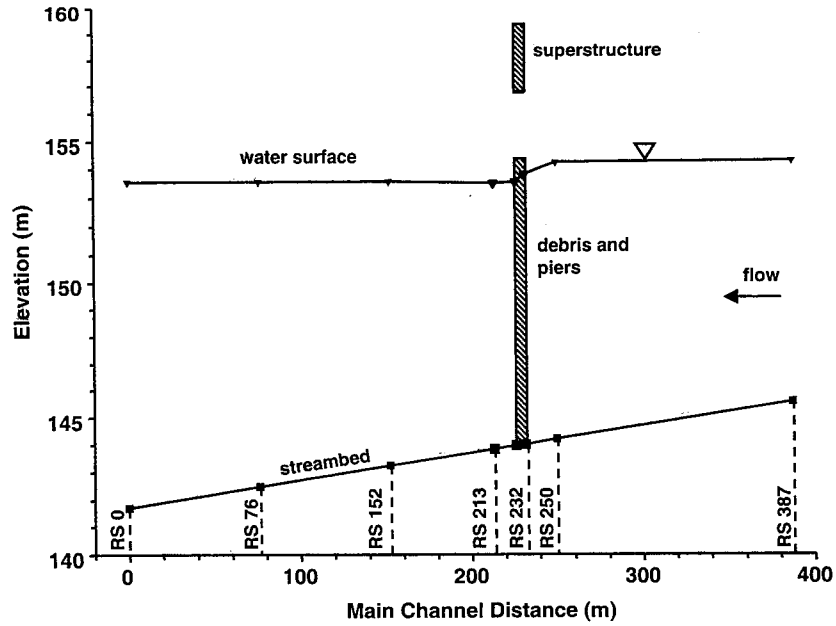


Figure 23. Example 2 computed water surface profile and stream thalweg elevation.

1. A debris accumulation of maximum effective width (24 m) forms on Pile Bent 2, with a smaller effective accumulation-transferring load to Pile Bent 3;
2. A debris accumulation of maximum effective width (24 m) forms on Pile Bent 3, with a smaller effective accumulation loading Pile Bent 2; and
3. A large log spans the opening and transfers or divides the load on the accumulation between the piers almost equally to each pier.

Although pressures on the debris accumulation are almost identical for each scenario, the distribution of total force to each of the piers may be substantially different from one situation to another. In the analysis of structural failure modes that include overturning of the entire structure about the streambed, substructure system shear or lateral bearing fail, and local buckling of substructure members, various load distributions should be considered. Tables 8 and 9 provide the resultant hydrostatic force and drag forces for Scenar-

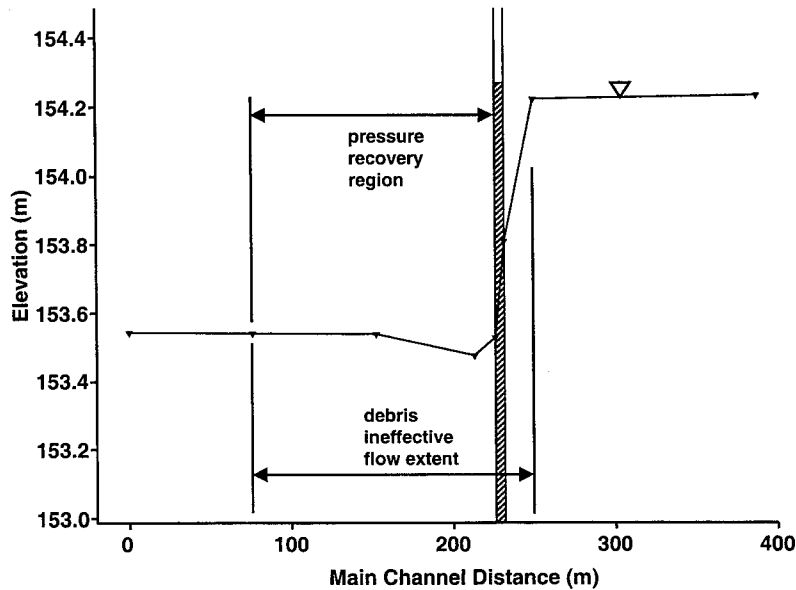


Figure 24. Example 2 computed water surface profile variation, with pressure-recovery regions and ineffective-flow extents.

TABLE 7 Example 2 HEC-RAS results

River Station (m)	Water Surface Elevation (m)	Flow Area (m <sup>2</sup> )	Main Channel Velocity (m/s)	Cross Section Average Velocity (m/s)
387	154.25	644	1.59	1.24
250	154.24	712	1.48	1.12
232 BR U	153.82	303	2.75	2.64
232 BR D	153.54	281	3.49	2.85
213	153.49	346	3.45	2.31
152	153.55	723	1.48	1.11
76	153.55	970	1.14	0.82
0	153.56	1083	1.04	0.74

ios 1 and 2, respectively. The following sections describe the force computations for both scenarios.

#### Scenario 1: Maximum Debris Accumulation on Pile Bent 2

During the formation of the hypothetical accumulation, the possibility exists that an accumulation of maximum extent (24 m wide) on Pile Bent 2 and a smaller accumulation (21.6 m wide) on Pile Bent 3 will form. Although the accumulations meet in the center and completely block flow between Pile Bents 2 and 3, only insignificant load and moment are assumed to be transferred between the two accumulations. This scenario produces the maximum resultant load on Pile Bent 2. Table 8 summarizes the drag-pressure force and the upstream, downstream, and net hydrostatic forces that are computed for the accumulations on Pile Bents 2 and 3 in this scenario. The drag pressure was applied to the same areas used to compute the upstream-hydrostatic pressures for Pile Bents 2 and 3. Table 8 provides the resultant forces for each bent and the forces' locations.

#### Scenario 2: Maximum Debris Accumulation on Pile Bent 3

This scenario is similar to Scenario 1, except that the maximum debris accumulation (24 m wide) is on Pile Bent 3 and the smaller accumulation (21.6 m wide) is on Pile Bent 2. The computational procedure is identical to that of Scenario 1, and Table 9 summarizes the results. The depth of the Pile Bent 3 accumulation is slightly shallower than that of Pile Bent 2; therefore, the area and maximum load of the Pile Bent 3 accumulation in this scenario are slightly different than those of the Pile Bent 2 load in Scenario 1.

#### Computation of the Contraction Ratio

The blockage ratios for each scenario were computed using Equation 8. The reference water surface for computing

blockage area was obtained at River Station 250 m as 154.24 m (see Table 7). In Scenario 1, the bottom of the debris accumulations for Pile Bents 2 and 3 were set at the streambed at elevations 145.2 m and 145.8 m, respectively (see Item 3 of Table 8). These bottom elevations represent full-depth debris accumulations (the debris extend from the water surface to the streambed). The total area blocked by these accumulations was computed as 400 m<sup>2</sup>. The value of  $A_c$  was obtained from the most contracted area in the bridge opening (281 m<sup>2</sup> at River Station 232, bridge downstream cross section [BR D]); that station also showed the highest cross-sectional velocity. The value of  $B$  was computed as 0.59. Although the computed blockage area for Scenario 2 was slightly different (398 m<sup>2</sup>) than that of Scenario 1, the blockage ratio was approximately the same value (0.59) as shown in Item 18 of Tables 8 and 9.

#### Selection of Reference Velocity for Drag Computations

The value of  $B$  was greater than 0.30; therefore, the average velocity in the contracted cross section was used as the reference velocity for computing the drag force. The highest cross-sectional average velocity was obtained at River Station 232 (BR D) at 2.85 m/s (see Table 7).

#### Drag Pressure and Forces

The pressure difference on the submerged-profile area of the debris perpendicular to the flow direction was computed using Equation 7. Because the blockage ratio ( $B$ ) was 0.59, the drag coefficient was 0.98 (see Table 3). Because the reference velocity was considered to be the main channel contracted-flow velocity (2.85 m/s), the drag pressure was 3.98 kN/m<sup>2</sup> (see Item 20 of Tables 8 and 9). The computed pressure multiplied by the projected area of the debris accumulation yields the drag-pressure force on each pier's accumulations. Item 21 of Tables 8 and 9 provides the drag forces for each scenario.

#### Transfer of Hydrodynamic Loads to the Structure

The recommendation for this example is that the resultant forces be applied as point loads at vertical locations, as shown in Tables 8 and 9. The location of the resultant forces for each debris segment was computed similarly to how the location of the resultant forces in Example 1 was computed. Consideration should be given to positioning the loads at locations where factors such as diagonal bracing, connections, or both may increase the structural susceptibility to failure. Less conservative distribution of the load to the structure may be warranted where additional information is available on the debris configuration, interaction of the debris mat with streambed and banks, and structural susceptibility.

**TABLE 8 Example 2, Load Scenario 1, summary of hydrostatic and drag force computations for debris accumulation spanning two piers, with largest accumulation on Pile Bent 2**

Item No.	Parameter	Pile Bent 2*	Pile Bent 3*	Computation and Reference*
1	WSE Upstream (m)	154.24	154.24	Table 7 HEC-RAS Output
2	WSE Downstream (m)	153.55	153.55	Table 7 HEC-RAS Output
3	Bottom Elevation of Segment (m)	145.17	145.80	HEC-RAS Input
4	Left Station of Segment (m)	27.6	51.6	HEC-RAS Input
5	Right Station of Segment (m)	51.6	73.2	HEC-RAS Input
6	WSE change (m)	0.69	0.69	(1) - (2)
7	W (m)	24.0	21.6	(5) - (4)
8	A <sub>nu</sub> (m <sup>2</sup> )	217.7	182.2	[(1) - (3)] x (7)
9	A <sub>sd</sub> (m <sup>2</sup> )	201.1	167.3	[(2) - (3)] x (7)
10	h <sub>cu</sub> for A <sub>nu</sub> (m)	4.54	4.22	[(1) - (3)] / 2
11	h <sub>cd</sub> for A <sub>sd</sub> (m)	4.19	3.88	[(2) - (3)] / 2
12	F <sub>nu</sub> (kN)	9684	7544	9.81 x (8) x (10)
13	F <sub>sd</sub> (kN)	8267	6361	9.81 x (9) x (11)
14	F <sub>n</sub> (kN)	1417	1183	(12) - (13)
15	V <sub>c</sub> (m/s)	2.85	2.85	Table 7 HEC-RAS Output
16	A <sub>D</sub> (m <sup>2</sup> )	217.7	182.2	(8)
17	A <sub>c</sub> (m <sup>2</sup> )	281	281	Table 7 HEC-RAS Output
18	B	0.59	0.59	[(8) <sub>b2</sub> + (8) <sub>b3</sub> ] / [(17) + (8) <sub>b2</sub> + (8) <sub>b3</sub> ]
19	C <sub>D</sub>	0.98	0.98	Table 3
20	P <sub>D</sub> (kN/m <sup>2</sup> )	3.98	3.98	[(19) x (15) <sup>2</sup> ] / 2
21	F <sub>D</sub> (kN)	866	725	(16) x (20)
22	Total Segment Force (kN)	2283	1908	(14) + (21)
23	Station of Hydrostatic Force (m)	39.6	62.4	[(4) + (5)] / 2
24	Elevation of Hydrostatic Force (m)	149.5	149.8	See Below **
25	Station of Drag Force (m)	39.6	62.4	[(4) + (5)] / 2
26	Elevation of Drag Force (m)	149.7	150.0	[(1) + (3)] / 2
27	Station of Resultant Force (m)	39.6	62.4	[(4) + (5)] / 2
28	Elevation of Resultant Force (m)	149.6	149.9	See Below ***

\*Computed table values were calculated to four-decimal precision and then rounded to the precision shown.

\* The computations provided include the referenced item number in parentheses. For example, "(20)" refers to Item 20.

\*\*Item 24 Computation: (24) = (3) + 
$$\frac{(12) \times \left[ \frac{(1) - (3)}{3} \right] - (13) \times \left[ \frac{(2) - (3)}{3} \right]}{(14)}$$

\*\*\*Item 28 Computation: (28) = 
$$\frac{(21) \times (26) + (24) \times (14)}{(22)}$$

**Example 3: Debris on Superstructure**

*Site Information*

The bridge in Figure 25 is built over a river in the eastern United States. The single-span, steel-girder superstructure becomes partially submerged during the design flood event. The stream has a history of chronic debris problems at other bridges upstream and downstream from the given site. Mature stands of trees on the floodplains and stream banks exist upstream of the bridge. The tree-lined banks are severely eroded throughout the watershed. Flood flows are estimated to be aligned with the bridge opening; however, an embankment on the right floodplain encroaches on the flow cross section at high stage, causing flow to contract into the bridge opening. The approach embankments contract floodplain flow such that all of the flow in the right floodplain is diverted into the main channel at the bridge. The design flow rate for

analysis of the debris loads was 1800 m<sup>3</sup>/s. The upstream clear width of the main channel between the tree-lined banks was 65 m.

*Debris-Delivery Potential and Maximum Debris Accumulation Geometry*

The potential for delivering debris to the bridge was estimated to be high because of a history of chronic debris-accumulation problems at other bridges upstream. Riparian trees constitute the source of the debris, as severely eroded tree-lined banks are present for approximately 50 mi upstream from the site. The width of the main channel at the bridge is about 70 m. The cross-stream clear width of the upstream channel between tree-lined banks was estimated to be 65 m; therefore, the sturdy length of the maximum-size tree that was

**TABLE 9 Example 2, Load Scenario 2, summary of hydrostatic and drag force computations for debris accumulation spanning two piers, with largest accumulation on Pile Bent 3**

Item No.	Parameter	Pile Bent 2*	Pile Bent 3*	Computation and Reference*
1	WSE Upstream (m)	154.24	154.24	Table 7 HEC-RAS Output
2	WSE Downstream (m)	153.55	153.55	Table 7 HEC-RAS Output
3	Bottom Elevation of Segment (m)	145.17	145.80	HEC-RAS Input
4	Left Station of Segment (m)	27.6	49.2	HEC-RAS Input
5	Right Station of Segment (m)	49.2	73.2	HEC-RAS Input
6	WSE change (m)	0.69	0.69	(1) – (2)
7	W (m)	21.6	24.0	(5) – (4)
8	$A_{hu}$ (m <sup>2</sup> )	195.8	202.6	[(1) – (3)] x (7)
9	$A_{hd}$ (m <sup>2</sup> )	180.9	186.0	[(2) – (3)] x (7)
10	$h_{cu}$ for $A_{hu}$ (m)	4.54	4.22	[(1) – (3)] / 2
11	$h_{cd}$ for $A_{hd}$ (m)	4.19	3.88	[(2) – (3)] / 2
12	$F_{hu}$ (kN)	8712	8386	9.81 x (8) x (10)
13	$F_{hd}$ (kN)	7437	7071	9.81 x (9) x (11)
14	$F_h$ (kN)	1275	1315	(12) – (13)
15	$V_c$ (m/s)	2.85	2.85	Table 7 HEC-RAS Output
16	$A_D$ (m <sup>2</sup> )	195.8	202.6	(8)
17	$A_c$ (m <sup>2</sup> )	281	281	Table 7 HEC-RAS Output
18	B	0.59	0.59	[(8) <sub>b2</sub> + (8) <sub>b3</sub> ] / [(17) + (8) <sub>b2</sub> + (8) <sub>b3</sub> ]
19	$C_D$	0.98	0.98	Table 3
20	$P_D$ (kN/m <sup>2</sup> )	3.98	3.98	[(19) x (15) <sup>2</sup> ] / 2
21	$F_D$ (kN)	779	806	(16) x (20)
22	Total Segment Force (kN)	2054	2121	(14) + (21)
23	Station of Hydrostatic Force (m)	38.4	61.2	[(4) + (5)] / 2
24	Elevation of Hydrostatic Force (m)	149.5	149.8	See Below **
25	Station of Drag Force (m)	38.4	61.2	[(4) + (5)] / 2
26	Elevation of Drag Force (m)	149.7	150.0	[(1) + (3)] / 2
27	Station of Resultant Force (m)	38.4	61.2	[(4) + (5)] / 2
28	Elevation of Resultant Force (m)	148.6	149.9	See Below ***

\*Computed table values were calculated to four-decimal precision and then rounded to the precision shown.

\* The computations provided include the referenced item number in parentheses. For example, "(20)" refers to Item 20.

$$**\text{Item 24 Computation: } (24) = (3) + \frac{(12) \times \left[ \frac{(1) - (3)}{3} \right] - (13) \times \left[ \frac{(2) - (3)}{3} \right]}{(14)}$$

$$***\text{Item 28 Computation: } (28) = \frac{(21) \times (26) + (24) \times (14)}{(22)}$$

transported to the site limited the length of the design log. The design length of the log was estimated from Figure 16 as 24 m.

The potential for debris transport to the bridge is high. The bridge superstructure becomes partially submerged; therefore, the entire superstructure that is located over or close to the main channel is susceptible to debris accumulation. The potential for debris accumulation on the superstructure is high.

The maximum width of the debris accumulation on the superstructure was taken to be the entire superstructure width. The depth of the accumulation was estimated to be 1.2 m below the superstructure, the maximum vertical extent recommended by Wellwood and Fenwick (21).

#### *Modeling Debris Blockage and Flow under the Superstructure*

The effective-flow superstructure bottom elevation was lowered by 1.2 m to represent the effects of debris blockage (see Figure 26) in the hydraulic model. Ineffective-flow areas were incorporated to represent flow recirculation downstream and upstream of the embankments; however, because the superstructure and debris allow flow to pass under the bridge across the entire width of the bridge opening, consideration of any additional ineffective-flow area was not necessary. The remaining model development was typical for bridges aligned

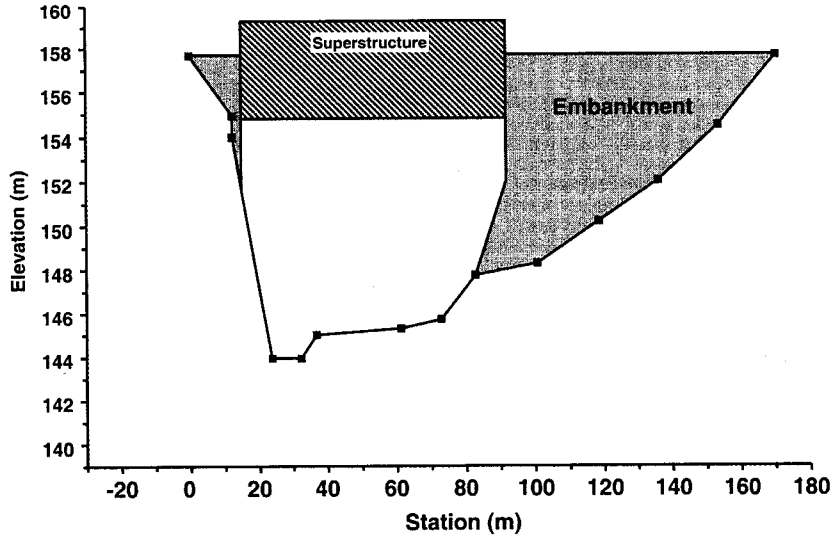


Figure 25. Example 3 upstream bridge cross section without debris.

with flow, with roadway-approach embankments that block flow, and with partially submerged bridge superstructures.

The submergence of the superstructure required modeling the flow as pressure flow. The flow through bridge openings in which both the upstream and downstream portions of the superstructure were submerged was modeled as flow through an orifice. An orifice discharge coefficient of 0.8 was used to model flow under the debris-encumbered superstructure.

*Energy-Loss Coefficients*

The Manning roughness coefficients that were used in this model were 0.03 for the main channel and 0.1 for the heavily wooded floodplains. The flow blockage of this example

required expansion and contraction coefficients for a moderately contracted bridge opening. The coefficients of contraction and expansion were estimated to be 0.3 and 0.5, respectively, for when the Manning roughness coefficients were 0.03 for the main channel and 0.1 for the heavily wooded floodplains. The coefficients were applied from River Station 463 m to River Station 0 m because of the large flow contraction and the extent of ineffective-flow areas associated with the right floodplain embankment.

*Hydraulic-Model Results*

Figure 27 shows the water surface profile and changes in flow depth from River Station 0 m to River Station 463 m.

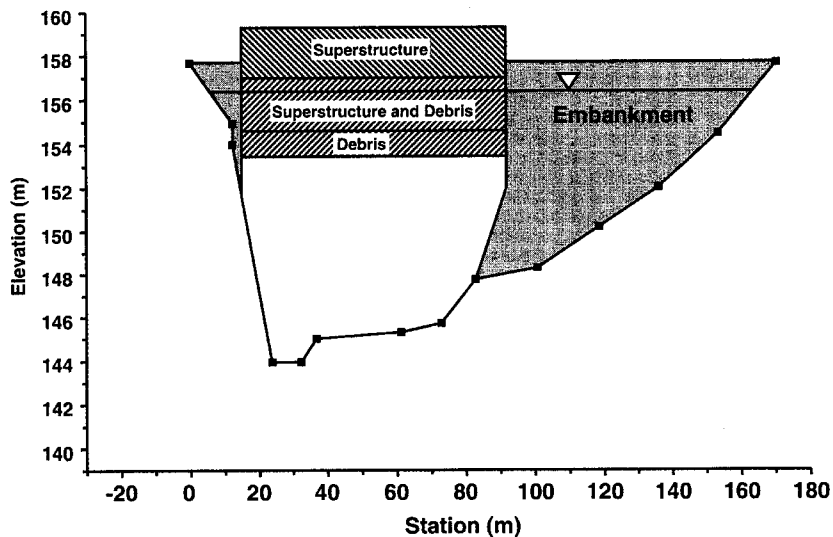


Figure 26. Example 3 upstream bridge cross section with debris.

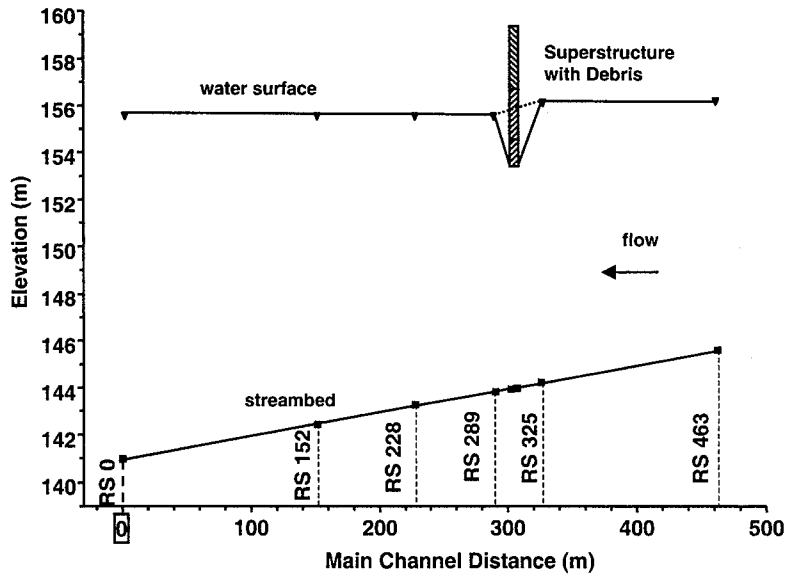


Figure 27. Example 3 computed water surface profile and stream thalweg elevation.

The highly exaggerated vertical scale of Figure 28 shows that almost all of the water surface elevation change in this example occurred in the area between the cross section immediately upstream of the bridge and the section immediately downstream of the bridge. Table 10, obtained from output tables generated by HEC-RAS, provides the corresponding numerical data.

*Water Surface Elevation and Hydrostatic-Pressure Variation*

In this example, the modeled water surface recovery (that is, the rise in elevation) downstream from the debris blockage was completed at the first river station cross section downstream from the bridge. Water surface elevations at

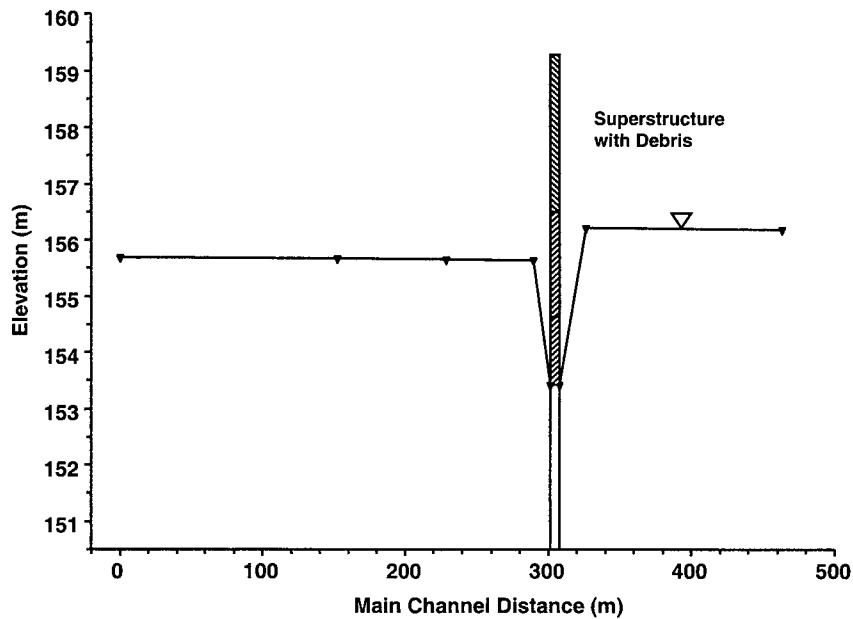


Figure 28. Example 3 computed water surface profile variation, with pressure-recovery regions and ineffective-flow extents.

**TABLE 10 Example 3 HEC-RAS results**

River Station (m)	Water Surface Elevation (m)	Flow Area (m <sup>2</sup> )	Main Channel Velocity (m/s)	Cross Section Average Velocity (m/s)
463	156.24	909	2.70	1.98
325	156.24	1024	2.30	1.76
307 BR U	153.43	559	3.39	3.22
307 BR D	153.43	563	3.36	3.20
289	155.66	916	2.40	1.96
228	155.67	1073	2.20	1.68
152	155.68	1285	2.01	1.40
0	155.68	1558	1.74	1.16

River Stations 325 m and 289 m were used for computing hydrostatic forces.

### Hydrostatic Pressure and Force

Computation of hydrostatic pressure distribution on the debris accumulation may be useful for distributing loads; however, the total load on the superstructure is required in this example; and so only the total hydrostatic loads on the upstream and downstream sides of the debris and superstructure were computed. Item 14 of Table 11 provides the

**TABLE 11 Example 3 summary of hydrostatic and drag force computations**

Item No.	Parameter	Value <sup>†</sup>	Computation and Reference*
1	WSE Upstream (m)	156.24	Table 10 HEC-RAS Output
2	WSE Downstream (m)	155.66	Table 10 HEC-RAS Output
3	Bottom Elevation of Debris Segment (m)	153.40	HEC-RAS Input
4	Left Station of Segment (m)	15.0	HEC-RAS Input
5	Right Station of Segment (m)	92.0	HEC-RAS Input
6	WSE Change (m)	0.58	(1) – (2)
7	W (m)	77.0	(5) – (4)
8	A <sub>hu</sub> (m <sup>2</sup> )	218.7	[(1) – (3)] x (7)
9	A <sub>hd</sub> (m <sup>2</sup> )	174.0	[(2) – (3)] x (7)
10	h <sub>cu</sub> for A <sub>hu</sub> (m)	1.42	[(1) – (3)] / 2
11	h <sub>cd</sub> for A <sub>hd</sub> (m)	1.13	[(2) – (3)] / 2
12	F <sub>hu</sub> (kN)	3046	9.81 x (8) x (10)
13	F <sub>hd</sub> (kN)	1929	9.81 x (9) x (11)
14	F <sub>h</sub>	1117	(12) – (13)
15	V <sub>c</sub> (m/s)	3.39	Table 10 HEC-RAS Output
16	A <sub>D</sub> (m <sup>2</sup> )	218.7	(8)
17	A <sub>C</sub> (m <sup>2</sup> )	559	Table 10 HEC-RAS Output
18	B	0.28	(8) / [(17) + (8)]
19	C <sub>D</sub>	1.90	Table 4
20	P <sub>D</sub> (kN/m <sup>2</sup> )	10.92	[(19) x (15) <sup>2</sup> ] / 2
21	F <sub>D</sub> (kN)	2388	(16) x (20)
22	Total Segment Force (kN)	3505	(14) + (21)
23	Station of Hydrostatic Force (m)	53.5	[(4) + (5)] / 2
24	Elevation of Hydrostatic Force (m)	154.7	See Below **
25	Station of Drag Force (m)	53.5	[(4) + (5)] / 2
26	Elevation of Drag Force (m)	154.8	[(1) + (3)] / 2
27	Station of Resultant Force (m)	53.5	[(4) + (5)] / 2
28	Elevation of Resultant Force (m)	154.8	See Below ***

<sup>†</sup>Computed table values were calculated to four-decimal precision and then rounded to the precision shown.

\* The computations provided include the referenced item number in parentheses. For example, "(20)" refers to Item 20.

$$\text{**Item 24 Computation: } (24) = (3) + \frac{(12) \times \left[ \frac{(1) - (3)}{3} \right] - (13) \times \left[ \frac{(2) - (3)}{3} \right]}{(14)}$$

$$\text{***Item 28 Computation: } (28) = \frac{(21) \times (26) + (24) \times (14)}{(22)}$$

total hydrostatic force on the debris, as represented by Equation 12. Items 1–5 of the same table provide input data necessary to compute the total hydrostatic force. Items 7–13 provide the computations necessary to determine areas, centroidal distances of the areas, and hydrostatic forces on the upstream and downstream sides of the accumulation. For a detailed description of each variable, refer to Equation 12. The hydrostatic force per unit length of superstructure was computed as 14.5 kN/m. The hydrostatic force for the total width of the superstructure against which debris had accumulated was computed as 77.0 m. The total hydrostatic pressure force was computed as 1,117 kN.

#### *Computation of the Contraction Ratio*

Drag coefficient and reference-velocity selection depend on the degree to which debris block the waterway opening. The blockage ratio ( $B$ ) was computed using Equation 8. The reference water surface elevation that was used to compute the blocked area was also used to compute the upstream-hydrostatic force area. The reference water surface elevation for this computation was obtained from River Station 325 m as 156.24 m (see Table 10). The bottom of the debris accumulation was located at elevation 153.40 m. The width of the debris accumulation was 77 m. The area of debris blockage ( $A_b$ ) at this station was 218.7 m<sup>2</sup>. The value of  $A_c$  was obtained from the most contracted area in the bridge opening. River Station 307 m (at the upstream face of the bridge) had the smallest area and, consequently, the highest average cross-sectional velocity. The value of  $A_c$  was taken as 559 m<sup>2</sup>. The value of  $B$  was computed as 0.28.

#### *Selection of Reference Velocity for Drag Computations*

The velocity of the contracted flow that was restricted between the streambed and the debris served as the reference velocity. The contracted flow under the bridge was contained mostly by the main channel; therefore, the average main-channel velocity served as the reference velocity. The maximum contracted velocity in the main channel was obtained from River Station 307 m (which is at the upstream face of the bridge) as 3.39 m/s (see Table 10).

#### *Drag Pressure*

The drag pressure on the submerged-profile area of the debris perpendicular to the flow direction was computed using Equation 7. The blockage ratio ( $B$ ) that was computed using Equation 8 was 0.28; the corresponding drag coefficient from Table 4 was 1.9. The reference velocity was taken to be the main channel contracted-flow velocity (3.39 m/s), as described

in the previous section. The drag pressure was computed as 10.92 kN/m<sup>2</sup>. Multiplying the drag pressure by the projected debris-accumulation area yields the drag-pressure force, Item 21 in Table 11. The drag force per unit length of superstructure was computed as 31 kN/m. The total drag force on the bridge was computed as 2,388 kN (Item 21 in Table 11).

#### *Transfer of Hydrodynamic Loads to the Structure*

The hydrostatic and drag loads given above should be applied to the structure at the elevations provided in Table 11. Consideration should be given to shear or sliding failure at the bridge bearings, as well as possible buckling of bracing beneath the deck of the structure. Overturning of the bridge is not kinematically possible in the absence of piers.

#### *Locations of the Resultant Forces*

The vertical locations of the resultant hydrostatic forces, drag forces, and total force were computed by adding the moments about convenient axes. Items 24, 26, and 28 of Table 11 provide the computation of each location.

#### *Transfer of Hydrodynamic Loads to the Structure*

As with the previous examples, the loads computed for Example 3 correspond to the pressure forces of the water on the debris. Transfer of the load from the debris to the structure depends on many factors, including the characteristics of the debris accumulation and the degree to which streambed and banks support the debris accumulation. A few large debris elements may transfer large portions of the load to a few points on the structure or to points on the streambed or banks. The recommendation for Example 3 is that the resultant force be applied at the vertical location, computed in Table 11, as a point load. Less conservative distribution of the load to the structure may be warranted where there is more information available on the debris configuration and structural susceptibility.

#### **Additional Considerations**

In Examples 1 and 2, only piers that were not shielded from debris were considered to have a debris load. Streams typically shift over the design life of a structure. Piers located on the floodplain, especially those near the channel, may become exposed to main-channel flow and to debris-transport conditions over time. At many sites, the shift can be rapid, while at other sites, migration of the channel may take decades. The susceptibility of floodplain piers to debris accumulation and forces should be considered where channel shift is possible.

As the channel shifts, it is likely that piers that were once susceptible to debris accumulation may no longer be susceptible. Therefore, in some situations, the loads developed on piers that are in the main channel could be applied to floodplain piers that may become susceptible over time because of channel shift.

In each of the three examples, the elevations for application of the drag, hydrostatic, and resultant forces were provided; however, the direction was not given. Under laboratory conditions and at observed debris accumulations during floods, debris accumulations on piers appear to align themselves with the flow direction. Because of the uncertainty associated with debris accumulation geometry and flood-flow direction, the resultant force should be applied using both consideration of the anticipated range of possible flow directions and the structure's susceptibility to the resultant forces over the range of flow directions that are possible over the life of the structure. For example, if the possible direction of flow is 20 deg to the axis of the pier and the pier is most susceptible to a force applied at 15 deg, then the force should be applied at 15 deg to the axis of the pier. For superstructures and debris accumulations that span adjacent piers, the

forces should be applied in at least two directions: (1) perpendicular to the face of the bridge and (2) in the direction of flow. Again, structure susceptibility and the possible variation of flow direction should be considered in selecting the appropriate design angle to use for applying the resultant forces.

In deep-flow conditions (that is, flow depths greater than 6 m) and under low-velocity conditions (that is, 1 to 2 m/s), debris accumulations may not extend to the streambed. Unfortunately, general information on the depth of debris accumulations is not available. Data specific to physiographic and ecological regions of each state are needed to develop more realistic debris accumulation depths and widths that are applicable to those regions. Engineering judgment that is based on the collection and analysis of debris geometric characteristics should be used to limit both the width and depth of debris accumulations.

Where deep scour is anticipated, increased estimates of the depth of debris that accumulate to the depth of scour may be necessary. For deep-flow conditions as described in the preceding paragraph, the extension of the debris into the scour hole may lead to unrealistically large debris accumulations.

---

## CHAPTER 4

# CONCLUSIONS AND RECOMMENDED RESEARCH

### CONCLUSIONS

Conclusions were drawn from the information obtained from the development of the State-of-Knowledge Account, from the analysis of experimental data and of the subsequent development of the debris-loading prediction methodology, and from the application of the draft specification to examples.

Information that was obtained during development of the State-of-Knowledge Account, especially that obtained from the review of reports of damaged bridges, provided the basis for the following conclusions:

- The effect of debris accumulations on the entire flow pattern, including flow depth and velocity, is important in the determination of debris forces. A common factor at sites where bridge damage occurs is severe flow contraction that is caused by debris accumulations on piers.
- Fine debris, such as leaves, tree branches, grasses, and other plant material tend to block a core region of woody-debris support matrix. The principal investigator's experience with examining debris accumulations in the mid-western and eastern United States is that this type of blockage of the woody-debris matrix is typical.
- Although debris accumulations are often considered to be floating rafts, they have been found to develop through the entire flow depth to the streambed on piers.
- Under conditions where trees are longer than the height of the superstructure above the streambed, debris accumulations can span the gap between the superstructure and streambed.
- If trees longer than bridge spans are transported to a bridge, then severe blockages in the bridge opening are possible.
- The methodology provided by Diehl (10) should be considered for use in the development of debris accumulation geometry.

Conclusions drawn from analysis of the experimental data and of the subsequent development of the debris-loading prediction methodology are as follows:

- The technique proposed by Koch et al. (22), in which the total streamwise force is partitioned into drag and hydrostatic components, provides a reliable basis for a debris-

loading prediction methodology that is consistent over a wide range of flow-blockage ratios.

- The contracted-flow velocity provides a consistent reference velocity for the prediction of drag forces. The drag coefficients that were developed in this study are based on the use of a contracted-flow velocity.
- The drag coefficients for debris forces on piers and superstructures depend heavily on the degree to which the debris and bridge block the channel flow for moderate and severe blockages (that is, for when  $B$  is greater than 0.30).
- For debris accumulations on both piers and superstructures, as flow-blockage ratio increases, the hydrostatic component of total force also increases while the drag component decreases. This trend is reflected in the decrease in value of drag coefficient that accompanies the increase in blockage ratio,  $B$ .
- For blockage ratios less than 0.30, drag coefficients for debris forces on piers and superstructures depend on Froude numbers ( $Fr$ ) in the range of 0.4–0.8. Drag coefficients decrease by 50 percent with the increase in Froude number within this range.

The following conclusions are drawn from the application of the draft specification to examples:

- Envelope curves that provide conservative estimates of drag force were developed for pier and superstructure drag coefficients. These envelope curves provide practical and reliable bases for a debris-loading specification.
- The debris-force prediction methodology that was developed requires water surface elevations and flow velocities that can be obtained directly from commonly used, one-dimensional flow models. The one-dimensional water surface elevation program HEC-RAS, version 2.2 (23), provides the water surface and flow-velocity parameters necessary to implement the force-prediction methodology.
- The drag coefficients that were developed in this study are inappropriate for use with the momentum approach for bridge analysis that is provided in HEC-RAS, version 2.2 (23), for flow contractions greater than about 20 percent. The location of hydrostatic force computations and the reference velocity that are implemented in the HEC-RAS model are different. One-dimensional

energy approaches should be used to evaluate flow parameters for debris-force prediction.

- Under complex flow conditions, two- or three-dimensional hydrodynamic models may be necessary to provide accurate flow parameters for effective implementation of the proposed force-prediction methodology.

## RECOMMENDATIONS

The objective of NCHRP Project 12-39 was to develop a rational debris-loading methodology on which a reliable and practical debris-loading specification could be based. A draft specification and commentary were developed for maximum debris loading on piers and superstructures in accordance with the objectives for the project. As a consequence, the debris forces that were estimated in the proposed specification will be conservative and may better represent an extreme event. Consideration should be given to future modification of the specification. It is recommended that the development of two separate specifications be considered: (1) one for the maximum debris-load configuration, which is similar to an extreme event such as ice loading and earthquakes, and (2) one for a less conservative debris load that is used in combination with other limit state conditions. The extreme-event specification should also consider scour. The reduction in force for the limit state conditions could be achieved by using a reduced debris-accumulation size. The reduction in debris-accumulation size should be based on physically meaningful parameters and field data.

The debris forces are highly sensitive to the area of the debris accumulation. An increase in debris-accumulation profile area not only affects the area over which the water pressure forces are applied, but also affects the pressures themselves by increasing stream-flow velocity and creating hydrostatic forces through a damming effect. Use of conservative estimates of debris extents directly leads to very conservative force prediction. Although the FHWA-sponsored study conducted by Diehl (10) has provided a rational basis for determining the width of debris accumulations, more state-specific information is needed to make the prediction methodology applicable to the geomorphological, hydrological, and ecological conditions of each state. State DOTs should consider the collection of information on debris accumulation geometry part of routine maintenance that is conducted to remove accumulations. A set of simple and approximate measurements of debris configurations and stream characteristics could be collected and assembled into a database, that, after a few years, could provide the basis for developing state-specific information on debris accumulation geometry. These data will provide the information necessary to reduce the maximum debris geometry conditions that are given in this draft specification. The data would also provide a basis for engineers to improve their judgment regarding application of the debris-loading specification.

The work of Diehl (10) has contributed substantially to the amount of information available on the characterization of debris accumulation shape and size from field observations. This work should be extended to obtain data at bridges where debris accumulate on superstructures, although obtaining such information is difficult and expensive. Little is known about the vertical dimensions of debris accumulations during flood events. The work of Diehl (10) should be extended to include measurement of the submerged extent of debris accumulations during flood events using side-scan sonar or other means. An alternative to using side-scan sonar may be measuring flow velocities downstream of the bridge with a velocity profiler to infer the blockage dimensions through examination of flow patterns in the wake.

The research in this study was limited to model-debris accumulations on piers and on superstructures aligned with flow. Future research that should be considered to improve force prediction includes additional experimental testing on debris on piers and superstructures skewed to the flow direction. In addition, superelevation of superstructures should be considered.

Little information is available for determining vertical forces such as buoyancy and lift. Additional research should be conducted to develop a method for evaluating these forces where debris accumulations are possible.

Debris accumulations were formed with model-debris elements in part of the experimental testing of this research project. This method of modeling debris was believed to provide debris accumulations that more closely represented the shape and roughness characteristics of prototype accumulations. Future experiments should be conducted to develop criteria for creating and scaling debris models. Additionally, model-debris experiments should be used to determine how debris accumulate on bridge components and how the shape of the accumulations relates to flow conditions. It is likely that the shape of accumulations depends heavily on flow conditions, as well as on the geometric conditions of the bridge and stream channel. Under high Froude number conditions and deep-water conditions, the recommended debris size is probably excessive.

Observations of debris transport during flood events are needed to determine the locations in stream channels that are most susceptible to high loads of debris transport. Secondary currents are known to play a large role in concentrating debris along certain areas of the channel. Site factors that may indicate when and where a lane of highly concentrated debris transport is likely to occur could provide engineers with information to avoid debris problems.

After the basic mechanics of debris transport and accumulation are better understood, then practical, reliable, statistically based models of debris accumulation geometry can be developed. A combination of field-based observations and laboratory modeling can provide the information necessary to develop such a statistical model for accumulation geometry.

Investigations on the development and application of two- and three-dimensional computational hydrodynamic models should be considered for determining flow parameters, as well as for computing hydrodynamic forces. Computational fluid-dynamics programs can compute pressure forces on submerged obstacles and predict secondary currents in channels. Two-dimensional hydrodynamic models are commonly used at bridge crossings. The application of these models should be investigated to determine the locations of stream channels where high-debris transport is likely, to evaluate the characteristics of flow around debris accumulations, and to predict the pressure distribution on large debris accumulations.

Scour is likely at sites where large debris accumulations endanger the bridge stability through lateral forces. The loss of lateral support resulting from scour of foundation soils

increases the susceptibility of the structure to debris forces. The additional exposed area of the piers may also contribute to additional hydrodynamic loads. Research is needed to determine the influence of scour on hydrodynamic loads.

As discussed in Chapter 3, the transfer of hydrodynamic loads from the debris to bridge components depends on the deformation of the debris accumulation and, therefore, also on the material properties of the debris accumulation. Research should be conducted to determine methods for distributing debris loads to bridge components.

The transport of large debris mats in rivers and their collision with bridge piers and superstructures has not been evaluated. Research to characterize the potential size of debris accumulations and the impact force that can be generated by the collision of these accumulations with bridge elements should be considered.

---

## REFERENCES

1. National Transportation Safety Board, *Highway Accident Report—Collapse of the Harrison Road Bridge Spans, Miamitown, Ohio, May 26, 1989*, Washington, D.C., 1990, 45 p.
  2. American Association of State Highway and Transportation Officials, *Standard Specifications for Highway Bridges*, thirteenth edition, Washington, D.C., 1983.
  3. American Association of State Highway and Transportation Officials, *AASHTO LRFD Bridge Design Specifications—Customary U.S. Units*, first edition, Washington, D.C., 1994.
  4. American Association of State Highway and Transportation Officials, *AASHTO LRFD Bridge Design Specifications—SI*, second edition, Washington, D.C., 1998.
  5. Parola, A. C., D. J. Hagerty, and S. Kamojjala, *NCHRP Report 417, "Highway Infrastructure Damage Caused by the 1993 Upper Mississippi River Basin Flooding"*, Transportation Research Board, National Research Council, Washington, D.C., 1998, pp. 1–195.
  6. Chang, F. F. M. and H. W. Shen, "Debris Problems in the River Environment," *Federal Highway Administration Report No. FHWA-RD-79-62*, 1979, 67 p.
  7. Parola A. C., S. Kamojjala, J. Richardson, and M. Kirby, "Numerical Simulation of Flow Patterns at a Bridge with Debris," *Conference Proceedings, ASCE Water Resources Engineering*, Memphis, T.N., 1998.
  8. Mueller, D. S. and A. C. Parola, "Detailed Scour Measurements Around a Debris Accumulation," *Conference Proceedings, ASCE Water Resources Engineering*, Memphis, T.N., 1998, p. 234.
  9. American Association of State Highway and Transportation Officials, *Standard Specifications for Highway Bridges*, fifteenth edition, Washington, D.C., 1992.
  10. Diehl, T. H., "Potential Drift Accumulation at Bridges," *Federal Highway Administration Report No. FHWA-RD-97-28*, 1997.
  11. O'Donnell, C. L., "Observation on the Causes of Bridge Damage in Pennsylvania and New York Due to Hurricane Agnes," *Highway Research Record No. 479*, Highway Research Board, National Research Council, Washington, D.C., 1973, pp. 20–36.
  12. Jempson, M. A. and C. J. Apelt, "Hydrodynamic Forces on Partially and Fully Submerged Bridge Superstructures," *Conference Proceedings, 16th ARRB Conference*, part 3, Perth, Western Australia, 1992, pp. 67–79.
  13. Montgomery, C. T., R. Gerard, W. J. Huiskamp, and R. W. Kornglsen, "Application of Ice Engineering to Bridge Design Standards," *Conference Proceedings, Cold Regions Engineering Specialty Conference*, Canadian Society for Civil Engineering, Montreal, Quebec, Canada, 1984, pp. 795–810.
  14. White, F. M., *Fluid Mechanics*, third edition, McGraw-Hill, New York, 1994.
  15. Apelt, C. J., "Flow Loads on Bridge Piers," *The Journal of the Institution of Engineers, Australia*, July–Aug. 1965, pp. 185–191.
  16. Apelt, C. J., "Flood Loads on Submerged Bridges," *Queensland Division Technical Papers*, Institution of Engineers Australia (Queensland Division), v. 27, no. 19, Publication No. QBG 1756, 1986a, p. 17–23.
  17. Apelt, C. J., "Flood Forces on Bridges," *Conference Proceedings, 13th AARB—5th REAAA Combined Conference*, Adelaide, Australia, 25–29 August 1986b, v. 13, part 6, Bridges, 1986b, p. 40–46.
  18. Apelt, C. J. and L. R. Issac, "Bridge Piers—Hydrodynamic Force Coefficients," *ASCE Journal of Hydraulics Division*, 1968, pp. 17–30.
  19. Denson, K. H., *Steady-State Drag, Lift and Rolling Moment Coefficients for Inundated Inland Bridges*, Mississippi Water Resources Research Institute, Mississippi State University, 1982, pp. 1–22.
  20. Naudascher, E. and H. J. Medlarz, "Hydrodynamic Loading and Backwater Effect of Partially Submerged Bridges," *Journal of Hydraulic Research*, vol. 21, no. 3, 1983, pp. 213–232.
  21. Wellwood, N. and J. Fenwick, "A Flood Loading Methodology for Bridges," *Conference Proceedings, 15th ARRB Conference*, part 3, 1989, pp. 315–341.
  22. Koch, A., M. Carstenjen, and L. Hainz, *Von Der Bewegung Des Wassers Und Den Dabei Auftretenden Kraften* ("Of the Movement of Water and the Power It Produces"), Springer (publisher), Berlin, Germany, 1926.
  23. Brunner, G. W., *HEC-RAS River Analysis System Hydraulic Reference Manual*, version 2.2, U.S. Army Corps of Engineers Hydrologic Engineering Center, Davis, C.A., 1998.
-

## **APPENDIX A**

### **SUPPORTING INFORMATION**

This appendix consists of five parts:

Part 1: State-of-Knowledge Account

Part 2: Laboratory Studies

Part 3: Analysis of Drag and Hydrostatic Force

Part 4: Draft Specification for and Commentary on Debris Accumulation Forces

Part 5: Bibliography

## PART 1: STATE-OF-KNOWLEDGE ACCOUNT

This state-of-knowledge account has five major sections. The first major section provides information on mean hydrodynamic forces, specifically drag, on submerged objects, including both background information and information on the factors that affect drag. Throughout this section, the importance of these factors to determining forces on bridges is discussed. The second major section discusses mean hydrodynamic forces on bridges and, specifically, their piers and superstructures. This section incorporates detailed discussion of drag equations. The third major section presents information on predicting and researching horizontal forces created by debris accumulations. The fourth major section provides information on the geometry of debris accumulations. The fifth major section summarizes the findings of investigations of bridge failures presumably caused by debris forces.

### MEAN HYDRODYNAMIC FORCES, SPECIFICALLY DRAG, ON SUBMERGED OBJECTS

Simplified force-determination methodologies for predicting total fluid forces on spheres, cylinders, and other common prismatic shapes in free-stream conditions are well established experimentally (White 1994; Munson, Young, and Okiishi 1990; Hoerner 1965). However, flow around debris and around bridge components in streams is complex, involving a free-surface boundary, nonuniform-flow velocities, and high levels of turbulence. In addition, channel boundaries and embankments confine flow such that severe contractions may be caused by bridge components and debris. The following subsections provide information on the factors that affect drag.

#### Hydrodynamic Forces, Specifically Drag: Background Information

When fluid moves around a body, an interaction between the body and the fluid occurs that can be described in terms of forces on the fluid-body interface (Munson, Young, and Okiishi 1990). The force on the body consists of tangential forces, derived from shear stresses, and normal forces, derived from normal stress. For nonstreamlined solid bodies, flow separation causes a downstream wake to form. The separation and wake prevent the complete recovery of pressure on the downstream sides of the obstacle. A net hydrodynamic force is created from the pressure variation between the upstream and downstream sides of the obstacle. As a consequence of the flow separation and wake formation, more than 97 percent of the hydrodynamic force on the object can be associated with

pressure variation for blunt obstacles (White 1994). Bridge superstructures, piers, and debris accumulations are blunt obstacles; therefore, a significant portion of drag is caused by pressure variation rather than tangential shear stresses.

The resultant forces on a submerged object can be separated into three components of force: drag, side, and lift. The drag force is considered the force in the streamwise direction. The lift force and side force run perpendicular to the streamwise direction. The resultant moment can also be separated into three moments, the directions of which align with the three forces.

This review focuses on the force in the streamwise direction and on factors that affect this force. Analytical modeling approaches for predicting drag force are limited because of the complexity of turbulent flow around three-dimensional, nonstreamlined bodies. Practical drag-force prediction methods have been based on empirical research, using a framework from dimensional analysis and small-scale laboratory data. The general form of the drag equation developed from dimensional analysis is

$$F_D = C_D \rho A_r \frac{(V_r)^2}{2} \quad (A1)$$

where

- $F_D$  = drag force, N.;
- $C_D$  = coefficient of drag;
- $\rho$  = fluid density, Kg/m<sup>3</sup>;
- $A_r$  = reference area, m<sup>2</sup>; and
- $V_r$  = reference velocity, m/s.

Drag coefficients ( $C_D$ ) for objects that are submerged in flow fields and that are not severely contracted by the object range from approximately 2.0, for a square plate oriented perpendicular to the flow, to 0.01, for air foils. The profile area of the obstacle perpendicular to the flow direction and the unobstructed-flow velocity typically serve as the reference area and reference velocity, respectively, in Equation A1. Drag coefficient depends on several factors, as described in the following.

#### Factors Affecting Drag

##### *Free-Stream Conditions (for Zero-Pressure Gradient)*

Free-stream conditions exist where pressure gradients in the streamwise direction away from an obstacle are negli-

ble and where the nonuniformity of the velocity distribution near the boundary is small (Schlichting 1979). Free-stream conditions for bridge piers or for submerged superstructures could be considered conditions in which (1) the total area that is blocked by piers, debris, and superstructure is sufficiently small to cause negligible increases in the contracted-flow velocity through the bridge opening; and (2) the difference in water surface elevation from the upstream side of the bridge to the downstream side is small when compared with the contracted-velocity head. An example of a free-stream condition is a small pier in a wide river or with a submerged superstructure in a very deep channel. Equations representing the forces on obstacles for free-stream conditions have been developed experimentally in the form of Equation A1. The coefficient of drag is a function of several geometric and flow parameters, including Reynolds number, angle of flow attack, and shape of the obstacle (White 1994). The Reynolds number ( $R_e$ ) is defined as

$$R_e = \frac{V_r D}{\nu} \quad (\text{A2})$$

where

- $R_e$  = Reynolds number;
- $V_r$  = reference velocity, m/s;
- $D$  = reference length of the object, m; and
- $\nu$  = kinematic viscosity,  $\text{m}^2/\text{s}$ .

For free-stream conditions, the reference velocity traditionally has been chosen as the uniform, undisturbed velocity (White 1994). When the flow around the object distorts the water surface, drag coefficients can vary with Froude number, which is defined as

$$Fr = \frac{V_r}{\sqrt{g Y_r}} \quad (\text{A3})$$

where

- $Fr$  = Froude number;
- $V_r$  = reference velocity (usually the average velocity at the average approach-flow depth), m/s;
- $g$  = gravitational acceleration constant ( $9.81 \text{ m/s}^2$ ); and
- $Y_r$  = reference depth (usually the average flow depth), m.

### *Turbulence Intensity*

Turbulence present in the approach flow alters the separation and reattachment of flow on the obstacle. Changes in drag coefficient, both decreases and increases, have been found for various Reynolds numbers and for various obstacle-edge conditions (Cheung and Melbourne 1983, Courchesne and Laneville 1982). The effects of turbulence intensity diminish with increased angle-of-flow incidence (Vickery 1966, Bear-

man 1978). For platelike, rectangular obstructions (that is, obstructions whose downstream widths are very short compared with their cross-stream widths), turbulence intensity can cause as much as an 80-percent increase in coefficient of drag (Courchesne and Laneville 1982).

### *Boundary Confinement (or Pressure Gradients)*

Boundaries may confine flow around bridge components, creating conditions substantially different from the idealized free-stream conditions. Pressure gradients that force flow to accelerate through contractions develop through the entire flow contraction. These pressure gradients result in water surface elevation variations through bridge contractions. The pressure gradients increase the separation velocities that lead to lower base pressures on the downstream side of the obstacle, causing increased drag. Richter and Naudascher (1976) found that the drop in mean-drag coefficient near the critical Reynolds number range becomes more pronounced with larger confinement. Drag coefficient increases when confinement below approximately Reynolds  $10^5$  increases, and it then decreases in the subcritical range. El-Sherbiny (1980) showed that for a conical obstruction confined in a pipe, the drag coefficient (using the approach velocity as reference velocity) increased without bound as the width of the obstruction approached the width of the flow conduit.

### *Velocity Nonuniformity*

Nonuniformity of flow velocity, both in the vertical direction from the streambed to the water surface and in the cross-stream direction, is typical in streams. Research that shows some of the effects of nonuniform-velocity distributions on drag coefficients was completed by Ranga Raju, Loeser, and Plate (1976) and by Sakamoto, Moriya, and Arie (1975, 1977). The research by Ranga Raju et al. (1976) examined the effect of typical nonuniform-velocity distributions, throughout smooth and rough boundary layers, on drag coefficients; thereby, they showed the effects of boundary layer thickness, zone of nonuniform velocity ( $\delta$ ), and size of obstruction ( $h$ ) for both smooth and rough boundaries. The drag coefficient ( $C_D$ ) decreases rapidly with increases in the relative boundary-layer thickness ( $\delta/h$ ). The reference velocity that was used for the drag coefficient was the free-stream flow velocity outside the boundary layer. The nonuniform flow effects also included the effect of the boundary.

### *Froude Number*

As shown by Rouse (1965), drag coefficient increases when Froude number increases and peaks when  $Fr = 0.7$ . Froude number was defined as

$$Fr = \frac{V_r}{\sqrt{gy}} \quad (\text{A4})$$

where

$Fr$  = Froude number;  
 $V_r$  = reference velocity, m/s;  
 $g$  = gravitational acceleration constant (9.81 m/s<sup>2</sup>); and  
 $y$  = water depth, m.

Further increase in  $Fr$  causes decrease in drag for a pier in a wide-open channel. The change in piezometric head between the front and rear face of the pier is produced by the standing gravity wave when the Froude number is about 1. For a row of circular cylinders in a wide channel, the flow becomes choked for an intermediate range of Froude numbers when the Froude number increases. The mean drag coefficient is a function of the Froude number and the blockage ratio (Hsieh 1964).

#### *Relation Between Fluid Flow and Forces: The One-Dimensional Momentum Equation*

The one-dimensional, flow-momentum equation, which does not consider bed or bank friction, is typically used to represent the relation between fluid forces and forces on submerged flow obstructions. Given a control volume of fluid that was contained between two cross sections, the following external forces act on the control volume: pressure forces, weight, and hydrodynamic forces. From the momentum equation, the vector sum of these forces is equal to the change of momentum. As shown by Naudascher (1991), the resulting steady, one-dimensional equation is

$$P_1 - P_2 + W_2 - F_b = \rho Q \beta_2 V_2 - \rho Q \beta_1 V_1 \quad (\text{A5})$$

where

$P_1$  = pressure-force vector on the upstream cross section, N;  
 $P_2$  = pressure-force vector on the downstream cross section, N;  
 $W_2$  = weight-force vector in the downstream direction, N;  
 $F_b$  = external opposing-force vector, acting on the control volume, caused by the reaction from the force of the moving fluid, N;  
 $\rho$  = fluid density, Kg/m<sup>3</sup>;  
 $Q$  = flow rate, m<sup>3</sup>/s;  
 $\beta_2$  = Boussinesq velocity coefficient for the downstream cross section;  
 $V_2$  = average velocity in the downstream cross section, m/s;  
 $\beta_1$  = Boussinesq velocity coefficient for the upstream cross section; and  
 $V_1$  = average velocity in the upstream cross section, m/s.

The Boussinesq velocity coefficient is defined as

$$\beta = \frac{1}{A} \int \left( \frac{v}{V} \right)^2 dA \quad (\text{A6})$$

where

$\beta$  = Boussinesq velocity coefficient;  
 $A$  = flow area, m<sup>2</sup>;  
 $v$  = velocity over the differential flow area, m/s;  
 $V$  = average flow velocity, m/s; and  
 $dA$  = differential flow area, m<sup>2</sup>.

Considering flow through bridge openings, Koch et al. (1926) proposed partitioning drag into two forces: one force associated with the variation in hydrostatic pressure through the bridge opening and another force caused by dynamic force, associated with the flow velocity. They described the total force with respect to the one-dimensional momentum equation for free-surface, shallow-water flow. Eichert and Peters (1970) presented what was essentially the same equation

$$(\gamma y_{c1} A_1 - \gamma y_{c3} A_3) + (\gamma y_{p3} A_{p3} - \gamma y_{p1} A_{p1}) - \left( \rho C_D A_{p1} \frac{V^2}{2} \right) = \rho Q (V_3 - V_1) \quad (\text{A7})$$

where

$\gamma$  = specific weight of the fluid, N/m<sup>3</sup>;  
 $y_{c1}$  = depth measured from the water surface to the centroid of the cross-sectional areas at Section 1, m;  
 $A_1$  = flow area at the upstream section from the bridge, m<sup>2</sup>;  
 $y_{c3}$  = depth measured from the water surface to the centroid of the cross-sectional areas at Section 3, m;  
 $A_3$  = flow area at the downstream section from the bridge, m<sup>2</sup>;  
 $y_{p3}$  = depth measured from the water surface to the centroid of the cross-sectional area at Section  $A_{p3}$ , m;  
 $A_{p3}$  = area of obstruction at the downstream Section 3, m<sup>2</sup>;  
 $y_{p1}$  = depth measured from the water surface to the centroid of the cross-sectional area at Section  $A_{p1}$ , m;  
 $A_{p1}$  = area of obstruction at the upstream Section 1, m<sup>2</sup>;  
 $\rho$  = fluid density, Kg/m<sup>3</sup>;  
 $C_D$  = drag coefficient;  
 $V$  = average flow velocity, m/s;  
 $Q$  = flow rate, m<sup>3</sup>/s;  
 $V_3$  = velocity at the downstream section, m/s; and  
 $V_1$  = velocity at the upstream section, m/s.

The equation assumes that the streambed is horizontal and that the forces caused by the streambed and bank friction are negligible.

The first term on the left side of Equation A7 ( $\gamma y_{c1} A_1 - \gamma y_{c3} A_3$ ) represents the pressure force on the upstream and

downstream sides of the control volume of the bridge opening. The second term ( $\gamma y_{p3} A_{p3} - \gamma y_{p1} A_{p1}$ ) represents the hydrostatic force on the piers. The third term  $\left( \rho C_D A_{p1} \frac{V^2}{2} \right)$  represents the dynamic force on the piers. The right side of the equation represents the change in momentum between the upstream and downstream cross sections of the bridge. The second and the third terms partition the total force on the pier as hydrostatic and dynamic components.

Under conditions of high bed slope and high bed and bank forces, the downstream component of weight and boundary drag terms must be included in the momentum equation. The formulation in HEC-RAS, version 2.2 (Brunner 1998), includes boundary drag terms (for example, friction slope) and weight terms. Rearranging Equation A7 and including the slope and weight terms, the momentum equation is written as

$$(\delta y_{c1} A_1 - \delta y_{c3} A_3) - \rho Q(V_3 - V_1) + \left[ \left( \frac{A_1 + A_3}{2} \right) \delta LS_o \right] - \left[ \left( \frac{A_1 + A_3}{2} \right) \delta LS_f \right] = \left( \rho C_D A_{p1} \frac{V^2}{2} \right) - (\delta y_{p3} A_{p3} - \delta y_{p1} A_{p1}) \quad (A8)$$

where

- $\delta = \rho g =$  unit weight of water, N/m<sup>3</sup>;
- $y_{c1} =$  depth measured from the water surface to the centroid of the cross-sectional areas at Section 1, m;
- $A_1 =$  flow area at the upstream section from the bridge, m<sup>2</sup>;
- $y_{c3} =$  depth measured from the water surface to the centroid of the cross-sectional areas at Section 3, m;
- $A_3 =$  flow area at the downstream section from the bridge, m<sup>2</sup>;
- $\rho =$  fluid density, Kg/m<sup>3</sup>;
- $Q =$  flow rate, m<sup>3</sup>/s;
- $V_3 =$  velocity at the downstream section, m/s;
- $V_1 =$  velocity at the upstream section, m/s;
- $L =$  distance between Section 1 and Section 3, m;
- $S_o =$  slope of the channel based on the mean bed elevation;
- $S_f =$  slope of the energy grade line (that is, friction slope);
- $C_D =$  drag coefficient;
- $A_{p1} =$  area of obstruction at the upstream Section 1, m<sup>2</sup>;
- $V =$  average flow velocity, m/s;
- $y_{p3} =$  depth measured from the water surface to the centroid of the cross-sectional area at Section  $A_{p3}$ , m;
- $A_{p3} =$  area of obstruction at the downstream Section 3, m<sup>2</sup>;
- $y_{p1} =$  depth measured from the water surface to the centroid of the cross-sectional area at Section  $A_{p1}$ , m;
- and
- $g =$  gravitational acceleration constant (9.81 m/s<sup>2</sup>).

As in the approach by Eichert and Peters (1970), the total force by the pier, in this equation, includes a dynamic component and a hydrostatic component.

Although the hydrostatic and drag forces are incorporated into the one-dimensional model HEC-RAS momentum-solution procedure to compute flow through bridges, the application of the pier forces is different from that presented in Equation A8. The force contribution of piers is applied in two of three control volumes that are used to compute water surface profiles through bridge openings. The drag and upstream hydrostatic forces of the pier are applied to a control volume immediately upstream of the bridge. The downstream hydrostatic force is placed on the control volume immediately downstream of the bridge. The velocity of the most upstream section of the three control volumes is used to compute the drag force.

## MEAN HYDRODYNAMIC FORCES ON BRIDGES AND, SPECIFICALLY, THEIR PIERS AND SUPERSTRUCTURES

### Mean Hydrodynamic Forces on Bridges

The total force on a bridge system is the sum of all the pressure forces acting on the system. The total pressure force can be separated conceptually into drag and other hydrostatic forces in the streamwise direction, lift and other buoyant forces in the vertical direction, and side forces in the cross-stream direction. These forces can create moments about the bridge (Denson 1982). To determine the hydrodynamic forces on bridge components, research has been conducted previously by Apelt (1965, 1986a, 1986b), Apelt and Issac (1968), Denson (1982), Jempson and Apelt (1992), Naudascher and Medlarz (1983), and Wellwood and Fenwick (1989). These researchers focused on the drag forces on the bridge structure for full and partial submergence. The drag coefficients, as described by Equation A1, vary widely, from about 0.6 to 3.5, depending on many factors; however, a major source of variation that prevents direct comparison of coefficients is inconsistency in the use of reference velocities and of reference areas.

Some investigators (Hsieh 1964, Mirajgaoker 1964) have differentiated between a resistance coefficient and a drag coefficient. The drag coefficient, for instance, has been defined for two-dimensional flow in an infinite, uniform fluid, whereas the resistance coefficient has embodied the effect of the surface wave that forms in open-channel flow. In this document, no distinction will be made between drag coefficient and coefficient of resistance.

### Mean Hydrodynamic Forces on Piers

Although many studies have been conducted on fluid forces on two-dimensional cylinders in practically unbounded

fluids of uniform-velocity distributions, relatively few studies have been conducted on the force created on objects that are placed in open-channel flow, where velocity gradients, relatively high turbulence, and waves on the free-water surface complicate the flow considerably.

Masch and Moore (1960) showed that the effects of three-dimensional flow from vertical variation in velocity cause variation as great as 40 percent in local drag coefficients for cylindrical objects. Hsieh (1964), using cylindrical model piers, found that the Froude number of the flow, as well as boundary geometry, influences the drag coefficient for cylindrical piers. He also found that the drag coefficient decreased with increase in depth for subcritical flow conditions. Pier spacing (the proximity effect) was shown to have a pronounced influence on drag-force coefficient under subcritical flow conditions. Hsieh (1964) showed that drag coefficient varies from 0.9 to 1.5, with variation in relative spacing  $S/D$ , from 30 to 5, where  $S$  represents the distance between pier centers, and  $D$ , the cylinder diameter. Also, he found that drag coefficient decreased with increase in Froude number for supercritical flow conditions. In addition, he found that the effects of flow depth and pier spacing on drag coefficient diminished with increase in Froude number above the critical Froude number. Mirajgaoaker's (1964) data on rectangular piers, rounded piers, and piers with upstream points showed a considerable decrease in drag coefficient with increase in Froude number above a critical Froude number. Mirajgaoaker also showed a considerable difference in drag coefficient for the three different pier shapes considered at the same flow conditions.

Apelt (1965) found that hydrodynamic loads perpendicular to the flow direction, termed "pier lift" ("side forces" in this review), can be substantial for even small-skew angles between pier axis and the approaching flow. In Apelt's study, lift for piers was defined as the cross-stream force perpendicular to the flow direction. Apelt and Issac (1968) conducted small-scale experiments to determine drag and lift coefficients for the piers.

### Mean Hydrodynamic Forces on Superstructures

Denson (1982) showed that three regimes of flow exist for inundated bridges with subcritical approach flows. The regimes appear to be characterized by the nature of the free-surface flow over the upstream and downstream bridge railings. Regime 1, low-inundation depth, corresponds to a shallow depth of flow over the upstream railing, similar to flow over a narrow weir. The water cascades over the upstream railing and plunges into subcritical flow on the bridge deck. Water flows around the downstream railings. Regime 2, moderate-inundation depth, corresponds to flow over the upstream railing that becomes supercritical and remains so over the deck and downstream railing. A hydraulic jump forms downstream of the superstructure. Regime 3, high-

inundation depths, corresponds to a deep flow over the railings and the deck such that subcritical flow conditions prevail over the entire width of the deck. From the illustrations provided in Denson (1982), a low-inundation depth regime exists when critical depth occurs and the upstream flow overtops the upstream railing.

Denson (1982) conducted small-scale flume investigations to determine the drag, lift, and rolling moments on representative two-lane bridge superstructures. Denson modeled three bridge superstructures: (1) 32.75-ft-wide deck with five AASHTO Type III prestressed concrete girders (45 in. deep) spaced on 4.94-ft centers, (2) 38.5-ft-wide deck with five W27 Beams (27 in. deep) spaced on 7.27-ft centers, and (3) 34.5-ft-wide deck with four steel girders (64 in. deep) spaced on 8.74-ft centers. Denson obtained drag coefficients that had maximum values of 5.0 (plate girder), but were generally in the area of 2.0 (AASHTO girder and W-beam). Denson reported maximum-lift coefficient values approximately equal to 6.0 and considered these values to be the most significant quantities measured in his study. Denson reported that total drag alone was not a significant quantity, except when accompanied by loss of positive reaction from hydrodynamic lift and buoyancy.

Naudascher and Medlarz (1983) investigated the force coefficient for partially submerged bridge superstructures to determine a relationship among the average-force coefficients, the number of beams, the beam geometry, and the flow conditions. Naudascher and Medlarz defined drag coefficient as follows:

$$C_f = \frac{1}{n} \frac{F(x)}{\rho \frac{h}{2} (V_m)^2} = C_f \left( \frac{V_m}{\sqrt{gy}}, \frac{h}{y}, \frac{y}{d}, \frac{e}{d}, \alpha, n \right) \quad (A9)$$

where

$C_f$  = mean drag coefficient per unit length on one of  $n$  beams;

$F(x)$  = water pressure force acting in the flow direction on the submerged bridge at point  $x$ , N;

$h$  = local depth of flow, m;

$\rho$  = fluid density, Kg/m<sup>3</sup>;

$V_m$  = average depth velocity, m/s;

$g$  = gravitational acceleration constant (9.81 m/s<sup>2</sup>);

$y$  = depth of bridge submergence, m;

$d$  = normal distance of the horizontal plate girders, m;

$e$  = width of horizontal plate girders, m;

$\alpha$  = angle between flow direction and bridge axis, deg; and

$n$  = number of girders.

$V_m/\sqrt{gy}$  is the local Froude number.

Jempson and Apelt (1992) reported on investigations conducted at the University of Queensland hydraulic laboratory

facilities on drag and lift coefficients for partially and fully submerged bridge superstructures. These investigations included small-scale model flume experiments and wind tunnel experiments. Jempson and Apelt (1992) reported the influence of relative submergence defined as

$$S_r = \frac{h}{H} \quad (\text{A10})$$

where

- $S_r$  = relative submergence, m;
- $h$  = upstream depth of flow above the bottom chord of the superstructure, m; and
- $H$  = height of the submerged portion of the superstructure, m.

Jempson and Apelt obtained peak values of  $C_D$  when  $S_r = 1.5$ .

Jempson and Apelt (1992) conducted small-scale model investigations of pressure distributions on two superstructures: a girder superstructure and an adjacent box beam. Integration of 32 temporally averaged pressure measurements along the surface of the two bridge superstructures was used to determine lift and drag coefficients. Jempson and Apelt found a substantial decrease in the drag and lift coefficients with increases in Reynolds number ( $R_e$ ).

Apelt (1986b) conducted experiments on a model section of a two-lane bridge. The model section consisted of a pier mounted symmetrically to a section of superstructure. Apelt (1986b) estimated the drag coefficient for the superstructure by itself under fully submerged conditions by assuming the drag coefficient for the pier and for the head stock was essentially the same as when the superstructure was not submerged. A value of 1.94 (the average of tests conducted without superstructure submergence) was used to approximate  $C_D$  for the head stock and pier. This technique resulted in an average  $C_D$  value of 1.99 for completely submerged girders and superstructure. Apelt found this result unsurprising, given that the value of  $C_D$  for a flat plate perpendicular to the flow is 2.

## HYDRODYNAMIC FORCES ON DEBRIS ACCUMULATIONS

Apelt (1986a) used a rectangular prism with drilled holes, narrow planks, and cylindrical logs arranged to simulate idealized debris mats for evaluating the drag forces experienced by the debris mats. He showed that, for the idealized debris, the forces depend on the internal geometry of the mat and on the percentage of the area of the openings through the mat. The preliminary research that was conducted by Apelt (1986a) on idealized debris mats has shown that the drag coefficient for idealized debris accumulations varied from 1.0 to 2.0, with corresponding variation in percentage of area openings from 10 percent to 30 percent. As shown by Apelt (1986a),

increase in the area of holes that are drilled through an idealized debris mat significantly decreases drag coefficient. In these experiments, debris mats were studied in the absence of bridge pier or superstructure models. Investigations of debris accumulation on bridge elements have not been reported.

Wellwood and Fenwick (1989) proposed a method for computing debris forces on bridges. The method considers an idealized debris accumulation geometry. The drag force is computed using the drag equation (Equation A1). Wellwood and Fenwick (1989) developed a method of predicting drag forces on superstructures for debris mats that extend below the superstructure. The net hydrodynamic load is given as

$$H_D = C_D \rho D \frac{V^2}{2} \quad (\text{A11})$$

where

- $H_D$  = net hydrodynamic load, N/m;
- $C_D$  = coefficient of drag;
- $\rho$  = fluid density, Kg/m<sup>3</sup>;
- $D$  = total depth of the debris below the water surface, m; and
- $V$  = restricted-flow velocity, m/s.

The method developed recommends using Equation A5 with either a reference velocity located at the midheight of the debris accumulation or the restricted-flow velocity. A drag coefficient of 1.04 was suggested for debris. A logarithmic velocity distribution was suggested to obtain the velocity at the midheight of the debris accumulation. The restricted-flow velocity was given as

$$V = \frac{Q}{A_r} \quad (\text{A12})$$

where

- $V$  = restricted-flow velocity, m/s;
- $Q$  = flow rate, m<sup>3</sup>/s; and
- $A_r$  = reference area, m<sup>2</sup>.

Wellwood and Fenwick's method appears to apply to debris accumulations that extend below the superstructure. The method produces a force per unit length of bridge.

## GEOMETRY OF DEBRIS ACCUMULATIONS

Although the occurrence of debris accumulations on bridges and the significance of the effects of debris on bridge elements are well established, only Wellwood and Fenwick (1989) and Diehl (1997) provide information on the geometry of debris accumulations. Diehl (1997) developed criteria for design debris blockages using evaluation of over 2,577 reported accumulations and 144 field investigations of drift accumulations.

Wellwood and Fenwick (1989) recommend that the width of the debris accumulation on a pier be equal to the average of adjacent-span lengths, up to a maximum of 20 m, with a minimum assumed vertical-accumulation depth of 1.2 m. Wellwood and Fenwick (1989) recommend that the accumulation extend the entire length of the superstructure, with a vertical extent equal to the width of the superstructure plus 1.2 m. In this State-of-Knowledge Account, the width of the superstructure refers to the difference between the top elevation of the railing system and the lowest elevation of the girder. The maximum vertical extent was limited to 3 m, unless site evidence warranted a larger extent.

Diehl (1997) developed suggested guidelines for the assessment of drift potential and recommends three phases to estimate the potential for (1) drift delivery to the bridge, (2) drift delivery to each bridge element, and (3) maximum accumulation geometry. As shown in Table A1, the method considers low, medium, and high potentials, as well as chronic conditions for debris delivery and accumulation on bridge elements. Diehl's method is based on a design log that is determined from the capacity of the watershed and stream to produce and transport debris. Although many factors are involved in the determination of the design log, Diehl simplified the determination, recommending use of the lowest value of the following:

- The width of the channel upstream from the site,
- The maximum length of sturdy logs, and
- (In much of the United States) 9 m (30 ft) plus one-quarter of the width of the channel upstream from the site.

The maximum sturdy-log length is the length of log that can withstand the hydrodynamic forces on the debris accumulation. It is not the maximum length of mature riparian and floodplain trees. The maximum sturdy-log length that is suggested ranges from 24 m (in the eastern U.S.) to 45 m (in California and in the Pacific Northwest). Diehl (1997) provided regional curves for the relation between stream width and sturdy log length.

The flow conditions at the bridge, the location of the bridge with respect to the path of debris transport, and the bridge geometric characteristics are considered in the determination of the potential maximum debris accumulation on bridge elements.

Bridge characteristics, specifically the length of gaps between substructure and superstructure elements, strongly influence the potential for drift accumulation. Diehl (1997) developed a procedure to evaluate the potential for accumulations using the conditions at piers, the conditions at superstructures, and a comparison of the horizontal and vertical gap size to the design log length. Horizontal gaps, such as those between piers, and vertical gaps, such as those extending from the superstructure to the streambed, are compared with the design log length. Gaps smaller than the design log length have a high potential for accumulation if flow through the gaps transports large amounts of debris. Table A2 shows the maximum debris-accumulation size based on the information of Diehl (1997) and that of Wellwood and Fenwick (1989).

If the distance between two piers is shorter than the design log length, then the region between the piers is considered to be a horizontal gap. If the distance between the bottom of the superstructure and the streambed or floodplain is shorter than the length of the design log, then the area between the streambed and superstructure is considered to be a vertical gap.

#### INVESTIGATIONS OF BRIDGE FAILURES PRESUMABLY CAUSED BY DEBRIS FORCES

An FHWA-sponsored survey of bridges that were subjected to a major flooding event found that the roadway decks of several bridges throughout New York and Pennsylvania had separated from their supporting substructures (O'Donnell 1973). Chang and Shen (1979) reported that the most frequent cause of damage to bridges is related to debris accumulation. Chang and Shen describe the type and geometry of bridges that are susceptible to damage from either debris impact or accumulation.

Three post-failure investigations of bridges provide information about some of the parameters and site conditions that

**Table A1 Major phases and tasks in evaluating potential for drift accumulation at a bridge**

Major Phase	Tasks
1. Estimate potential for drift delivery.	a. Estimate potential for drift delivery to the site. b. Estimate size of largest drift delivered. c. Assign location categories to all parts of the highway crossing.
2. Estimate drift potential on individual bridge elements.	a. Assign bridge characteristics to all submerged parts of the bridge. b. Determine accumulation potential for each part of the bridge.
3. Calculate hypothetical accumulations for the entire bridge.	a. Calculate hypothetical accumulation of medium potential. b. Calculate hypothetical accumulation of high potential. c. Calculate hypothetical chronic accumulation.

**TABLE A2 Maximum extent of debris accumulation**

Accumulation Type	Width	Height
Pier	L	Y
Superstructure	S	H + 1.2 m below superstructure
Horizontal Gap	W	Smaller of D or Y
Vertical Gap	W	D

L=design log length, H = vertical height of superstructure, W = width of gap, D = vertical extent of gap, Y = flow depth, S = span.

must be considered in the practical and reliable evaluation of forces caused by debris accumulation on bridges. A National Transportation Safety Board (NTSB) investigation (1990) provides information on the characteristics of the Great Miami River and floodplain at the site of a collapse of a temporary bridge at Harrison Road near Cincinnati, Ohio. Aerial photos and site diagrams illustrate the complexities, such as channel curvature, floodplain, and main-channel-flow interaction and flow contraction associated with high-way embankments. Two collapsed bridges studied by Parola et al. (1998a) on small, incised streams in Nebraska and Missouri showed the effect of severe-flow contraction.

Flow conditions, debris surface geometry, and channel topography were measured at a bridge on the Brazos River in Texas during a flood event in 1995. Measurements of the debris geometry (Diehl 1997), measurement of flow veloc-

ities around the debris accumulation (Mueller and Parola 1998), and computational modeling of flow around the debris accumulation at the bridge (Parola et al. 1998b) illustrate the conditions under which debris forces must be computed. A highly nonuniform flow, significant contraction of the waterway, and channel bends all contributed to the flow conditions around the debris accumulation. Although detailed measurements of the flow velocity and channel topography were made, debris forces were not measured.

Examination of the documented site conditions where bridges have collapsed (NTSB 1990 and Parola et al. 1998a) and where detailed flow conditions were measured during a flood event revealed the following conditions of flow that may be typical of bridges that are susceptible to debris accumulation and consequential damage.

- It may not be possible to locate a consistent position for determining an approach-flow reference velocity. Stream bends, backwater effects, and the interaction of floodplain and main channel cause highly nonuniform flows that make it very uncertain and subjective to select a representative velocity in the approach to the bridge (equivalent to the reference velocity).
- Accumulations composed of large woody debris affect flow across the entire bridge cross section for even medium-sized rivers. Woody-debris accumulations can obstruct more than 50 percent of the waterway opening at a bridge.
- Fine materials block large portions of the debris matrix, making a core region of the accumulation effectively impermeable.
- If trees longer than bridge spans are transported to a bridge, then the bridge opening may be completely blocked.

## PART 2: LABORATORY STUDIES

### INTRODUCTION

Three experimental studies were conducted under NCHRP Project 12-39 to determine drag coefficients for debris on piers and superstructures. The first study involved a series of small-scale experiments conducted in the Bridge Force Testing Facility at the University of Queensland, Brisbane, Australia. These small-scale tests were completed at a scale of 1:25. The second study involved a series of tests completed at the Riprap Testing Facility of the U.S. Army Corps of Engineers Waterways Experiment Station (WES) in Vicksburg, Mississippi. These tests were completed at a scale of about 1:16. The third study involved a series of tests completed at the University of Louisville Hydraulics Laboratory. This last study used plates to examine the effects of severe flow blockage. The following sections describe the experimental apparatuses, instrumentations, models (if applicable), procedures, and resulting data sets of each study.

### SMALL-SCALE EXPERIMENTS AT THE UNIVERSITY OF QUEENSLAND

#### Apparatus

These experiments were completed in the test flume in the Department of Civil Engineering at the University of Queensland. Figure A1 shows the flume. This flume had a low-head, high-flow circuit, with maximum-flow capacity of 0.5 m<sup>3</sup>/sec. The working section was rectangular in shape, 1 m wide, 1.5 m deep, and 6.7 m long. At the downstream end, the walls were clear plexiglass for a length of 3.7 m. The flow was supplied by an axial flow pump that was directly coupled to a variable-speed electric motor. The pump returned flow from a sump tank at the downstream end of the flume to a forebay, which was 4.8 m wide, 6.8 m long and, 1.8 m deep. The 400-mm-diameter delivery pipe from the pump discharged into the forebay through a diffuser that was designed to achieve uniform distribution of the flow across the upstream end of the forebay while minimizing the exit energy losses. After leaving the diffuser, the flow passed through a grillage of concrete blocks, which improved the uniformity of the flow distribution before the flow entered the main forebay. A 3-m-long streamlined horizontal contraction guided the flow from the forebay into the flume.

The water level in the flume was adjusted by adding or removing water as required; a float-controlled, make-up valve ensured that the water level was maintained constant at a given setting. The flow rate was varied continuously by varying the speed of the pump motor.

The velocity distribution in the working section was uniform, within about 2 percent, over the upper half of the flow cross section (where the model-bridge superstructures were tested) except in the wall boundary layers, which were about 50 mm thick.

#### Instrumentation

Time-averaged velocities in the working section were measured with a miniature OTT-meter. The velocity was inferred from the rate of revolution of a calibrated rotor. The rotors used were 30 and 50 mm in diameter. To obtain a correct measurement, the revolutions were timed for 90 s to give a true average reading.

The OTT-meter was mounted from above the flume on a two-dimensional, traversing mechanism. This mechanism allowed the location of the meter to be set accurately to within 0.5 mm. The approach-velocity distribution was measured 1.225 m upstream from the centerline of the model bridge.

Water levels were measured at four locations in the test flume: 2.62 m and 1.225 m upstream from the model bridge centerline and 1.225 m and 1.66 m downstream from the centerline. At the most upstream and downstream locations, water level was measured with pointer gauges. At the other two locations, the water level was measured with piezometers that connected tapings in the side of the flume close to the floor to a sensitive Validyne pressure transducer, type P305D, with maximum allowable differential head of 14 mm of water.

The forces on models in the working section were measured with a custom-designed dynamometer system capable of measuring force in the horizontal and vertical directions and measuring the moment of the total force about a horizontal axis that was normal to the direction of flow. The dynamometer system consisted of a rigid frame, to which the model was fixed, that was supported on a horizontal axle set across the top of the working section. Displacement and rotation of the axle were prevented by five force transducers. Two transducers were set at each end of the horizontal axle such that one on each side restrained horizontal movement and the other restrained vertical movement. The fifth transducer was set approximately 800 mm downstream from the axle in the same horizontal plane. This transducer prevented rotation of the frame about the axle by applying a vertical force. Each of the five transducers was mounted on a micrometer screw so that precise adjustment could be made to the position of the transducer along the line of action of the force that it restrained and, thereby, measured. The contact between the model support frame and each force transducer

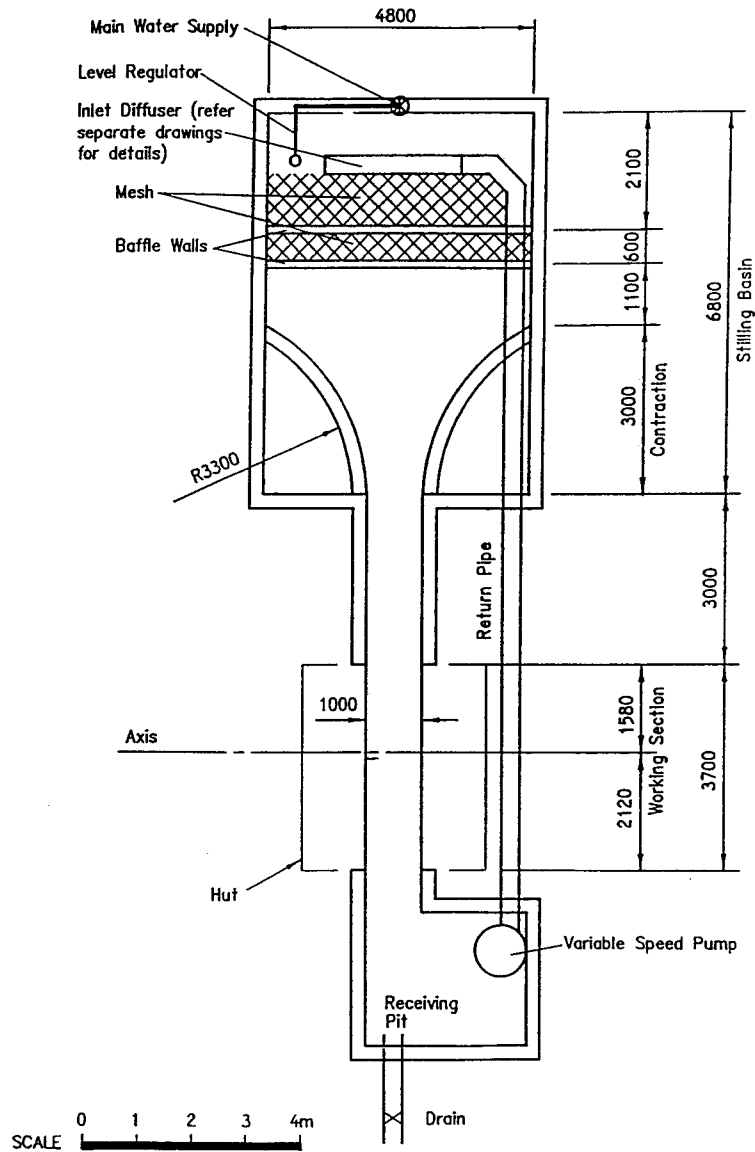


Figure A1. University of Queensland test flume.

was made through a precision roller bearing to minimize friction in the system.

Vertical counterweights reduced the load that the weight of the bridge model applied to the vertical-force transducers, thus keeping the forces that were applied to these transducers within their operational range.

Preloads were applied to all load cells to ensure that each roller bearing remained in contact with its bearing surface at all times and that the force transducers operated above the low end of their operating range. The horizontal preload was applied using a weight that was suspended on a string. The string was connected to the upstream end of the frame and ran over a pulley so that the horizontal preload would act in the downstream direction. The moment preload about the frame axle was applied using a weight that was suspended from the

upstream end of the frame. The counterweights served as the vertical preload and were set to ensure that the force transducers were above the low end of their operating range.

Before measurements of hydrodynamic forces and moment were made, each transducer was reset, by adjustments of the micrometer screws, to the position it occupied before the application of the model hydrodynamic loads. Two dial gauges measured the horizontal deflection, two measured the vertical deflection, and one measured the rotation around the axle. One horizontal gauge and one vertical gauge were positioned (in the direction of flow) on each of the left and right sides of the frame. The gauges were positioned 21 cm upstream of the axle. The gauge to measure rotation about the axle was positioned next to the force transducer that was used to prevent rotation. Thus, the frame and model were

always in the same position when forces were measured with the transducers, and the weight of the system did not affect force measurements. The force transducers that were used were strain gauge transducers with four active strain gauges, giving a full, wheatstone bridge circuit. The force-measuring system is calibrated in place with a system of weights and pulleys.

The Data Acquisition System (DAS) provided eight differential channels, six of which were used, at a throughput rate of 100,000 Hz. This system provided a maximum sampling rate of 16,666 Hz per channel of data. It used a 16-bit, analogue-to-digital converter that provided a resolution of 1 bit in 65,536 (0.1526 millivolts/bit). Each channel contained a signal-conditioning module with an input rate of 10,000 Hz. The full-scale input and gain selection was accomplished using a combination of switches and a programmable gain amplifier (software selected). The system is run with a 486 DX2-66 PC.

The output from the force transducers was a voltage. The force transducers were calibrated such that the voltage output equaled a load in kilograms. An initial bench calibration adjusted the span on the amplifier so that a 10-kg load was approximately equivalent to 1 V. Calibration was then done with the force transducers on the rig. The calibration on the rig was used for all calculations of forces.

The preload facilities were used to apply the loads for calibration. The two horizontal-force transducers were calibrated together, as were the vertical-force transducers. The moment transducer was calibrated independently of the vertical- and horizontal-force transducers. The output from the transducers not being calibrated was recorded to check for cross-talk, for example. When the horizontal-force transducers were being calibrated, the outputs from the vertical-force and moment transducers were recorded. Cross-talk occurred when a portion of the load being applied to the transducers in one direction was detected by the transducers measuring in a different direction. The cross-talk was negligible in this system.

Calibration was carried out whenever the model structure to be tested was changed and at frequent intervals throughout the testing of each model.

**Models of Superstructures and Piers**

Tests were conducted on models of four different types of superstructure and three different types of pier. Tests included force and flow measurements on piers and superstructures with debris. Table A3 provides the number of tests conducted for each pier and superstructure.

All pier and superstructure models were constructed from aluminum in the University of Queensland Department of Civil Engineering workshop to a scale of 1:25. The details of the models are given in the following sections.

*Superstructure A*

Superstructure A was a typical, prestressed, concrete I-beam girder bridge, with concrete deck and solid, New Jersey-type guardrails. The four I-beams were AASHTO Type IV. Figure A2 provides the dimensions of the model of Superstructure A.

*Superstructure B*

Superstructure B was a typical steel-girder bridge, with concrete deck and New Jersey-type guardrails. Figure A3 provides the dimensions of the Superstructure B model. The deck and guardrails were identical to those in Superstructure A; therefore, only the girders needed to be changed to produce the Superstructure B model from Superstructure A. The same comment applies to the models of Superstructures C and D. The overall dimensions of the steel girders were true to scale, but the thickness of webs and flanges were not.

*Superstructure C*

Superstructure C was a typical spread box-beam bridge, with concrete deck and New Jersey-type guardrails. Figure A4 provides the dimensions of the Superstructure C model.

*Superstructure D*

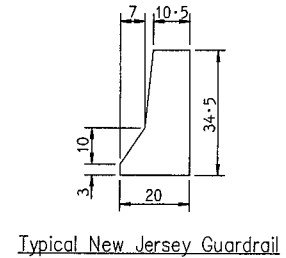
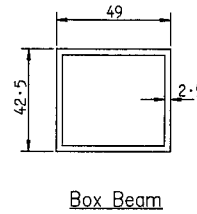
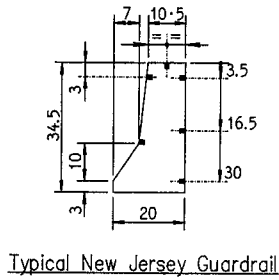
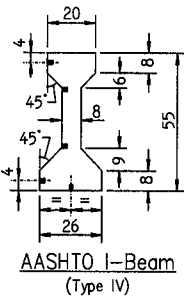
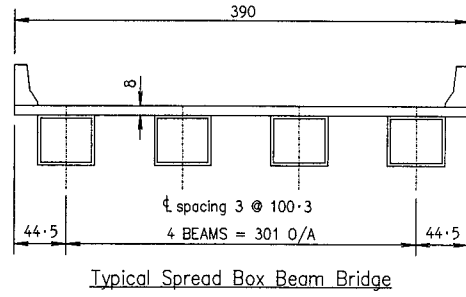
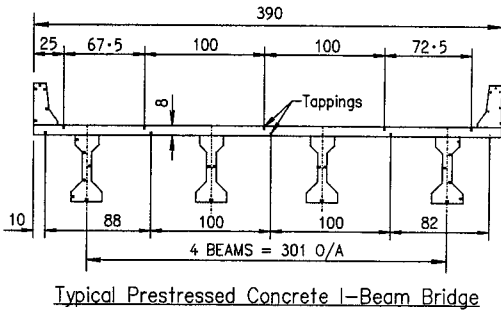
Superstructure D was a typical adjacent box-beam bridge, with concrete deck and New Jersey-type guardrails. Figure A5 provides the dimensions of the Superstructure D model.

*Pier Type A*

Pier Type A was a typical two-column pier, with a rectangular pier cap. Figure A6 provides the dimensions of the Pier Type A model. In preliminary tests, a large endplate was fixed to the lower end of the model pier to eliminate end effects. However, tests with and without the endplate gave

**TABLE A3 Summary of Queensland experiments**

Structure Type	Number of Tests		
	Flat Plate	Rough Cone	Rough Wedge
Pier A	6	8	---
Pier B	9	7	---
Pier C	4	3	---
Superstructure A	12	---	9
Superstructure B	3	---	---
Superstructure C	10	---	3
Superstructure D	4	---	---



$L_r = 25$

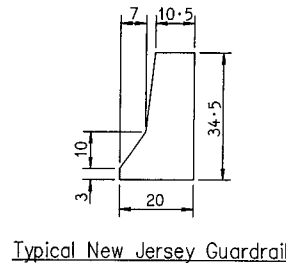
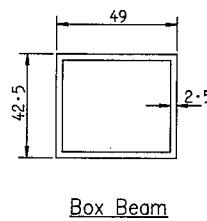
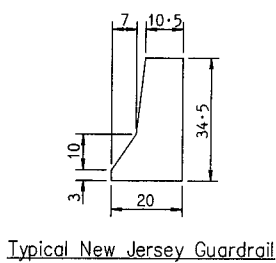
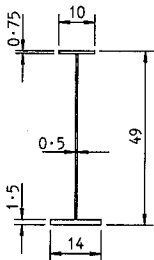
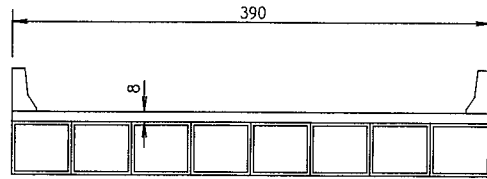
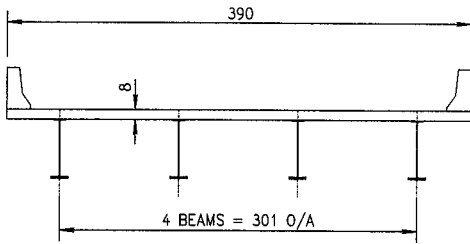
Model dimensions are in millimetres.

$L_r = 25$

Model dimensions are in millimetres.

Figure A2. Superstructure A.

Figure A4. Superstructure C.



$L_r = 25$

Model dimensions are in millimetres.

$L_r = 25$

Model dimensions are in millimetres.

Figure A3. Superstructure B.

Figure A5. Superstructure D.

similar results for the hydrodynamic forces on the pier; therefore, the model was tested without the endplate in the main test series.

*Pier Type B*

Pier Type B was a typical solid, rectangular pier, with a rectangular pier cap. Figure A7 provides the dimensions of the Pier Type B model.

*Pier Type C*

Pier Type C was a four-steel, H-pile bent pier, with the dimensions of the Harrison Road bridge pile-bent pier. The Harrison Road bridge failed under the influence of debris loading. Figure A8 provides the dimensions of the Pier Type C model. The cross-sectional shapes of the H-piles and angle bracings were constructed from sheet aluminum.

**Models of Debris**

*Debris for Superstructures*

In conjunction with the construction of Superstructure A, five models of debris rafts were constructed for preliminary "ranging" tests. For tests on superstructures without piers,

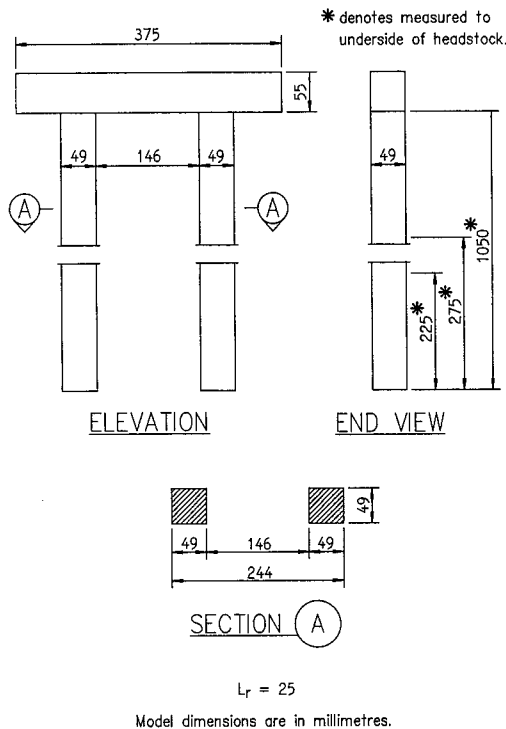


Figure A6. Pier Type A.

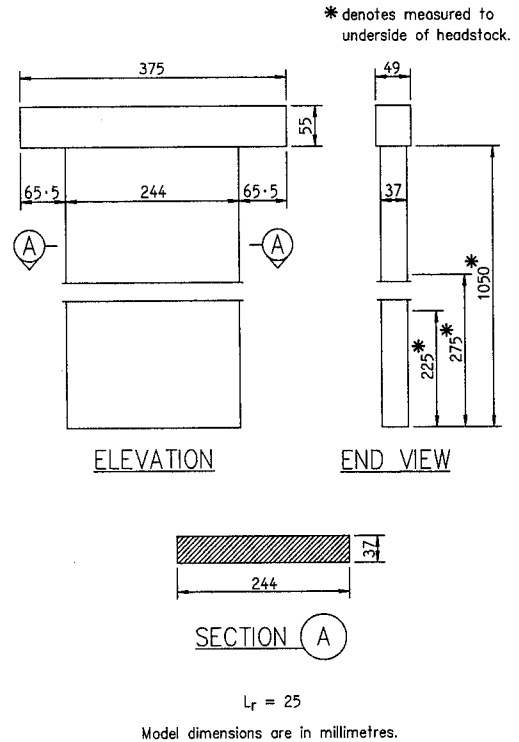


Figure A7. Pier Type B.

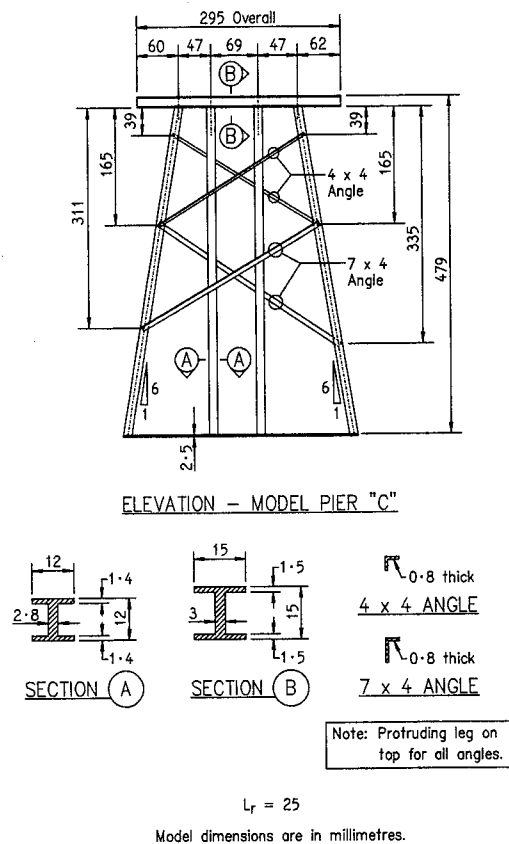


Figure A8. Pier Type C.

the conditions were two-dimensional; therefore, the models of debris rafts for use in such tests were essentially prismatic. The four model debris rafts were

- Flat plate,
- Smooth wedge,
- Trial rough wedge, and
- Rough wedge.

Figures A9–A11 provide the dimensions of these models.

### Debris for Piers

For tests on piers when the water level was below the superstructure, the debris raft was simulated as a half-cone. The flat-plate model, in this case, was a triangular plate fixed to the upstream face of the pier model. Figures A12–A14 show these debris models.

### Procedure

The following procedure was followed to measure forces on the models using the direct-force measurement system.

1. Fill flume to desired level.
2. Ensure that the bridge is not supported by load cells.
3. Position bridge at level to be tested.
4. Apply vertical counterweights and moment preload.
5. Remove rear safety bolt.
6. Lower bridge onto vertical-force transducers.
7. Move horizontal-force transducers up against bearer plates.
8. Apply horizontal preload.
9. Zero dial gauges.
10. Record voltage output for each force transducer (this is the zero against which all changes in load are measured).
11. Set pump to desired speed and allow system to reach equilibrium (approximately 45 min).
12. Return bridge to undeflected position (The undeflected position is the zero position set in Step 9. The bridge is moved back to the undeflected position using the micrometer screw on the force transducer mountings. Given the dynamic nature of the flow [the dial gauge readings fluctuate], it is not possible to return

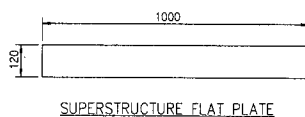
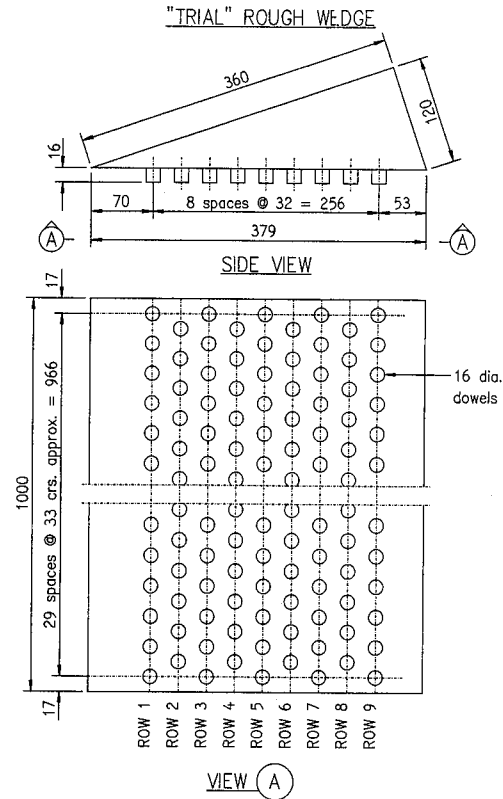


Figure A9. Flat plate debris.



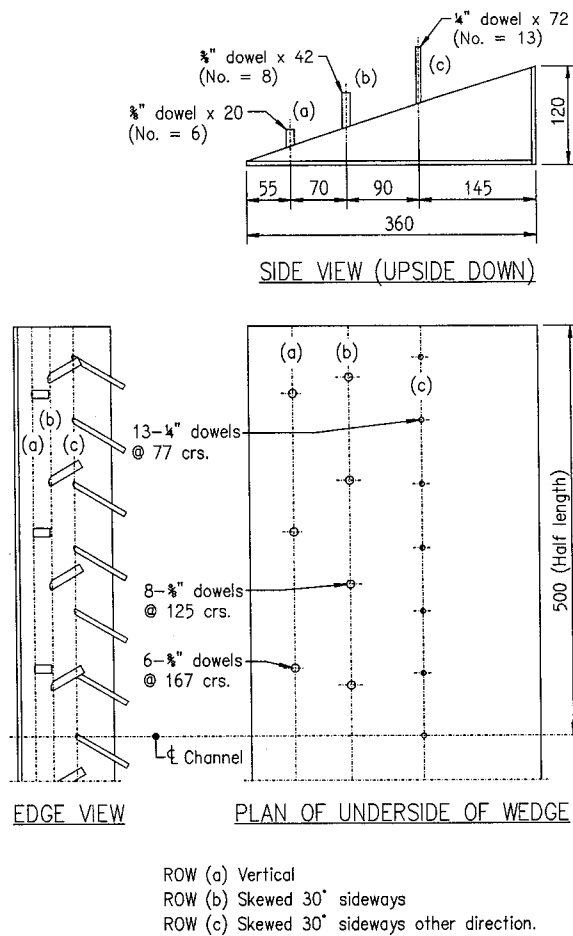
Each row is offset from adjacent rows  
i.e. 30 dowels in ROW 1; 29 dowels in ROW 2 etc.

NOTE: Rough Wedge = Trial Rough Wedge with extra roughness added without disturbing existing roughness.

Figure A10. Trial rough wedge debris.

the bridge exactly to the undeflected position. This problem pertains more to the vertical direction than to the horizontal direction [that is, the flow direction], possibly because of fluctuations of the separated boundary layer.

13. Record voltage reading for each force transducer (The fluctuations of dial gauges noted in Step 12 are also evident in the force-transducer outputs. These fluctuations are inevitable, because the deflections of the force transducers equal the movements of the frame. The outputs from the drag and moment transducers are nearly static, but the output from the lift transducers vary considerably. The outputs from the transducers are recorded with the DAS until enough data are obtained to give accurate average values. Typically, data are logged for 2 min at 2 Hz, but longer periods and higher frequencies are used when large fluctuations in voltage are observed.)
14. Record velocities at depths corresponding to the bridge midheight. The velocity is recorded at 10 positions across the channel. The readings are taken at



NOTE: Rough Wedge = Trial Rough Wedge with extra roughness shown above added without disturbing existing roughness

Figure A11. Extra roughness.

- 100-mm intervals, with the first and last being 50 mm from the flume wall.
- 15. Record water temperature.
- 16. Adjust flow for next test conditions, allowing approximately 15 min for equilibrium. Repeat from Step 12.
- 17. When test sequence is completed, stop pump and remove preloads.
- 18. Move force transducers away from bearer plates.

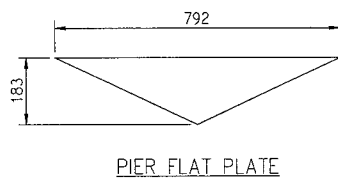


Figure A12. Flat plate debris model for piers.

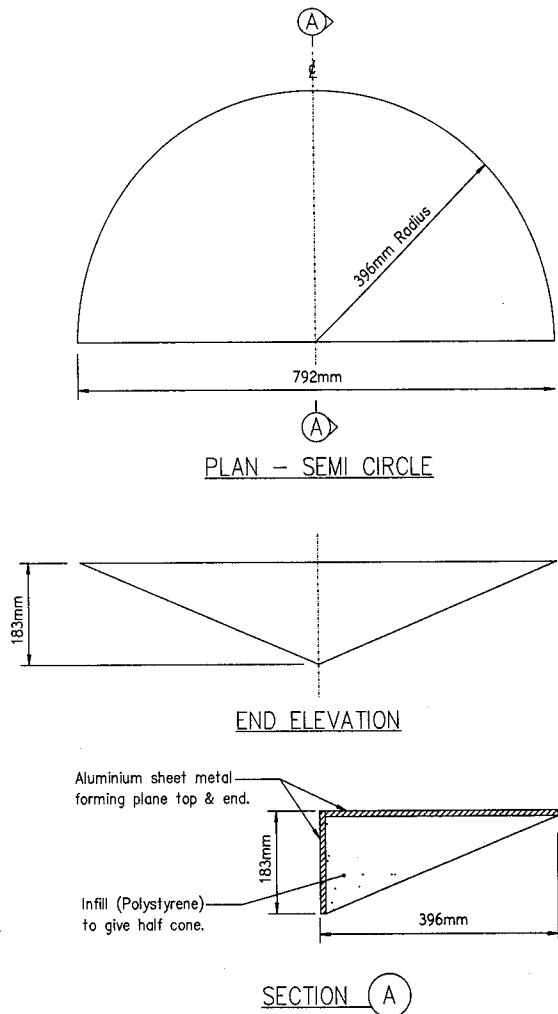


Figure A13. Smooth cone debris model for piers.

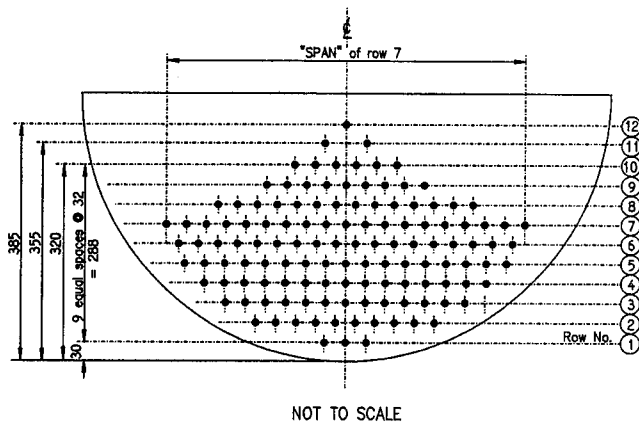
**University of Queensland Idealized-Model Debris Data Set**

Tables A4 and A5 provide the collected data and computed variables that will be described in the Part 3 analysis. The variables include the upstream and downstream flow depth, approach-flow velocity, contracted-flow velocity, hydrostatic force component, drag force component, total streamwise force, contracted-flow blockage ratio, and drag coefficient (which is computed using the contracted-flow velocity as described in Part 3).

**WES MEDIUM-SCALE DEBRIS ACCUMULATION GEOMETRY AND FORCE-MEASUREMENT EXPERIMENTS**

Medium-scale tests were conducted to determine the variation of drag coefficient for debris accumulations on piers and superstructures. A 1:16 scale model of a typical steel-

"REGULAR" ROUGHNESS



VIEW UNDER SIDE OF CONE.  
 DIMENSIONS GIVEN ARE MEASURED ALONG THE SURFACE  
 I.E. NOT PROJECTED.

- THE ROUGHNESS ELEMENTS ARE 16mm DIA. DOWELS PROJECTING NORMAL TO SURFACE A DISTANCE OF 16mm.
- THE SPACING ALONG ROWS IS APPROXIMATE 33mm C/C
- FROM ROW TO ROW, DOWELS ARE "STAGGERED" ONE HALF SPACING EXCEPT FOR ROWS 11 & 12 AND ROW 4

Row No.	1	2	3	4	5	6	7	8	9	10	11	12
Span (mm)	70	295	395	465	530	550	590	420	260	170	70	-
No. of Dowels	3	10	13	15	17	18	19	14	9	6	2	1

Figure A14. Regular roughness model for cone debris.

girder bridge, with concrete deck and New Jersey-type guardrails, was used. This structure was geometrically similar to Superstructure B (Figure A3) used in the University of Queensland experiments, except for the thickness of the model girder plates and flanges. Total force in the streamwise direction was measured for flow conditions with debris on a superstructure and piers.

**Apparatus**

Figure A15 shows a schematic of the flume and pumping station. The maximum capacity of the pumping station was 5.7 m<sup>3</sup>/s at a maximum depth of 1.2 m. The flume was approximately 238 m long, with four bends fully lined with a filter cloth and 76-mm crushed limestone. Tests for this study were performed in the straight section, 47 m downstream of the pump discharge.

Figure A16 shows the primary and secondary support structure of two beams cantilevered upstream from a two-pier, steel-support structure. The secondary support structure consisted of metal telescoping rods and a pulley system

extending from the primary supports to the ungauged model-bridge sections. The telescoping rods in Figure A17 were positioned to prevent translation and rotation of the ungauged bridge when submerged. Figures A18–A20 show the pulley system used to counterweight the gauged section of the bridge. The twelve 25.4-mm-diameter telescoping rods were constructed of aluminum. The pulley system was composed of wire cable and ten 12.7-mm-diameter pulleys.

**Instrumentation**

Velocity profiles were measured 8.2 m upstream of the model bridge, with a Pitot tube accurate to 3 mm of velocity head. Point gauges accurate to 0.3 mm were used to measure water surface elevations upstream and downstream of the bridge sections. Forces on the gauged model-bridge section were measured using four force transducers. A 12-V battery excited the force transducers. The analog output from the force transducer was measured with a Keithley Metrabyte DAS-20 data-acquisition board, controlled by data-acquisition software (LabTech Notebook). The force transducers were calibrated before each test and examined after each test.

The maximum depth of the accumulation was measured with an L-shaped probing rod that extended upstream and under the accumulation. The vertical portion of the rod was calibrated such that the bottom of the accumulation could be referenced to the water surface elevation point gauges. The probing-rod accuracy was approximately 3 mm.

The drag force was measured by a single force transducer in the center of the bridge section approximately 0.7 m above the bridge-deck surface. Force transducers with full-scale ratings of 111, 222, 445, and 890 N were used to measure drag forces. Although lift forces were measured, they were not considered in this study. The force transducers were accurate to within 0.04 percent of full scale.

**Models**

The model bridge constructed at a 1:16 scale was similar to a typical two-lane bridge, with steel girders and New Jersey-type railing system. The model bridge had a total length of 5.5 m and was 0.61 m wide. The central 1.82-m section of the bridge was isolated for drag measurements from the remaining bridge and was held in place by vertically positioned tendons. The drag force transducer maintained the streamwise position of the gauged bridge. The sections of the model bridge are referred to as the gauged section and ungauged sections, as shown in Figure A16. The ungauged sections lacked some of the details of the gauged section and were constructed from plywood.

The debris elements were modeled with 0.61-m-long tree limbs, cut from various species of trees, with diameters of 12.7–25.4 mm. All branches were removed. Fine debris

TABLE A4 University of Queensland idealized-model data set for piers

Test #	Depth US (mm)	Depth DS (mm)	V <sub>a</sub> (m/s)	V <sub>c</sub> (m/s)	F <sub>h</sub> (N)	F <sub>D</sub> (N)	F <sub>T</sub> (N)	B	Method 3 C <sub>D</sub>
<b>Pier A</b>									
PWD2FP	400.0	388.8	1.030	1.312	7.48	58.87	66.35	0.19	0.82
PWD3FP	329.3	316.2	0.935	1.250	8.66	48.58	57.24	0.22	0.78
PWD4FP	252.0	231.7	0.786	1.160	12.89	36.28	49.17	0.26	0.71
PWD6FP	331.4	307.4	1.136	1.536	14.92	57.87	72.79	0.20	0.61
PWD7FP	330.8	328.2	0.721	0.952	1.82	42.62	44.44	0.24	1.17
PWD8FP	330.6	333.6	0.540	0.711	-2.17	30.65	28.48	0.25	1.52
PWD1RC	999.8	1008.1	0.470	0.531	-6.69	23.74	17.05	0.12	1.49
PWD2RC	399.3	405.9	1.009	1.270	-3.19	34.18	30.99	0.22	0.51
PWD3RC	331.5	336.9	0.920	1.207	-2.60	29.33	26.74	0.25	0.50
PWD4RC	248.8	243.2	0.937	1.359	2.61	21.75	24.36	0.29	0.31
PWD6RC	330.4	335.3	1.116	1.467	-2.35	32.24	29.89	0.25	0.37
PWD7RC	330.0	341.3	0.720	0.942	-5.52	25.61	20.08	0.26	0.72
PWD8RC	330.0	342.1	0.558	0.730	-5.93	18.36	12.44	0.26	0.86
PWD9RC	332.0	346.3	0.379	0.494	-7.05	14.98	7.93	0.27	1.53
<b>Pier B</b>									
PWD10FP	1000.9	1007.9	0.470	0.523	-5.17	24.15	18.98	0.11	1.72
PWD11FP	400.9	399.2	0.853	1.069	1.20	46.33	47.53	0.20	1.01
PWD12FP	329.8	316.3	0.917	1.217	8.91	47.58	56.49	0.21	0.82
PWD13FP	249.4	237.0	0.610	0.888	8.23	28.93	37.16	0.28	0.98
PWD14FP	199.7	179.4	0.602	0.991	12.89	28.63	41.52	0.32	0.80
PWD14FPR	198.9	181.0	0.559	0.916	11.52	27.11	38.63	0.33	0.88
PWD15FP	331.6	312.2	1.136	1.515	12.38	55.20	67.58	0.20	0.62
PWD16FP	331.7	328.5	0.704	0.923	2.24	37.59	39.83	0.23	1.13
PWD17FP	330.6	331.1	0.540	0.707	-0.36	31.01	30.66	0.24	1.59
PWD10RC	1000.1	1009.1	0.470	0.523	-4.37	13.46	9.08	0.11	0.96
PWD11RC	400.2	406.9	0.852	1.063	-3.24	23.44	20.20	0.21	0.51
PWD12RC	329.5	329.9	0.935	1.225	-0.19	24.07	23.88	0.24	0.41
PWD13RC	249.8	250.5	0.657	0.939	-0.33	17.70	17.37	0.30	0.53
PWD16RC	331.1	333.6	0.739	0.965	-1.19	19.32	18.12	0.24	0.53
PWD17RC	329.6	335.2	0.539	0.704	-2.70	15.30	12.61	0.25	0.79
PWD18RC	328.3	335.8	0.395	0.515	-3.63	10.92	7.30	0.25	1.06
<b>Pier C</b>									
PWD19FP	408.5	405.1	0.781	0.959	2.37	31.08	33.46	0.18	0.90
PWD20FP	328.2	319.7	0.754	0.981	5.77	30.91	36.68	0.21	0.86
PWD21FP	251.1	238.1	0.596	0.857	8.60	23.73	32.33	0.27	0.88
PWD22FP	199.4	188.0	0.504	0.809	7.61	20.67	28.28	0.34	0.87
PWD19RC	408.2	412.7	0.780	0.954	-2.16	17.73	15.57	0.19	0.52
PWD20RC	326.8	329.8	0.734	0.948	-1.43	16.43	15.00	0.23	0.49
PWD21RC	246.1	247.3	0.622	0.884	-0.57	14.29	13.72	0.30	0.50

material was modeled using dried hay. A single sheet of polyethylene was draped over the upstream surface of accumulations to model complete debris-matrix blockage of natural debris accumulations by very fine debris and sediment. Figures A21 and A22 show the debris models used in the study.

### Procedure

Before flow conditions were established in the flume, force transducers were calibrated. After flow conditions had been established for approximately 30 min, debris was placed in the flow 8.5 m upstream of the bridge in clusters of 4–10 elements. After an initial accumulation of at least two debris elements was established on the bridge pier, single elements

of debris were placed in the flow upstream of the bridge. To develop debris accumulations on the partially submerged superstructure, single elements of debris were placed at various locations across the flume. Debris elements that did not accumulate were collected downstream of the test section of the flume and reintroduced upstream.

For determining the variation of velocity in the central portion of the channel and for computing drag on small accumulations, velocity was measured along three profiles in the central part of the channel upstream of the bridge. The measurements were obtained at vertical increments of 0.1 times the depth of flow in each profile. The profiles were spaced every 0.3 m from the center of the channel and 8.2 m upstream of the test bridge.

Water surface elevations were measured with point gauges located in the same cross section as the velocity measure-

TABLE A5 University of Queensland idealized-model data set for superstructures

Test #	Depth US (mm)	Depth DS (mm)	V <sub>a</sub> (m/s)	V <sub>c</sub> (m/s)	F <sub>h</sub> (N)	F <sub>D</sub> (N)	F <sub>T</sub> (N)	B	Method 3 C <sub>D</sub>
<b>Superstructure A</b>									
SWD1FP	980.2	974.7	0.464	0.524	6.20	15.36	21.56	0.12	0.93
SWD3FP	322.5	298.6	0.926	1.259	17.13	42.50	59.62	0.34	0.45
SWD4FP	232.5	195.6	0.737	1.238	27.71	31.01	58.72	0.47	0.34
SWD5FP	213.5	175.6	0.647	1.211	30.51	27.49	58.00	0.52	0.31
SWD7FP	402.9	384.0	0.772	0.986	15.01	41.48	56.49	0.28	0.71
SWD8FP	416.3	403.6	0.624	0.825	12.14	29.23	41.37	0.28	0.72
SWD9FP	424.3	414.8	0.405	0.542	9.98	11.99	21.96	0.28	0.68
SWD9FPR	426.1	417.4	0.427	0.577	9.32	16.63	25.95	0.28	0.83
SWD9AFP	426.1	421.7	0.285	0.385	4.81	4.99	9.79	0.28	0.56
SWD9BFP	429.5	427.1	0.184	0.250	2.73	1.51	4.23	0.28	0.40
SWD10FP	353.1	324.3	1.012	1.323	21.18	34.72	55.89	0.31	0.33
SWD11FP	368.5	349.6	0.950	1.215	13.15	42.12	55.27	0.29	0.48
SWD2RW	399.3	393.4	0.990	1.266	6.50	25.25	31.75	0.28	0.26
SWD3RW	332.5	316.6	0.895	1.231	15.71	14.57	30.28	0.34	0.16
SWD4RW	229.4	209.7	0.810	1.351	15.64	19.78	35.43	0.47	0.18
SWD5RW	206.4	183.1	0.694	1.259	18.94	15.99	34.93	0.52	0.17
SWD7RW	415.8	414.8	0.778	0.915	8.72	15.64	24.36	0.28	0.31
SWD8RW	414.1	411.2	0.624	0.824	5.90	11.84	17.74	0.28	0.29
SWD9RW	436.5	439.1	0.435	0.609	5.53	4.35	9.88	0.28	0.20
SWD10RW	351.8	343.6	0.949	1.270	5.41	25.39	30.80	0.31	0.26
SWD11RW	375.3	365.1	0.976	1.265	8.29	23.15	31.44	0.29	0.24
<b>Superstructure B</b>									
SWD14AFP	372.0	364.1	0.380	0.542	8.46	15.85	24.31	0.32	0.90
SWD15AFP	399.3	393.4	0.375	0.525	6.52	15.41	21.94	0.30	0.93
SWD15CFP	420.1	412.6	0.445	0.605	8.08	17.22	25.30	0.28	0.78
<b>Superstructure C</b>									
SWD18FPR	955.2	951.9	0.459	0.522	3.77	16.43	20.20	0.13	1.00
SWD19FP	349.1	325.9	0.982	1.312	17.18	45.32	62.51	0.31	0.44
SWD20AFP	308.2	298.6	0.327	0.530	10.96	10.33	21.29	0.39	0.61
SWD21AFP	259.2	245.5	0.315	0.583	15.48	9.68	25.16	0.47	0.48
SWD22AFP	210.5	189.7	0.298	0.701	23.02	10.85	33.87	0.58	0.37
SWD24FP	365.7	344.7	0.736	1.021	19.20	38.05	57.25	0.31	0.61
SWD25FP	372.8	359.2	0.534	0.756	13.88	27.37	41.24	0.31	0.80
SWD26FP	379.2	372.4	0.405	0.584	7.59	18.13	25.72	0.31	0.89
SWD27AFP	338.8	330.9	0.364	0.558	8.94	16.37	25.31	0.35	0.88
SWD28AFP	352.6	344.7	0.389	0.567	8.36	17.01	25.37	0.33	0.88
SWD18RWR	960	959.5	0.459	0.525	0.59	5.24	5.82	0.13	0.32
SWD24RW	365.4	357.3	0.735	1.015	7.89	12.51	20.41	0.31	0.20
SWD25RW	369.6	366.3	0.551	0.773	3.43	11.86	15.29	0.31	0.33
<b>Superstructure D</b>									
SWD31AFP	339.1	327.3	0.380	0.578	13.15	14.22	27.37	0.35	0.71
SWD32AFP	358.7	349.0	0.373	0.550	10.72	15.60	26.32	0.33	0.86
SWD32CFP	383.2	374.5	0.366	0.530	9.99	12.49	22.48	0.31	0.74
SWD32CFPR	383.8	374.6	0.386	0.558	10.57	12.82	23.39	0.31	0.69

ments. A single point gauge was at the centerline of approach. A second gauge was downstream and outside the wake that was created by the debris accumulation.

The profile area of the debris accumulations was measured using a probing rod attached to the downstream instrumentation beam. The maximum depth of each accumulation was

measured along a cross section 0.5 m downstream of the bridge. The cross-stream extents of the accumulations were measured using 40-mm markings painted on the gauged and ungauged sections of the bridge. Upstream extents were measured from a rod that was painted with 40-mm markings and was attached to the center of the bridge gauged section.

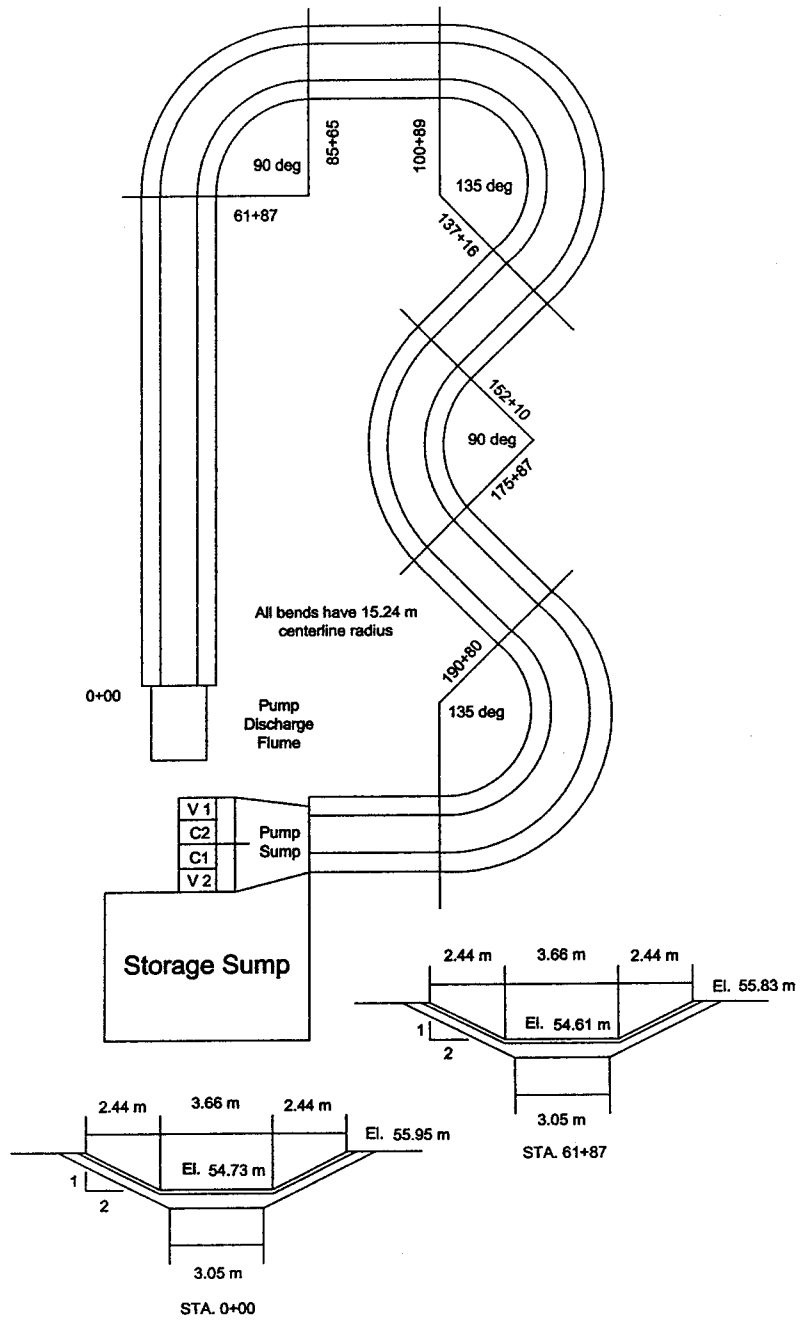


Figure A15. WES flume.

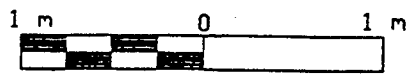
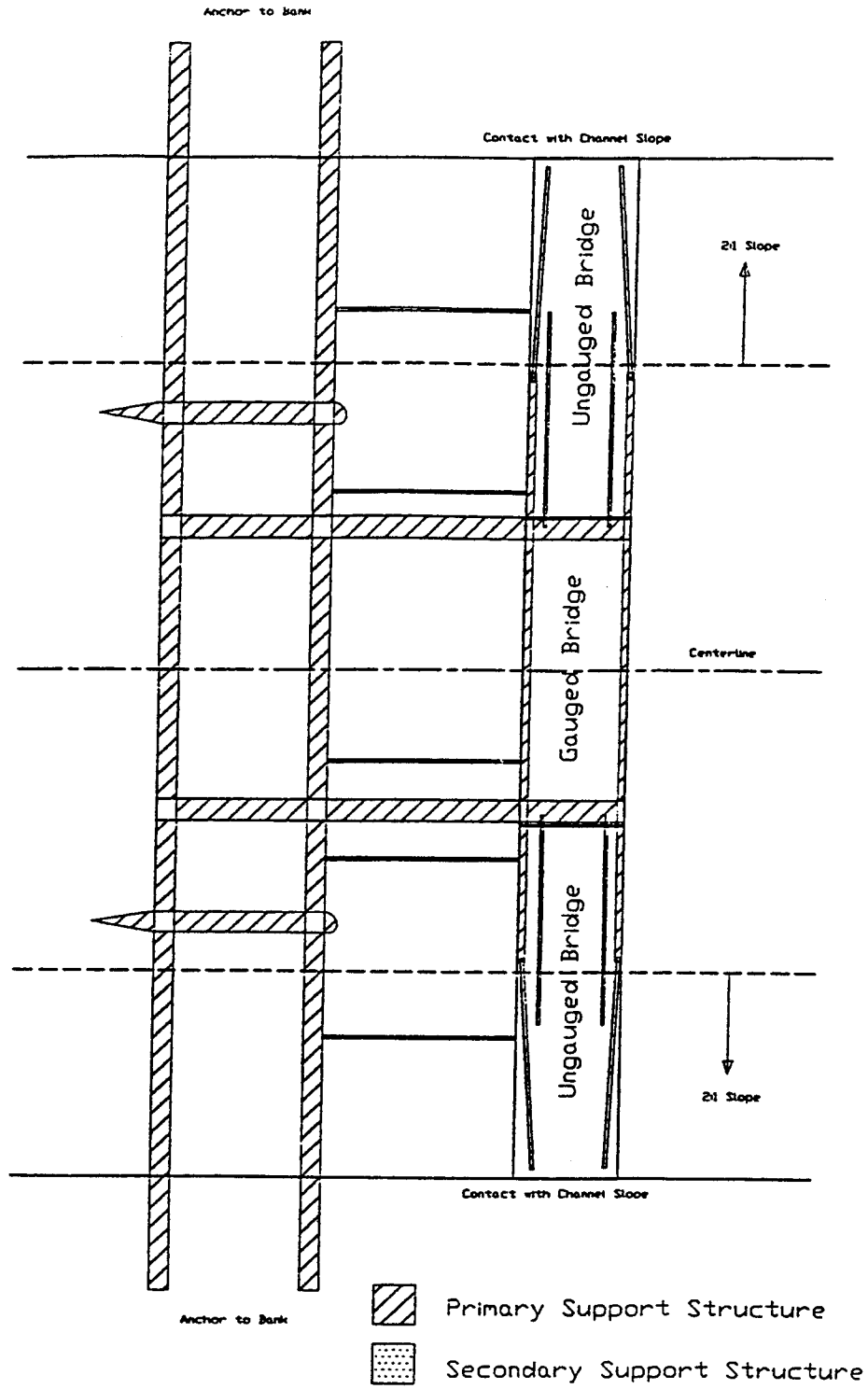


Figure A16. Primary and secondary support structures for testing mechanism.

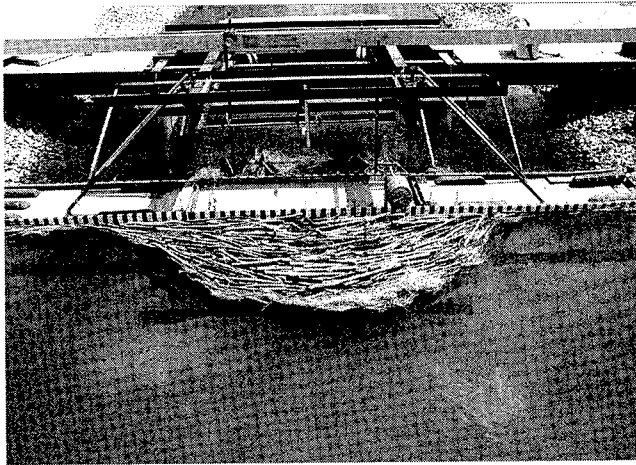


Figure A17. Testing mechanism, front view.

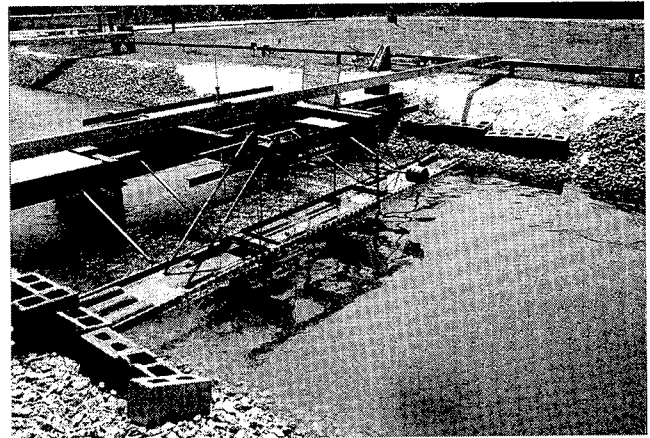


Figure A18. Testing mechanism, side view.

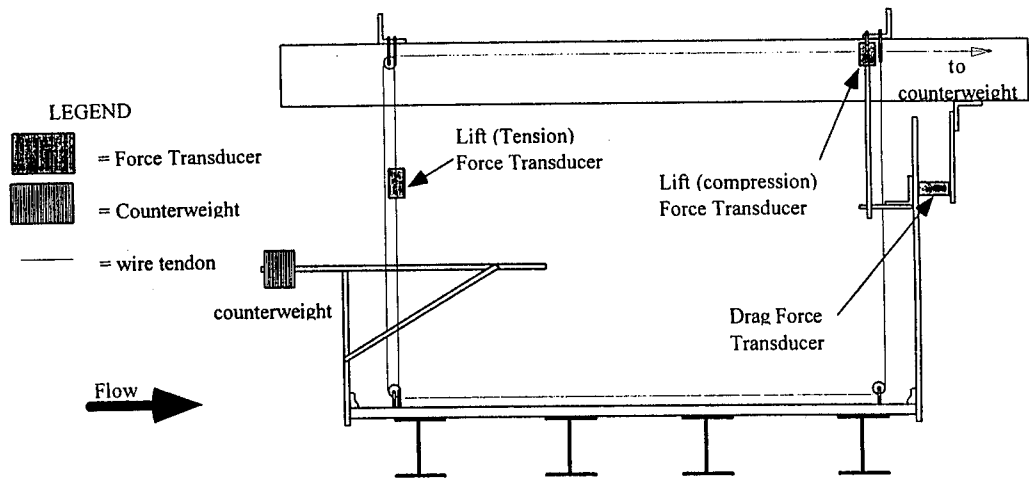


Figure A19. Diagram of gauged bridge section, side view.

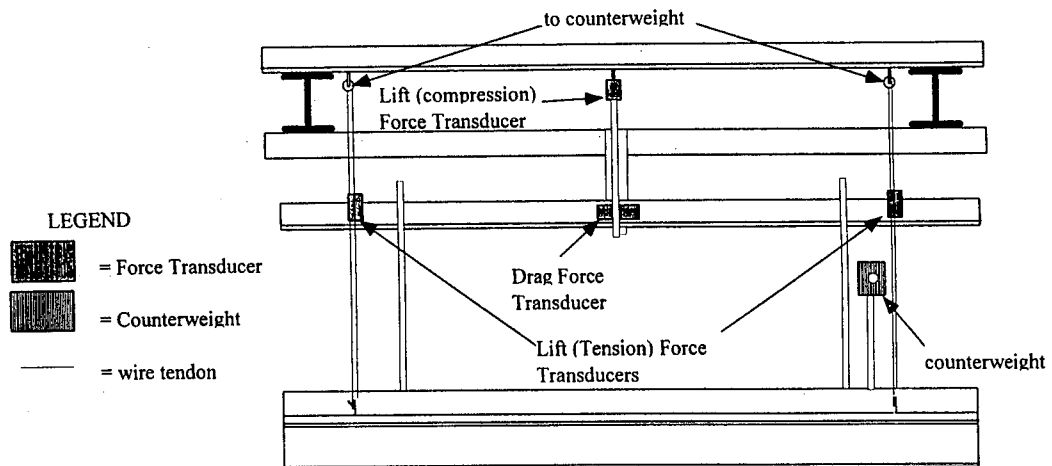


Figure A20. Diagram of gauged bridge section, front view.

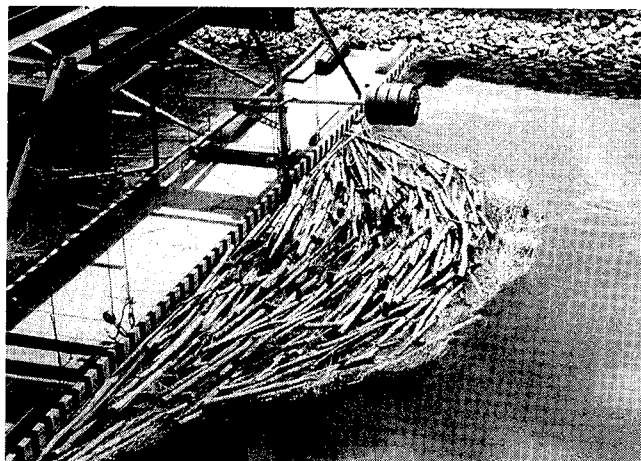


Figure A21. Typical debris accumulation, composed of coarse debris with layer of fine debris.

A layer of fine debris was added to the accumulation, and force measurements were repeated. Lastly, an impermeable membrane made of polyethylene sheets was draped over the upstream surface area of the accumulation and held in position by the flow. The cross-section dimensions were measured when the shape of the accumulation changed noticeably. Generally, the accumulation shape and size were considered constant for the measurements with fine debris

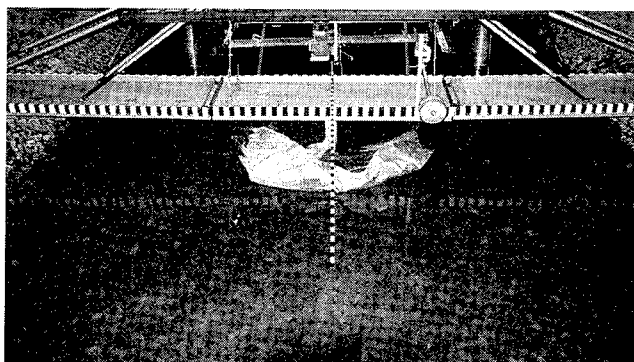


Figure A22. Typical debris accumulation, composed of coarse debris with layer of impermeable membrane.

and for those with the impermeable membrane. Figures A21 and A22 show examples of accumulations with fine debris and with the impermeable membrane.

#### WES Medium-Scale, Woody-Debris Model Data Set

Tables A6 and A7 provide the collected data and computed variables that will be described in the Part 3 analysis. The variables are the same as those described for Tables A4 and A5.

TABLE A6 WES medium-scale, woody-debris model data set for piers

Test #	Depth US (mm)	Depth DS (mm)	$V_a$ (m/s)	$V_c$ (m/s)	$F_h$ (N)	$F$ (N)	$F_T$ (N)	$B$	Method 3 $C_D$
<b>Woody Debris Elements Only</b>									
8.22.3	0.5715	0.5410	0.722	0.824	9.84	203.67	213.51	0.12	1.78
8.23.2	0.5410	0.5163	0.443	0.566	13.32	91.66	104.98	0.22	1.03
8.23.4	0.5313	0.5157	0.453	0.647	11.48	165.25	176.73	0.30	1.05
8.24.3	0.3673	0.3603	0.790	1.179	3.69	149.57	153.26	0.33	0.40
8.26.3	0.5599	0.5550	0.425	0.485	1.60	71.79	73.40	0.12	1.83
8.26.5	0.5642	0.5508	0.421	0.618	11.36	153.23	164.58	0.32	0.93
8.27.1	0.4572	0.4505	0.379	0.475	2.80	80.74	83.54	0.20	1.69
8.27.6	0.3097	0.3018	0.299	0.429	3.13	23.47	26.60	0.30	0.64
8.29.1	0.4572	0.4444	0.379	0.563	8.42	121.83	130.24	0.33	1.13
<b>Woody Debris Elements with Fine Debris</b>									
8.23.3	0.5368	0.5215	0.448	0.568	8.06	116.18	124.24	0.21	1.34
8.26.4	0.5599	0.5550	0.425	0.485	1.60	60.98	62.59	0.12	1.56
8.26.7	0.5642	0.5508	0.421	0.618	11.36	224.75	236.11	0.32	1.37
8.27.2	0.4630	0.4505	0.374	0.469	5.27	87.47	92.74	0.20	1.85
8.27.8	0.3097	0.3018	0.299	0.429	3.13	38.95	42.08	0.30	1.06
8.27.11	0.3206	0.3054	0.288	0.434	6.82	76.77	83.58	0.34	1.76
8.29.3	0.4935	0.4374	0.346	0.563	43.78	234.46	278.23	0.39	1.67
8.30.1	0.3075	0.2890	0.302	0.441	7.47	65.48	72.95	0.32	1.63
<b>Woody Debris Elements with Impermeable Membrane</b>									
8.23.5	0.5450	0.4999	0.439	0.641	35.14	170.73	205.86	0.31	1.02
8.26.6	0.5642	0.5508	0.421	0.618	11.36	193.26	204.62	0.32	1.17
8.27.7	0.3097	0.3018	0.299	0.429	3.13	32.32	35.45	0.30	0.88
8.27.10	0.3206	0.3054	0.288	0.434	6.82	62.71	69.53	0.34	1.44
8.29.2	0.4889	0.4380	0.350	0.562	38.82	207.39	246.21	0.38	1.53

TABLE A7 WES medium-scale, woody-debris model data set for superstructures

Test #	Depth US (mm)	Depth DS (mm)	$V_a$ (m/s)	$V_c$ (m/s)	$F_h$ (N)	$F_D$ (N)	$F_T$ (N)	B	$C_D$ Method 3
<b>Woody Debris Elements</b>									
9.4.1	0.6898	0.6693	0.245	0.308	9.55	22.84	32.38	0.21	0.94
9.4.2	0.6873	0.6794	0.368	0.508	6.55	143.04	149.59	0.27	1.33
9.4.4	0.8504	0.8041	0.932	0.982	150.39	209.91	360.30	0.26	1.87
9.5.1	0.5313	0.5157	0.453	0.489	21.74	19.05	40.79	0.22	0.88
9.5.2	0.5145	0.5047	0.305	0.326	7.39	8.67	16.06	0.19	1.08
<b>Woody Debris Elements with Fine Debris</b>									
9.4.3	0.6892	0.6724	0.367	0.505	13.67	186.10	199.77	0.27	1.74
9.5.3	0.5258	0.4983	0.297	0.595	22.59	44.27	66.86	0.50	0.29
9.5.4	0.5617	0.5005	0.423	0.888	67.40	187.44	254.84	0.52	0.40

### SMALL-SCALE EXPERIMENTS AT THE UNIVERSITY OF LOUISVILLE HYDRAULICS LABORATORY

The variation in drag coefficient for up to 40 percent of debris blockage in the bridge opening was investigated in the WES medium-scale experiments. The WES medium-scale experiments and the Task 7 examinations of two bridges (Parola et al. 1998a) demonstrate that debris blockages greater than 50 percent can occur. Debris accumulations that block more than 40 percent of the bridge opening may characterize conditions where bridges collapse. Therefore, data were needed to describe the variation in the drag coefficient with area-based blockage ratios in excess of 40 percent ( $B > 0.4$ ). A small-scale experimental investigation was conducted at the University of Louisville Hydraulics Laboratory to determine the variation in drag coefficient for severely blocked bridge openings.

In severely blocked conditions, the flow was blocked from the water surface to the streambed across large portions of the channel. To model these situations, a plate that blocked portions of a rectangular flume obstructed flow, and the force on the plate was measured. The plate width was varied from 10–90 percent of the flume width. Flow velocity and depth were varied to represent a wide range of flow conditions. Drag coefficients were computed from the drag force and from the computed flow velocity.

### Apparatus

A force-measuring apparatus was constructed from the components of the medium-scale testing apparatus, as shown in Figures A23–A26. Aluminum plates of the following widths blocked flow in the channel: 91 mm, 183 mm, 274 mm, 366 mm, 457 mm, 549 mm, 732 mm, and 823 mm.

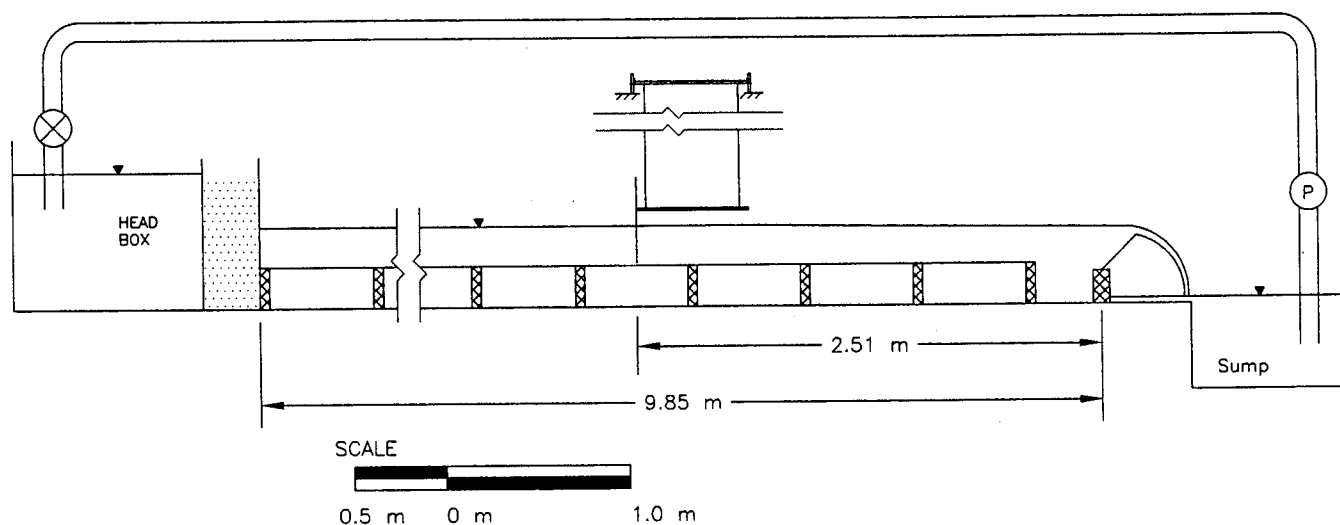


Figure A23. University of Louisville test apparatus.

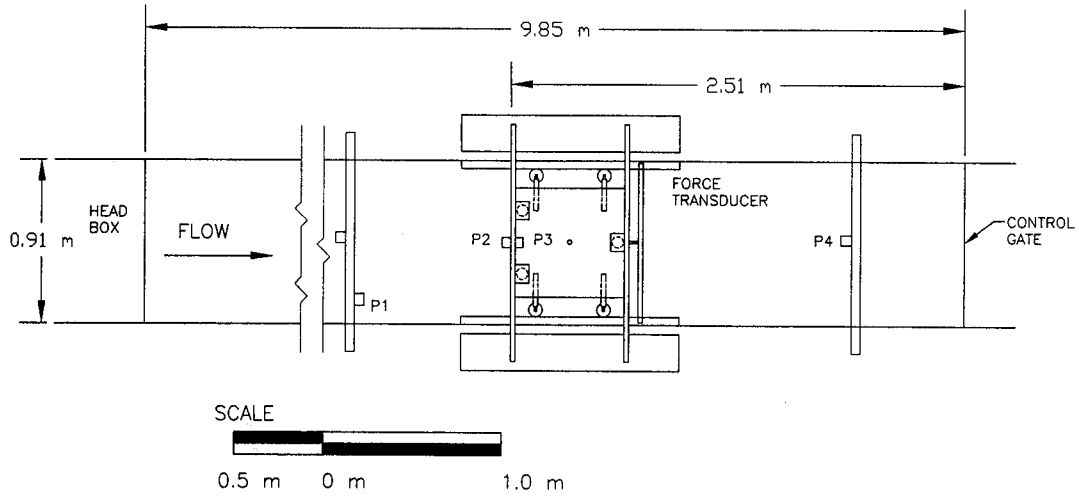


Figure A24. Plan view of flume and test apparatus (P indicates gauge location; blockage plate located between P2 and P3)

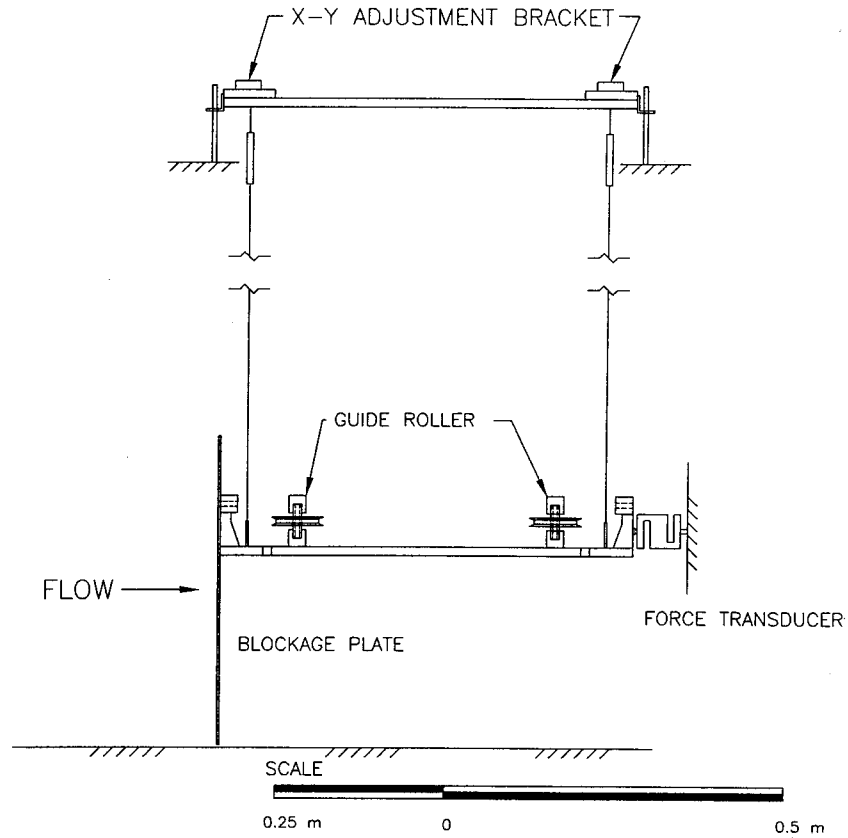


Figure A25. Diagram of test apparatus, side view.

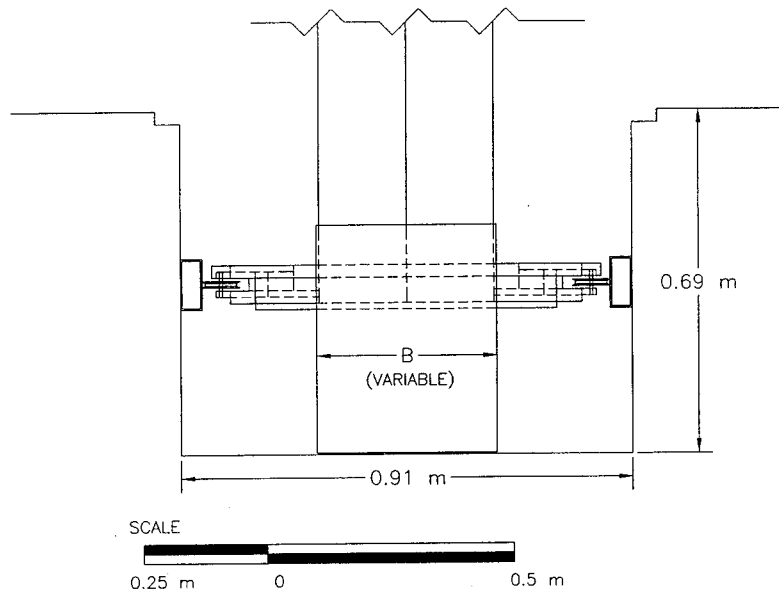


Figure A26. Diagram of test apparatus, front view.

### Instrumentation

The forces on the plates were measured using a Rice Lake Weighing Systems 50-lb force transducer, model RL20000A-50 (serial number AB 72371). The force transducer was excited by a 12-V battery. Output from the force transducer was measured and recorded with the same data-acquisition system described in the medium-scale experiments. Approach-flow velocities and cross-stream velocity distribution were measured with the Nixon Stream Flowmeter low-speed probe.

The water surface elevations were measured with point gauges ( $\pm 0.3$  mm), located 0.76 m and 0.04 m upstream and 0.04 m and 1.88 m downstream of the blockage plate. Point gauges were located at positions shown in Figure A24. The drag force was measured by a single force transducer in the center of the flume. A force transducer with full-scale rating of 222 N was used to measure drag forces. The force transducer was accurate to within 0.04 percent of full scale.

### Procedure

The force transducer was calibrated with a blockage plate mounted to the front of the test apparatus. To obtain a consistent reference for the four point gauges, the flume was flooded and allowed to stand overnight. The following day, water surface elevations were measured at the point gauges. Then, the reservoir was drained to its normal operating level.

Flow in the flume was established at an approximately predetermined flow depth and velocity. Velocity measurements were taken for 30 s, at 0.95 m upstream of the blockage plate, every 10 s. The velocity measurements were obtained at 10 evenly spaced intervals across the channel at 0.2, 0.4, 0.6, 0.8, and 0.9 times the water depth. The total flow was computed from the area weighted-average velocity. Water surface elevations at each point gauge were measured. The streamwise force on the plate was measured.

A series of flow conditions was obtained by holding the flow constant and by changing the tailwater elevation. Force measurements and water surface elevation measurements were obtained. A series of plates was tested while holding the flow rate constant. Several series of tests were conducted with different flow rates.

### University of Louisville Vertical-Plate, Flow-Blockage Data Set

Table A8 provides the collected data and the computed variables that will be described in the Part 3 analysis. In addition to the variables included in Tables A4–A7, three additional drag coefficients are provided. The vertical flat-plate experiments conducted at the University of Louisville were used to examine the variation of four different drag coefficients. The methods for computing the drag coefficients will be described in Part 3.

TABLE A8 University of Louisville vertical-plate, flow-blockage data set

Test #	Depth US (mm)	Depth DS (mm)	V <sub>a</sub> (m/s)	V <sub>c</sub> (m/s)	F <sub>h</sub> (N)	F <sub>D</sub> (N)	F <sub>T</sub> (N)	B	C <sub>D</sub>			
									Method 1	Method 2	Method 3	Method 4
81505-1A	102.7	0.1	0.66	0.72	0.58	1.91	2.49	0.05	1.67	1.42	0.99	1.17
81505-1B	138.3	135.5	0.55	0.59	0.17	1.42	1.59	0.05	1.48	1.31	1.15	1.31
81505-1C	173.1	170.7	0.44	0.47	0.18	1.20	1.39	0.05	1.55	1.39	1.18	1.31
81505-1D	205.7	203.8	0.37	0.39	0.17	0.98	1.15	0.05	1.49	1.34	1.10	1.22
81505-1E	235.6	235.2	0.33	0.34	0.04	0.89	0.93	0.05	1.54	1.40	1.33	1.47
81705-1A	114.0	99.6	0.67	0.72	0.69	2.14	2.82	0.05	1.86	1.57	1.07	1.26
81705-1B	139.3	134.0	0.55	0.58	0.32	1.47	1.79	0.05	1.54	1.36	1.06	1.20
81705-1C	175.2	171.4	0.44	0.46	0.29	1.25	1.54	0.05	1.63	1.46	1.11	1.24
81705-1D	207.2	204.3	0.37	0.39	0.27	1.07	1.33	0.05	1.64	1.48	1.11	1.23
81705-1E	235.3	234.1	0.33	0.35	0.13	1.07	1.19	0.05	1.85	1.67	1.47	1.63
81510-1A	118.2	99.8	0.64	0.77	1.79	4.80	6.60	0.10	2.16	1.51	0.95	1.35
81510-1B	140.8	134.5	0.54	0.62	0.78	3.29	4.07	0.10	1.74	1.33	1.02	1.33
81510-1C	175.8	171.5	0.44	0.49	0.67	2.76	3.43	0.10	1.81	1.43	1.08	1.37
81510-1D	202.7	200.2	0.38	0.42	0.45	2.27	2.72	0.10	1.70	1.36	1.09	1.36
81510-1E	236.2	234.1	0.33	0.36	0.44	2.05	2.49	0.10	1.78	1.43	1.13	1.40
81710-1A	118.8	99.5	0.64	0.76	1.88	5.07	6.95	0.10	2.29	1.61	1.01	1.44
81710-1B	142.0	135.0	0.54	0.61	0.87	3.60	4.47	0.10	1.93	1.47	1.12	1.46
81710-1C	174.6	170.1	0.44	0.49	0.69	3.16	3.85	0.10	2.05	1.63	1.27	1.60
81710-1D	206.3	203.7	0.37	0.42	0.48	2.62	3.10	0.10	2.00	1.60	1.31	1.64
81710-1E	234.7	232.7	0.33	0.37	0.42	2.40	2.82	0.10	2.08	1.67	1.38	1.71
92810-1B	128.6	123.1	0.43	0.49	0.62	2.49	3.11	0.10	2.27	1.77	1.33	1.70
92810-1C	158.5	157.5	0.35	0.40	0.14	2.00	2.14	0.10	2.21	1.77	1.64	2.06
92810-1D	189.6	188.1	0.30	0.33	0.25	1.56	1.81	0.10	2.04	1.64	1.38	1.71
92810-1E	213.4	212.7	0.26	0.29	0.13	1.42	1.56	0.10	2.08	1.69	1.53	1.89
92810-1F	241.4	240.0	0.23	0.26	0.30	1.25	1.55	0.10	2.05	1.67	1.26	1.56
80220-1A	115.8	95.4	0.49	0.67	3.85	10.14	13.99	0.20	4.00	2.14	1.32	2.48
80220-1B	134.1	124.9	0.43	0.56	2.13	7.87	10.00	0.20	3.55	2.07	1.51	2.59
80220-1C	165.8	158.6	0.35	0.44	2.09	6.27	8.36	0.20	3.45	2.12	1.41	2.30
80220-1D	192.0	189.0	0.30	0.38	1.02	5.25	6.27	0.20	3.31	2.07	1.67	2.67
80420-1A	134.4	112.4	0.49	0.66	4.85	13.03	17.88	0.20	4.39	2.44	1.53	2.76
80420-1B	149.6	135.0	0.44	0.58	3.71	10.36	14.08	0.20	3.86	2.26	1.45	2.48
80420-1C	177.4	168.9	0.38	0.48	2.63	8.41	11.04	0.20	3.67	2.25	1.54	2.52
80420-1D	204.5	197.6	0.33	0.42	2.48	7.25	9.73	0.20	3.62	2.26	1.49	2.39
81520-1A	138.6	118.8	0.55	0.76	4.56	12.59	17.15	0.20	3.29	2.22	1.49	2.39
81520-1B	159.4	150.6	0.48	0.63	2.44	9.30	11.74	0.20	2.77	1.60	1.18	2.04
81520-1C	188.6	184.8	0.41	0.52	1.27	7.61	8.88	0.20	2.66	1.62	1.35	2.22
81520-1D	215.8	212.5	0.36	0.45	1.26	6.49	7.76	0.20	2.59	1.60	1.29	2.08
81720-1A	135.0	115.8	0.56	0.80	4.31	12.28	16.58	0.20	3.13	1.57	1.02	2.03
81720-1B	160.0	151.9	0.48	0.63	2.26	9.34	11.60	0.20	2.79	1.62	1.22	2.12
81720-1C	189.2	183.2	0.41	0.52	2.00	7.74	9.74	0.20	2.72	1.65	1.22	2.01
81720-1D	214.8	212.4	0.36	0.46	0.92	6.94	7.86	0.20	2.75	1.71	1.48	2.39
81720-1E	241.7	239.4	0.32	0.40	0.99	6.05	7.04	0.20	2.69	1.69	1.41	2.25
82420-2A	96.9	74.6	0.47	0.66	3.42	7.43	10.85	0.20	3.78	1.94	1.05	2.04
82420-2B	115.5	105.2	0.40	0.52	2.03	5.25	7.28	0.20	3.14	1.83	1.12	1.93
82420-2C	148.4	142.6	0.31	0.40	1.51	3.96	5.47	0.20	3.00	1.85	1.15	1.86
82420-2D	175.5	171.7	0.27	0.33	1.18	3.34	4.52	0.20	2.97	1.86	1.21	1.92
82420-2E	203.0	199.9	0.23	0.29	1.12	2.85	3.96	0.20	2.91	1.84	1.12	1.77
82420-3A	71.0	61.3	0.36	0.48	1.15	2.76	3.91	0.20	3.32	1.85	1.08	1.94
82420-3B	85.3	79.3	0.30	0.39	0.88	2.45	3.33	0.20	3.47	2.08	1.33	2.22
81530-1A	153.3	119.4	0.50	0.83	12.40	28.11	40.51	0.30	5.38	1.95	1.09	3.01
81530-1B	168.5	149.7	0.46	0.71	8.02	22.33	30.35	0.30	4.68	1.91	1.22	3.00
81530-1C	199.3	186.8	0.39	0.58	6.47	17.21	23.69	0.30	4.23	1.90	1.18	2.64
81530-1D	222.8	212.0	0.35	0.51	6.30	15.08	21.38	0.30	4.13	1.91	1.11	2.40
81530-1E	249.9	245.2	0.31	0.45	3.12	12.94	16.07	0.30	3.96	1.87	1.42	3.01
81730-1B	169.4	150.8	0.45	0.71	7.99	20.60	28.58	0.30	4.34	1.78	1.09	2.65
81730-1C	196.3	185.9	0.39	0.59	5.33	17.66	22.99	0.30	4.28	1.91	1.33	2.99
81730-1D	220.3	211.7	0.35	0.52	4.98	15.30	20.29	0.30	4.14	1.91	1.29	2.79
81730-1E	244.7	238.5	0.32	0.46	4.02	13.61	17.63	0.30	4.08	1.92	1.35	2.88
83030-1A	79.6	61.0	0.28	0.43	3.51	6.58	10.09	0.30	7.59	3.27	1.53	3.55
83030-1B	98.5	90.2	0.23	0.34	2.10	4.85	6.95	0.30	6.80	3.14	1.78	3.85
83030-1C	127.1	121.8	0.18	0.26	1.77	3.74	5.51	0.30	6.65	3.18	1.68	3.50
83030-1D	157.3	153.8	0.15	0.21	1.46	2.85	4.31	0.30	6.19	3.00	1.46	3.02
83030-1E	181.1	178.6	0.13	0.18	1.21	2.45	3.65	0.30	6.09	2.97	1.50	3.09
83030-1F	208.2	205.8	0.11	0.16	1.33	2.14	3.47	0.30	6.07	2.97	1.12	2.28
90930-1A	113.1	90.8	0.37	0.57	6.10	12.59	18.69	0.30	5.98	2.46	1.27	3.08
90930-1B	126.8	111.0	0.33	0.50	5.04	10.72	15.76	0.30	5.68	2.50	1.32	3.01
90930-1C	150.6	142.1	0.28	0.41	3.34	8.76	12.10	0.30	5.45	2.52	1.56	3.37
90930-1D	180.1	172.7	0.23	0.34	3.50	7.38	10.89	0.30	5.45	2.59	1.36	2.87
90930-1E	204.2	198.7	0.21	0.30	2.97	6.32	9.29	0.30	5.26	2.53	1.34	2.79
90930-1F	229.2	225.0	0.19	0.27	2.56	5.20	7.76	0.30	4.85	2.35	1.19	2.46
90930-1G	250.2	246.7	0.17	0.24	2.33	5.07	7.40	0.30	5.14	2.50	1.35	2.77
90930-1H	270.4	267.7	0.16	0.23	1.95	4.63	6.58	0.30	5.05	2.46	1.42	2.92
91030-1A	83.8	64.4	0.31	0.47	3.86	7.61	11.46	0.30	7.09	2.98	1.47	3.49
91030-1B	103.6	94.6	0.25	0.37	2.39	5.78	8.18	0.30	6.54	3.00	1.76	3.84
91030-1C	133.2	127.3	0.20	0.28	2.06	4.18	6.24	0.30	5.98	2.85	1.45	3.03
91030-1D	160.0	156.9	0.16	0.24	1.32	3.43	4.74	0.30	5.83	2.82	1.73	3.59
91030-1E	183.8	181.0	0.14	0.21	1.37	3.25	4.62	0.30	6.31	3.07	1.77	3.65
91030-1F	211.2	208.9	0.12	0.18	1.30	2.89	4.19	0.30	6.42	3.14	1.73	3.54
91030-1G	232.0	230.7	0.11	0.16	0.81	2.27	3.08	0.30	5.51	2.70	1.74	3.55
91030-1H	250.5	249.4	0.11	0.15	0.74	2.14	2.87	0.30	5.59	2.74	1.79	3.66
93030-1C	140.8	122.8	0.40	0.58	5.81	16.15	21.96	0.30	5.88	2.73	1.75	3.76
93030-1D	166.1	155.4	0.34	0.48	4.21	13.57	17.78	0.30	5.76	2.84	1.96	3.97

(Continued)

TABLE A8 (Continued)

Test #	Depth US (mm)	Depth DS (mm)	V <sub>a</sub> (m/s)	V <sub>c</sub> (m/s)	F <sub>h</sub> (N)	F <sub>D</sub> (N)	F <sub>T</sub> (N)	B	C <sub>D</sub>			
									Method 1	Method 2	Method 3	Method 4
93030-1E	191.7	184.4	0.29	0.41	3.36	11.16	14.53	0.30	5.43	2.75	1.92	3.79
93030-1F	217.9	211.8	0.26	0.36	3.21	9.79	13.00	0.30	5.37	2.76	1.85	3.61
80240-1A	151.2	101.7	0.38	0.72	22.37	35.94	58.31	0.40	9.06	2.52	0.95	3.42
80240-1B	162.7	137.7	0.35	0.65	13.42	30.74	44.16	0.40	8.30	2.49	1.40	4.67
80240-1C	176.2	150.4	0.33	0.58	15.06	28.82	43.88	0.40	8.39	2.64	1.26	4.00
80240-1D	197.8	180.2	0.29	0.51	11.89	26.11	38.00	0.40	8.47	2.80	1.52	4.62
80440-1A	158.5	106.8	0.42	0.83	24.51	49.24	73.75	0.40	9.68	2.46	1.23	4.86
80440-1B	179.2	131.6	0.37	0.68	26.44	42.79	69.23	0.40	9.44	2.82	1.08	3.61
80440-1C	190.2	159.8	0.35	0.63	19.01	39.19	58.20	0.40	9.14	2.84	1.46	4.71
80440-1D	212.1	190.0	0.32	0.55	15.88	31.72	47.60	0.40	8.21	2.68	1.34	4.10
80440-1E	232.2	212.1	0.29	0.50	15.96	28.56	44.52	0.40	8.06	2.70	1.19	3.55
80840-1A	124.7	86.4	0.34	0.64	14.46	23.58	38.04	0.40	8.96	2.53	0.98	3.46
80840-1B	140.8	119.3	0.30	0.54	10.00	18.33	28.33	0.40	7.80	2.43	1.10	3.54
80840-1C	159.1	142.0	0.27	0.47	9.21	15.84	25.05	0.40	7.55	2.48	1.04	3.16
80840-1D	185.0	173.9	0.23	0.40	7.13	13.26	20.38	0.40	7.29	2.49	1.15	3.37
80940-1B	93.9	77.8	0.25	0.45	4.95	8.45	13.40	0.40	7.89	2.45	1.02	3.28
80940-1C	116.7	109.1	0.20	0.35	3.07	6.45	9.52	0.40	7.33	2.47	1.29	3.84
80940-1D	145.4	139.8	0.16	0.28	2.86	5.25	8.11	0.40	7.31	2.55	1.16	3.33
83050-1B	106.1	88.4	0.21	0.47	7.70	12.72	20.42	0.50	11.46	2.43	0.96	4.53
83050-1C	130.1	118.9	0.18	0.37	6.24	9.65	15.89	0.50	10.54	2.43	0.86	3.73
83050-1D	157.6	150.2	0.15	0.30	5.09	7.61	12.70	0.50	9.94	2.38	0.79	3.29
83050-1E	181.1	175.5	0.13	0.26	4.46	6.49	10.96	0.50	9.69	2.36	0.74	3.03
83050-1F	205.7	201.5	0.11	0.23	3.82	5.74	9.56	0.50	9.69	2.38	0.79	3.23
83050-1G	226.8	223.4	0.10	0.21	3.42	5.16	8.58	0.50	9.56	2.36	0.79	3.22
83050-1H	245.7	242.6	0.09	0.19	3.38	4.72	8.10	0.50	9.44	2.33	0.66	2.67
90850-1B	152.7	125.0	0.28	0.61	17.20	25.35	42.55	0.50	9.60	1.96	0.63	3.09
90850-1C	174.3	153.0	0.24	0.51	15.59	22.77	38.36	0.50	9.78	2.17	0.68	3.09
90850-1D	196.9	179.7	0.21	0.45	14.48	20.91	35.39	0.50	10.09	2.33	0.72	3.10
90850-1E	217.6	204.7	0.19	0.40	12.18	18.82	31.00	0.50	10.00	2.36	0.83	3.53
90850-1F	241.4	230.7	0.18	0.36	11.29	16.50	27.80	0.50	9.69	2.33	0.73	3.06
90850-1G	260.9	252.4	0.16	0.33	9.76	15.08	24.83	0.50	9.55	2.31	0.82	3.37
90850-1H	276.8	269.5	0.15	0.31	8.92	14.19	23.11	0.50	9.51	2.31	0.86	3.53
91050-1B	117.3	93.0	0.22	0.48	11.43	17.13	28.55	0.50	13.05	2.79	0.93	4.34
91050-1C	139.3	123.9	0.19	0.39	9.06	14.77	23.83	0.50	13.23	3.04	1.17	5.11
91050-1D	166.1	156.8	0.16	0.32	6.71	11.08	17.79	0.50	11.72	2.79	1.10	4.62
91050-1E	188.4	179.4	0.14	0.28	7.40	9.74	17.14	0.50	11.62	2.81	0.68	2.79
91050-1F	214.3	209.5	0.12	0.25	4.55	8.32	12.87	0.50	11.23	2.75	1.24	5.09
91050-1G	234.7	230.0	0.11	0.23	4.88	7.70	12.58	0.50	11.35	2.79	1.02	4.15
91050-1H	253.3	249.6	0.10	0.21	4.16	7.25	11.41	0.50	11.51	2.84	1.21	4.91
91050-1I	288.2	284.8	0.10	0.20	4.05	6.76	10.81	0.50	11.35	2.81	1.12	4.55
73060-1A	113.4	57.8	0.22	0.64	25.60	28.82	54.42	0.60	19.85	2.25	0.25	2.22
73060-1B	116.1	78.4	0.21	0.62	19.67	26.33	46.01	0.60	18.53	2.18	0.55	4.69
73060-1C	131.1	106.7	0.19	0.52	15.57	20.95	36.52	0.60	16.46	2.19	0.56	4.23
80260-1A	193.5	105.9	0.30	0.94	70.29	90.83	161.12	0.60	19.25	1.95	0.44	4.35
80260-1B	199.3	131.9	0.29	0.88	59.83	79.89	139.72	0.60	17.41	1.91	0.48	4.37
80260-1C	207.6	152.7	0.28	0.81	53.01	72.64	125.65	0.60	16.46	1.95	0.53	4.45
80260-1D	222.5	178.4	0.26	0.73	47.38	64.10	111.48	0.60	15.52	1.99	0.52	4.05
80260-1E	245.3	212.2	0.24	0.64	40.59	55.56	96.14	0.60	14.76	2.03	0.55	3.98
81860-1	109.1	82.1	0.20	0.57	13.84	16.32	30.16	0.60	13.88	1.68	0.26	2.12
81860-1A	130.1	113.3	0.17	0.45	10.96	12.72	23.68	0.60	12.75	1.77	0.25	1.77
81860-1B	156.3	146.2	0.14	0.36	8.19	10.50	18.69	0.60	12.51	1.85	0.41	2.75
81860-1C	180.1	172.9	0.12	0.31	6.81	8.90	15.71	0.60	12.14	1.85	0.43	2.84
81860-1D	204.8	199.4	0.11	0.27	5.85	7.74	13.59	0.60	11.95	1.85	0.45	2.92
81860-1E	232.8	229.0	0.09	0.24	4.70	6.76	11.46	0.60	11.81	1.84	0.56	3.59
82160-1	111.2	80.8	0.20	0.55	15.66	18.99	34.65	0.60	16.42	2.03	0.36	2.88
82160-1A	133.5	114.8	0.16	0.44	12.46	14.46	26.91	0.60	14.83	2.09	0.29	2.05
82160-1B	157.2	144.8	0.14	0.36	10.05	12.01	22.06	0.60	14.38	2.13	0.35	2.35
82160-1C	181.9	173.2	0.12	0.31	8.29	10.28	18.56	0.60	14.14	2.16	0.42	2.73
82160-1D	207.2	200.1	0.11	0.27	7.76	9.12	16.88	0.60	14.22	2.20	0.33	2.12
82460-1	111.2	79.0	0.19	0.55	16.43	20.19	36.63	0.60	17.63	2.19	0.41	3.29
82460-2A	166.1	94.1	0.28	0.91	50.26	66.32	116.58	0.60	18.32	1.75	0.42	4.44
82460-2B	174.6	107.7	0.27	0.81	50.67	58.40	109.07	0.60	16.92	1.88	0.25	2.24
82460-2C	184.1	135.2	0.26	0.73	41.89	50.89	92.78	0.60	15.51	1.88	0.33	2.74
82460-2D	202.0	166.6	0.23	0.64	35.01	43.81	78.82	0.60	14.60	1.94	0.39	2.93
82460-2E	223.4	195.7	0.21	0.56	31.14	37.90	69.04	0.60	13.91	1.96	0.35	2.48
82460-2F	244.4	223.5	0.19	0.51	26.24	33.67	59.91	0.60	13.48	1.96	0.43	2.98
83080-1	150.9	30.5	0.15	1.05	78.13	76.78	154.90	0.80	60.19	1.26	-0.02	-1.06
83080-1A	150.9	42.3	0.15	1.05	75.06	77.58	152.63	0.80	60.82	1.27	0.04	1.98
83080-1B	157.3	74.3	0.15	1.05	68.76	72.55	141.31	0.80	59.17	1.14	0.06	3.09
83080-1C	169.2	114.0	0.14	0.89	55.92	64.81	120.73	0.80	56.66	1.32	0.18	7.77
83080-1D	186.2	143.7	0.12	0.73	50.16	57.03	107.18	0.80	54.70	1.60	0.19	6.59
83080-1E	204.2	169.4	0.11	0.63	46.51	50.71	97.22	0.80	53.14	1.71	0.14	4.40
83080-1F	223.7	192.8	0.10	0.56	46.04	45.86	91.90	0.80	52.48	1.79	-0.01	-0.20
83080-1G	239.9	215.4	0.10	0.52	39.90	42.17	82.07	0.80	51.58	1.81	0.10	2.77
83080-1H	257.3	236.7	0.09	0.48	36.40	38.52	74.92	0.80	50.43	1.81	0.10	2.77
90680-1	64.9	16.6	0.11	0.72	14.08	14.15	28.23	0.80	52.11	1.17	0.01	0.23
90680-1A	66.1	28.6	0.11	0.72	12.70	13.43	26.14	0.80	50.30	1.09	0.06	2.73
90680-1B	78.0	55.6	0.09	0.56	10.71	10.99	21.69	0.80	47.70	1.22	0.03	1.22
90680-1C	100.6	88.0	0.07	0.38	8.50	8.41	16.91	0.80	45.96	1.56	-0.02	-0.51
90680-1D	125.6	118.0	0.06	0.30	6.62	6.89	13.52	0.80	46.37	1.69	0.07	1.83
90680-1E	148.4	142.8	0.05	0.25	5.83	5.92	11.75	0.80	46.64	1.75	0.02	0.65
90680-1F	171.6	167.5	0.04	0.22	4.97	5.20	10.18	0.80	47.10	1.80	0.08	2.09
90680-1G	189.0	185.5	0.04	0.20	4.69	4.80	9.49	0.80	47.64	1.83	0.04	1.14

(Continued)

TABLE A8 (Continued)

Test #	Depth US (mm)	Depth DS (mm)	V <sub>a</sub> (m/s)	V <sub>c</sub> (m/s)	F <sub>h</sub> (N)	F <sub>D</sub> (N)	F <sub>T</sub> (N)	B	C <sub>D</sub>			
									Method 1	Method 2	Method 3	Method 4
90880-1H	209.1	206.2	0.03	0.18	4.31	4.40	8.71	0.80	48.17	1.86	0.04	1.04
90880-1I	221.3	218.7	0.03	0.17	4.09	4.18	8.27	0.80	48.26	1.87	0.04	1.03
90880-1J	230.4	228.0	0.03	0.16	3.94	4.05	7.98	0.80	48.62	1.88	0.05	1.35
90880-1K	263.0	261.2	0.03	0.14	3.38	3.56	6.93	0.80	48.56	1.89	0.10	2.50
90880-1	237.7	40.9	0.18	1.29	196.13	195.14	391.28	0.80	70.57	1.36	-0.01	-0.36
90880-1A	237.7	88.7	0.18	1.29	173.97	195.32	369.29	0.80	70.63	1.36	0.15	7.72
90880-1B	242.0	118.4	0.18	1.29	159.35	188.20	347.55	0.80	69.25	1.28	0.20	10.62
90880-1C	253.6	149.7	0.17	1.11	149.90	176.90	326.80	0.80	68.11	1.54	0.24	10.40
90880-1D	266.1	173.6	0.16	0.98	145.49	166.18	311.68	0.80	67.04	1.78	0.22	8.35
90880-1E	280.7	200.7	0.15	0.89	137.77	154.98	292.74	0.80	65.84	1.92	0.21	7.31
90980-1	173.7	35.3	0.15	1.10	103.47	104.13	207.61	0.80	71.89	1.36	0.01	0.45
90980-1A	174.7	49.6	0.15	1.10	100.38	104.49	204.87	0.80	72.45	1.35	0.05	2.85
90980-1B	178.9	85.7	0.15	1.10	88.22	99.60	187.81	0.80	70.72	1.26	0.14	8.08
90980-1C	189.9	117.1	0.14	0.87	79.95	90.48	170.43	0.80	68.03	1.74	0.20	7.91
90980-1D	205.4	150.6	0.13	0.75	69.79	80.73	150.52	0.80	65.45	1.93	0.26	8.87
90980-1E	221.3	176.1	0.12	0.67	64.26	73.44	137.70	0.80	63.91	2.04	0.25	7.92
90980-1F	240.8	202.4	0.11	0.60	60.88	66.99	127.87	0.80	63.31	2.14	0.19	5.77
90980-1G	257.3	223.7	0.10	0.55	57.81	62.36	120.18	0.80	62.80	2.19	0.16	4.58
90980-1H	273.7	243.9	0.10	0.51	55.18	58.36	113.54	0.80	62.45	2.22	0.12	3.41
72990-1A	234.4	52.6	0.11	1.37	210.00	216.45	426.44	0.90	196.23	1.19	0.04	5.85
72990-1B	239.3	79.3	0.10	1.37	205.16	216.81	421.97	0.90	200.32	1.17	0.06	10.76
72990-1C	251.8	127.3	0.10	1.37	189.96	209.60	399.56	0.90	203.36	1.08	0.10	19.06
72990-1D	267.0	164.0	0.09	1.37	178.67	197.46	376.12	0.90	202.83	0.96	0.09	19.30
81890-1A	216.7	45.6	0.10	1.31	180.45	180.20	360.64	0.90	195.78	1.18	0.00	-0.27
81890-1B	221.8	71.1	0.10	1.31	177.47	177.62	355.09	0.90	197.36	1.13	0.00	0.16
81890-1C	231.6	110.1	0.10	1.31	166.92	176.10	343.03	0.90	204.02	1.07	0.06	10.63
81890-1D	242.3	143.7	0.09	1.31	153.03	168.99	322.01	0.90	204.51	0.99	0.09	19.32
81890-1E	257.2	169.3	0.09	1.31	150.73	160.18	310.91	0.90	205.38	0.88	0.05	12.11
81890-1F	270.9	192.0	0.08	1.06	146.85	152.08	298.93	0.90	205.07	1.21	0.04	7.06
82090-1A	222.5	76.0	0.10	1.31	176.00	183.13	359.13	0.90	203.90	1.16	0.05	7.94
82090-1B	233.1	111.9	0.09	1.31	168.29	178.91	347.20	0.90	208.35	1.08	0.06	12.36
82090-1C	244.1	146.0	0.09	1.31	154.02	172.63	326.66	0.90	210.21	1.00	0.11	22.67
82090-1D	257.5	169.3	0.09	1.31	151.51	161.87	313.38	0.90	207.58	0.89	0.06	13.29
82090-1E	273.7	199.0	0.08	1.04	142.12	153.73	295.84	0.90	209.16	1.28	0.10	15.80
82790-1A	208.8	68.2	0.10	1.29	156.75	162.18	318.93	0.90	185.89	1.13	0.04	6.23
82790-1B	218.5	108.5	0.10	1.29	144.77	158.09	302.86	0.90	189.30	1.05	0.09	15.95
82790-1C	233.4	140.4	0.09	1.29	139.91	149.46	289.37	0.90	190.73	0.93	0.06	12.18
82790-1D	245.6	161.5	0.09	1.29	137.79	142.08	279.87	0.90	190.47	0.84	0.03	5.74
82790-1E	261.8	189.0	0.08	1.06	132.08	134.20	266.29	0.90	191.40	1.12	0.02	3.02
82790-1F	274.3	208.4	0.08	0.95	128.03	128.15	256.18	0.90	191.23	1.26	0.00	0.19
82790-1G	277.9	219.9	0.08	0.93	116.20	125.35	241.55	0.90	189.44	1.28	0.09	13.82
82890-1A	205.4	42.1	0.10	1.29	162.67	165.47	328.14	0.90	186.69	1.17	0.02	3.17
82890-1B	210.0	72.3	0.10	1.29	156.45	162.23	318.68	0.90	186.97	1.12	0.04	6.66
90190-1	98.8	16.5	0.07	0.91	38.19	36.79	74.98	0.90	175.80	1.10	-0.04	-6.71
90190-1A	98.8	28.9	0.07	0.91	35.93	37.01	72.93	0.90	176.87	1.11	0.03	5.18
90190-1B	103.0	57.5	0.07	0.91	29.39	35.32	64.71	0.90	175.75	1.02	0.17	29.49
90190-1C	125.9	90.7	0.06	0.75	30.69	32.03	62.71	0.90	191.87	1.10	0.05	8.04
90190-1D	147.2	121.5	0.05	0.56	27.79	28.69	56.48	0.90	199.48	1.50	0.05	6.24
90190-1E	161.5	141.5	0.04	0.50	24.39	26.51	50.90	0.90	201.28	1.62	0.13	16.11
90190-1F	176.2	159.2	0.04	0.45	22.95	24.51	47.46	0.90	201.98	1.70	0.11	12.87
90190-1G	193.2	178.1	0.04	0.40	22.57	22.73	45.30	0.90	204.82	1.78	0.01	1.49
90190-1H	204.5	190.8	0.04	0.38	21.80	22.11	43.90	0.90	210.39	1.85	0.03	2.96
90190-1I	223.4	211.6	0.03	0.34	20.66	20.60	41.25	0.90	213.41	1.91	-0.01	-0.66
90190-1J	234.1	223.4	0.03	0.33	19.70	19.79	39.50	0.90	214.41	1.93	0.01	1.00
90190-1K	247.2	237.6	0.03	0.31	18.73	18.90	37.64	0.90	216.03	1.96	0.02	1.98
90190-1L	259.1	250.3	0.03	0.29	18.04	18.19	36.23	0.90	217.42	1.98	0.02	1.81
90190-1M	271.3	263.3	0.03	0.28	17.21	17.57	34.78	0.90	219.58	2.01	0.04	4.47
81890-1C	231.6	110.1	0.10	1.31	166.92	176.10	343.03	0.90	204.02	1.07	0.06	10.63
81890-1D	242.3	143.7	0.09	1.31	153.03	168.99	322.01	0.90	204.51	0.99	0.09	19.32
81890-1E	257.2	169.3	0.09	1.31	150.73	160.18	310.91	0.90	205.38	0.88	0.05	12.11
81890-1F	270.9	192.0	0.08	1.06	146.85	152.08	298.93	0.90	205.07	1.21	0.04	7.06
82090-1A	222.5	76.0	0.10	1.31	176.00	183.13	359.13	0.90	203.90	1.16	0.05	7.94
82090-1B	233.1	111.9	0.09	1.31	168.29	178.91	347.20	0.90	208.35	1.08	0.06	12.36
82090-1C	244.1	146.0	0.09	1.31	154.02	172.63	326.66	0.90	210.21	1.00	0.11	22.67
82090-1D	257.5	169.3	0.09	1.31	151.51	161.87	313.38	0.90	207.58	0.89	0.06	13.29
82090-1E	273.7	199.0	0.08	1.04	142.12	153.73	295.84	0.90	209.16	1.28	0.10	15.80
82790-1A	208.8	68.2	0.10	1.29	156.75	162.18	318.93	0.90	185.89	1.13	0.04	6.23
82790-1B	218.5	108.5	0.10	1.29	144.77	158.09	302.86	0.90	189.30	1.05	0.09	15.95
82790-1C	233.4	140.4	0.09	1.29	139.91	149.46	289.37	0.90	190.73	0.93	0.06	12.18
82790-1D	245.6	161.5	0.09	1.29	137.79	142.08	279.87	0.90	190.47	0.84	0.03	5.74
82790-1E	261.8	189.0	0.08	1.06	132.08	134.20	266.29	0.90	191.40	1.12	0.02	3.02
82790-1F	274.3	208.4	0.08	0.95	128.03	128.15	256.18	0.90	191.23	1.26	0.00	0.19
82790-1G	277.9	219.9	0.08	0.93	116.20	125.35	241.55	0.90	189.44	1.28	0.09	13.82
82890-1A	205.4	42.1	0.10	1.29	162.67	165.47	328.14	0.90	186.69	1.17	0.02	3.17
82890-1B	210.0	72.3	0.10	1.29	156.45	162.23	318.68	0.90	186.97	1.12	0.04	6.66
90190-1	98.8	16.5	0.07	0.91	38.19	36.79	74.98	0.90	175.80	1.10	-0.04	-6.71
90190-1A	98.8	28.9	0.07	0.91	35.93	37.01	72.93	0.90	176.87	1.11	0.03	5.18
90190-1B	103.0	57.5	0.07	0.91	29.39	35.32	64.71	0.90	175.75	1.02	0.17	29.49
90190-1C	125.9	90.7	0.06	0.75	30.69	32.03	62.71	0.90	191.87	1.10	0.05	8.04
90190-1D	147.2	121.5	0.05	0.56	27.79	28.69	56.48	0.90	199.48	1.50	0.05	6.24
90190-1E	161.5	141.5	0.04	0.50	24.39	26.51	50.90	0.90	201.28	1.62	0.13	16.11
90190-1F	176.2	159.2	0.04	0.45	22.95	24.51	47.46	0.90	201.98	1.70	0.11	12.87
90190-1G	193.2	178.1	0.04	0.40	22.57	22.73	45.30	0.90	204.82	1.78	0.01	1.49
90190-1H	204.5	190.8	0.04	0.38	21.80	22.11	43.90	0.90	210.39	1.85	0.03	2.96
90190-1I	223.4	211.6	0.03	0.34	20.66	20.60	41.25	0.90	213.41	1.91	-0.01	-0.66
90190-1J	234.1	223.4	0.03	0.33	19.70	19.79	39.50	0.90	214.41	1.93	0.01	1.00
90190-1K	247.2	237.6	0.03	0.31	18.73	18.90	37.64	0.90	216.03	1.96	0.02	1.98
90190-1L	259.1	250.3	0.03	0.29	18.04	18.19	36.23	0.90	217.42	1.98	0.02	1.81
90190-1M	271.3	263.3	0.03	0.28	17.21	17.57	34.78	0.90	219.58	2.01	0.04	4.47

## PART 3: ANALYSIS OF DRAG AND HYDROSTATIC FORCE

### INTRODUCTION

*NCHRP Report 417*, "Highway Infrastructure Damage Caused by the 1993 Upper Mississippi River Basin Flooding" (Parola et al. 1998a) and an examination of other case studies that are described in the State-of-Knowledge Account (see Part 1) have shown that blockage of large portions of the stream channels by debris is an important aspect of site conditions where bridges have collapsed because of debris forces. Analysis of the data was conducted to determine the most reliable parameters for determining drag and hydrostatic forces. The large amount of data available from the University of Louisville plate-blockage tests spanned the entire range of flow blockage (5–90 percent) and a wide range of subcritical flow Froude numbers. Therefore, analysis of the University of Louisville blockage data was used to determine the appropriate reference velocity for the drag equation and to determine the effectiveness of partitioning the total horizontal streamwise force into drag and hydrostatic components. The analysis focused on the variation of drag coefficient as a function primarily of flow-blockage ratio. The influence of flow Froude number and Reynolds number were also considered.

After the appropriate reference velocities and the method for partitioning drag and hydrostatic forces were established, drag coefficients for the small-scale, idealized-debris data from the University of Queensland and for the medium-scale data from WES were developed and compared with the plate data. The Queensland and WES data sets essentially served as verification data for the relation established among the simplified plate-blockage tests.

### METHODS OF DATA ANALYSIS

Drag coefficients were computed from the University of Louisville full-depth, vertical-plate data, using the combinations of reference velocity and forces shown in Table A9. The variation of drag coefficient was then examined for each of the computation methods.

In Method 1, the drag force was considered as the total horizontal force on the test apparatus, and the approach-flow velocity was considered as the reference velocity.

In Method 2, the drag force was considered as the total horizontal force on the test apparatus. The average-flow velocity in the contracted section of the bridge opening was considered as the reference velocity.

In Method 3, the drag force was considered the difference between (a) the total horizontal force on the bridge; and (b) the hydrostatic force, which is computed from the difference

between the total force created by the upstream hydrostatic pressure and that created by the downstream hydrostatic pressure. The reference velocity used to compute the drag coefficient in Method 3 was the average flow velocity in the contracted section of the bridge opening.

In Method 4, the drag force was considered to be the same as in Method 3. The average approach velocity was used as the reference velocity.

The four methods for computing drag coefficients produce substantially different drag coefficients. The details of each method are provided in the following sections.

#### Method 1: Use Approach Flow as Reference Velocity

The drag coefficient for Method 1 was computed as

$$C_D = \frac{F_x}{\rho A_{OV} \frac{(V_a)^2}{2}} \quad (\text{A13})$$

where

$C_D$  = drag coefficient;

$A_{OV}$  = projected area of an obstruction normal to the flow direction and below the upstream water surface,  $\text{m}^2$ ;

$V_a$  = average approach-flow velocity,  $\text{m/s}$ ;

$F_x$  = water pressure force acting in the flow direction on the submerged bridge at point  $x$ ,  $\text{N}$ ; and

$\rho$  = fluid density,  $\text{Kg/m}^3$ .

The average approach-flow velocity was computed as

$$V_a = \frac{Q}{A_T} \quad (\text{A14})$$

where

$V_a$  = average approach-flow velocity,  $\text{m/s}$ ;

$Q$  = flow rate,  $\text{m}^3/\text{s}$ ; and

$A_T$  = flow area based on water surface elevation and channel geometry 0.95 m upstream of the upstream face of the plate.

The Method 1 Froude number for the approach flow was computed as

$$Fr = \frac{V_a}{\sqrt{gY_a}} \quad (\text{A15})$$

TABLE A9 Drag coefficient analysis method

Method	Reference Velocity for Drag Coefficient Computation	Force for Drag Coefficient Computation
1	Approach	Total
2	Contracted	Total
3	Contracted	Total - Hydrostatic
4	Approach	Total - Hydrostatic

where

$Fr$  = Froude number;  
 $V_a$  = average approach-flow velocity, m/s;  
 $g$  = gravitational acceleration constant (9.81 m/s<sup>2</sup>); and  
 $Y_a$  = approach-flow water depth at 0.95 m upstream of the upstream face of the plate, m.

The Method 1 Reynolds number for the approach flow was computed as

$$Re = \frac{WV_a}{\nu} \quad (A16)$$

where

$Re$  = Reynolds number,  
 $W$  = blockage width, m;  
 $V_a$  = average approach-flow velocity, m/s; and  
 $\nu$  = kinematic viscosity, m<sup>2</sup>/s.

### Method 2: Use Average Contracted Flow as Reference Velocity

The drag coefficient for Method 2 was computed as

$$C_D = \frac{F_x}{\rho A_{OU} \frac{(V_c)^2}{2}} \quad (A17)$$

where

$C_D$  = drag coefficient;  
 $F_x$  = water pressure force acting in the flow direction on the submerged bridge at point  $x$ , N;  
 $\rho$  = fluid density, Kg/m<sup>3</sup>;  
 $A_{OU}$  = projected area of an obstruction normal to the flow direction and below the upstream water surface, m<sup>2</sup>; and  
 $V_c$  = contracted-flow velocity, m/s.

The average contracted-flow velocity was computed as

$$V_c = \frac{Q}{A_c} \quad (A18)$$

where

$V_c$  = contracted-flow velocity, m/s;  
 $Q$  = flow rate, m<sup>3</sup>/s; and

$A_c$  = unobstructed cross-sectional flow area in the contracted section, m<sup>2</sup>.

The contracted-flow velocity and area were computed, assuming there were no losses from the approach-flow section to the contraction, as

$$WSE_a + \frac{V_a}{2g} = WSE_c + \frac{V_c}{2g} \quad (A19)$$

where

$WSE_a$  = approach-flow water surface elevation, m;  
 $V_a$  = average approach-flow velocity, m/s;  
 $g$  = gravitational acceleration constant (9.81 m/s<sup>2</sup>);  
 $WSE_c$  = contracted-flow water surface elevation, m; and  
 $V_c$  = contracted-flow velocity, m/s.

In some flow cases, critical conditions were computed in the plate contraction. For these conditions, critical depth and velocity were assumed as the contracted-flow conditions. The Method 2 Froude number for the contracted flow was computed as

$$Fr_c = \frac{V_c}{\sqrt{gY_c}} \quad (A20)$$

where

$Fr$  = contracted-flow Froude number;  
 $V_c$  = contracted-flow velocity, m/s;  
 $g$  = gravitational acceleration constant (9.81 m/s<sup>2</sup>); and  
 $Y_c$  = average flow depth in the flow contraction, m.

The Method 2 Reynolds number for the contracted flow was computed as

$$Re_c = \frac{WV_c}{\nu} \quad (A21)$$

where

$Re_c$  = contracted-flow Reynolds number;  
 $W$  = blockage width, m;  
 $V_c$  = contracted-flow velocity, m/s; and  
 $\nu$  = kinematic viscosity, m<sup>2</sup>/s.

### Method 3: Use Contracted Flow as Reference Velocity and Use Hydrostatic Pressure Reduction

In this method, the force was partitioned into a drag force and a hydrostatic force. The drag force was computed as

$$F_D = F_x - F_{hx} \quad (\text{A22})$$

where

- $F_D$  = drag force, N;
- $F_x$  = water pressure force on the plate in the streamwise direction that is due to stream flow, N; and
- $F_{hx}$  = hydrostatic force attributed to average streamwise-pressure gradients, N.

The variation in mean water surface elevation is considered to create the hydrostatic force on the plate. The hydrostatic force on the upstream side of the plate was computed as

$$F_{hu} = w h_{cou} A_{ou} \quad (\text{A23})$$

where

- $F_{hu}$  = hydrostatic force on the upstream side of the obstruction, N;
- $w$  = specific weight of water (9,810 N/m<sup>3</sup>);
- $h_{cou}$  = vertical distance from the water surface to the centroid of area  $A_{ou}$ , m; and
- $A_{ou}$  = projected area of an obstruction normal to the flow direction and below the upstream water surface, m<sup>2</sup>.

Likewise, the hydrostatic force on the downstream side of the plate was computed as

$$F_{hd} = w h_{cod} A_{od} \quad (\text{A24})$$

where

- $F_{hd}$  = hydrostatic force on the downstream side of the obstruction, N;
- $w$  = specific weight of water (9,810 N/m<sup>3</sup>);
- $h_{cod}$  = vertical distance from the water surface to the centroid of area  $A_{od}$ , m; and
- $A_{od}$  = projected area obstructed by the plate normal to the flow direction and below the downstream water surface, m<sup>2</sup>.

The hydrostatic force attributed to average streamwise pressure gradients was computed as

$$F_{hx} = F_{hu} - F_{hd} \quad (\text{A25})$$

where

- $F_{hx}$  = hydrostatic force attributed to average streamwise pressure gradients, N;
- $F_{hu}$  = hydrostatic force on the upstream side of the obstruction, N; and
- $F_{hd}$  = hydrostatic force on the downstream side of the obstruction, N.

The Method 3 drag coefficient was computed as

$$C_D = \frac{F_D}{\rho A_{ou} \frac{(V_c)^2}{2}} \quad (\text{A26})$$

where

- $C_D$  = drag coefficient;
- $F_D$  = drag force, N;
- $\rho$  = fluid density, Kg/m<sup>3</sup>;
- $A_{ou}$  = projected area of an obstruction normal to the flow direction and below the upstream water surface, m<sup>2</sup>; and
- $V_c$  = contracted-flow velocity, m/s.

The reference velocity was computed as the contracted-flow velocity from Equation A18. The contracted-flow velocity and area were computed, assuming there were no losses from the approach-flow section to the contraction, using Equation A19. The Froude number for the constricted flow was computed using Equation A20. The Reynolds number for the constricted flow was computed using Equation A21.

### Method 4: Use Approach Flow as Reference Velocity and Use Hydrostatic Pressure Reduction

This method is similar to Method 3, except that the approach-flow velocity instead of the contracted-flow velocity was used as the reference velocity in the drag equation. The horizontal force was separated into hydrostatic force and drag force. The drag force of the submerged portions of the full-depth rectangular plate was computed using Equation A22.

The hydrostatic force difference was computed using Equation A25. The drag coefficient for Method 4 was computed as

$$C_D = \frac{F_D}{\rho A_{ou} \frac{(V_a)^2}{2}} \quad (\text{A27})$$

where

- $C_D$  = drag coefficient;
- $F_D$  = drag force, N;
- $\rho$  = fluid density, Kg/m<sup>3</sup>;

$A_{ou}$  = projected area of an obstruction normal to the flow direction and below the upstream water surface, m<sup>2</sup>; and

$V_a$  = average approach-flow velocity, m/s.

## RESULTS OF ANALYSIS

Drag coefficients from the University of Louisville full-depth plate experiments were computed using the four methods described in the previous section. The variation of drag coefficient with Froude number, Reynolds number, and blockage ratio was examined. Flow-blockage ratio was defined as

$$B = \frac{A_b}{A_b + A_c} \quad (\text{A28})$$

where

$B$  = flow-blockage ratio;

$A_b$  = flow area blocked by debris in the contracted bridge section, m<sup>2</sup>; and

$A_c$  = unobstructed cross-sectional flow area in the contracted section, m<sup>2</sup>.

The most influential factor regarding variation of drag coefficient was found to be flow-blockage ratio. Against each method, the variation of drag coefficient was examined to determine the effect of flow-blockage ratio, Froude number, and Reynolds number. However, only the description of the Method 3 results includes the effect of Froude number and Reynolds number.

### Method 1 Results

The drag coefficient was calculated from the total force (that is, there was no partitioning into drag and hydrostatic forces), and the approach-flow velocity was considered the reference velocity. The drag coefficient, based on this method, varies dramatically from about 1.5 at 5-percent blockage to 220 at 90-percent blockage, as shown in Figure A27. The effect of flow-blockage ratio above 40 percent is dramatic. As flow becomes highly contracted, the drag coefficient increases rapidly and approaches infinity at a 100-percent blockage (that is, the structure becomes a dam). The very high drag coefficient is associated with the large total force that develops as the flow-blockage ratio increases from 60–90 percent, although the effect is apparent at a flow-blockage ratio of 20 percent. In addition, the

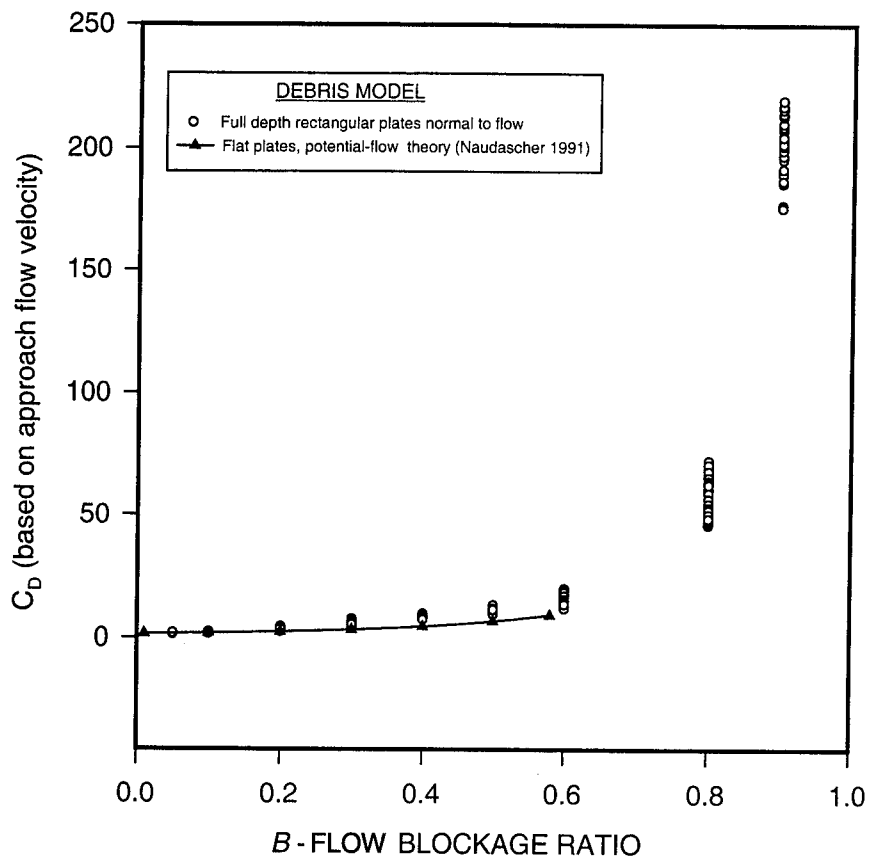


Figure A27. Method 1 variation of drag coefficient with blockage ratio.

approach velocity (used as the reference velocity) decreases as the blockage ratio increases because of the backwater effect. Naudascher (1991) predicted this effect theoretically, as indicated in Figure A27. The lack of accuracy in predicting velocity under even moderately contracted conditions, in combination with the high sensitivity of the drag coefficient to small changes in blockage ratio, limits the usefulness of this method.

### Method 2 Results

The drag coefficient was calculated from the total force (that is, there was no partitioning into drag and hydrostatic forces), and the contracted-flow velocity was considered the reference velocity. Figure A28 shows the variation of drag coefficient with blockage ratio. The drag coefficient varies from a range typical of a plate in free-stream flow at low blockage ratios, increases to a maximum value at approximately 30-percent blockage, and decreases with increased blockage widths. Overall, the drag coefficient varies from about 0.8, at 90-percent blockage, to 3.2, at 30-percent blockage. Method 2 is satisfactory for blockage widths shorter than 60 percent; however, as the blockage ratio approaches 100 percent, the forces have an unacceptably high variation. As the blockage ratio approaches 100 percent (that is, dam condition), the forces approach the difference in hydrostatic pressures between the upstream and downstream sides of the obstruction. This force difference can be calculated well within the accuracy of known water-surface-elevation dif-

ferences from the upstream to the downstream sides of the obstruction.

### Method 3 Results

Figure A29 shows the variation of the Method 3 drag coefficient with blockage ratio. The reduction of the total force by the hydrostatic force reduces the drag coefficient for blockage widths greater than approximately 30 percent. The drag coefficient approaches zero at the limit of 100-percent blockage, where the total force becomes completely hydrostatic. At low blockage ratios, the effect of flow contraction and the low water-surface-elevation differences associated with low contraction effects have a small effect on the drag coefficient. The drag coefficient tends to increase to a maximum at about 30-percent blockage. Although forces increase beyond 30-percent blockage, the partitioning into hydrostatic and drag forces causes the drag coefficient to decrease. This method provides drag coefficients similar to those obtained for flat plates in free-stream conditions under low-blockage conditions. At high-blockage conditions, the effect of drag is diminished while the pressure distribution approaches hydrostatic conditions upstream and downstream of the obstacle. Computation of drag coefficients using the model of Method 3 shows a gradual transition from drag-dominated force conditions at low-blockage ratios to hydrostatic-dominated force conditions at high-blockage ratios.

Figures A30 and A31 show the effects of Froude number and Reynolds number on the Method 3 drag coefficient. For

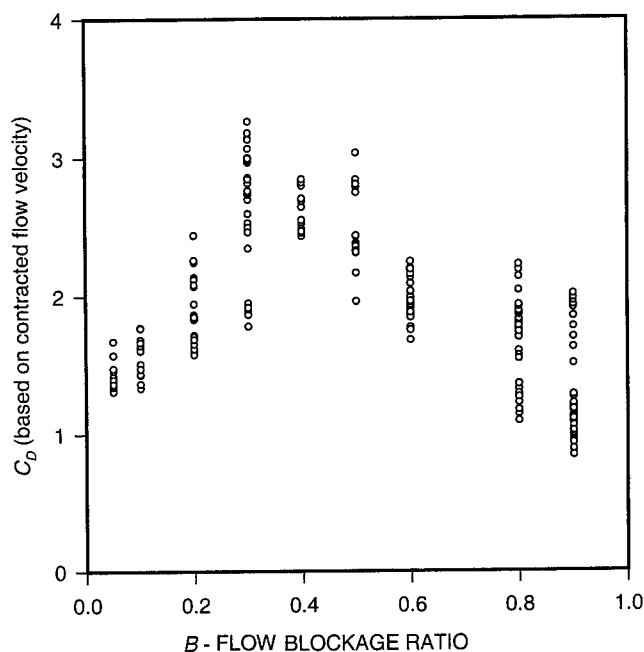


Figure A28. Method 2 variation of drag coefficient with blockage ratio.

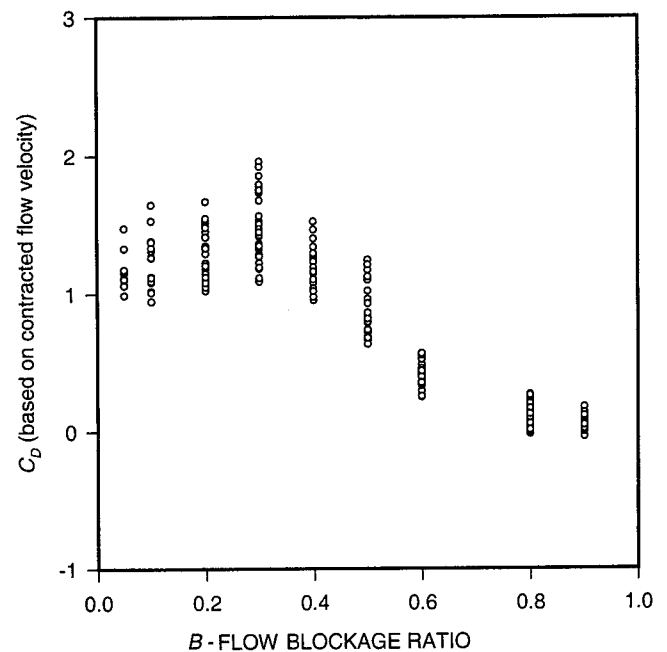


Figure A29. Method 3 variation of drag coefficient with blockage ratio.

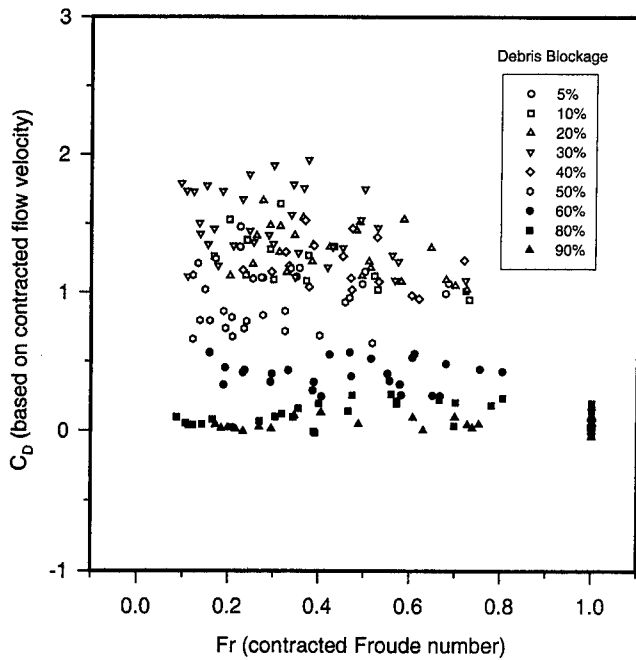


Figure A30. Method 3 variation of drag coefficient with Froude number.

blockage less than 40 percent, a trend of decreasing drag coefficient with increased Froude number is apparent. A conservative envelope relation between drag coefficient and Froude number is

$$C_D = 3 - 2.5Fr \tag{A29}$$

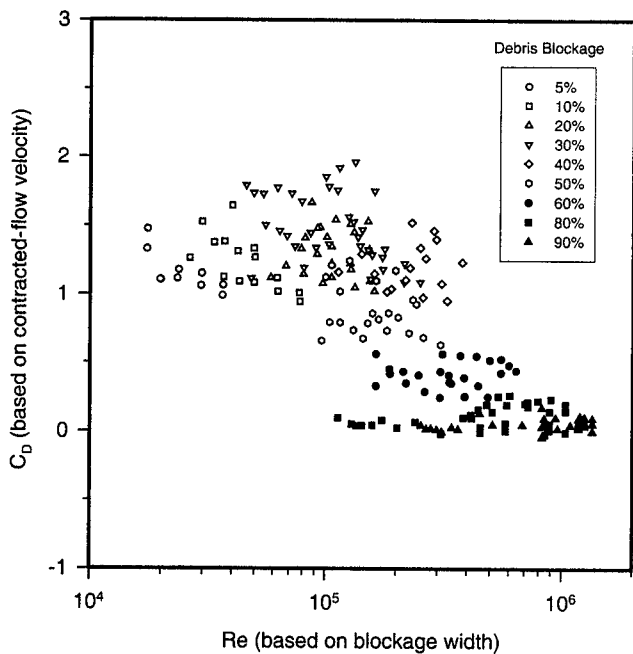


Figure A31. Method 3 variation of drag coefficient with Reynolds number.

in the ranges of  $0.4 < Fr < 0.8$  and  $B < 0.4$

where

$C_D$  = drag coefficient and  
 $Fr$  = Froude number.

The trend of decreasing drag coefficient with Froude number may continue for higher Froude numbers. A trend is not apparent for the variation of Method 3 drag coefficient with Reynolds number.

#### Method 4 Results

Figure A32 shows the variation of Method 4 drag coefficient with blockage ratio. Use of the approach velocity as a reference velocity causes extremely large variations in drag coefficient at high-blockage ratios. As presented in the description of Method 2 results, the variation of drag coefficient at high-blockage ratios provides a large variation in drag force in conditions where the total force is primarily hydrostatic.

#### MEAN AND ENVELOPE DRAG COEFFICIENT RELATIONS FOR FULL-DEPTH PLATES

Line segments were developed to envelope the full-depth plate data for a blockage ratio lower than 0.77. The line segments were forced to a drag coefficient of zero at 100-percent blockage, at which point all of the force is considered to be hydrostatic. Figure A33 shows the line segments, as well as

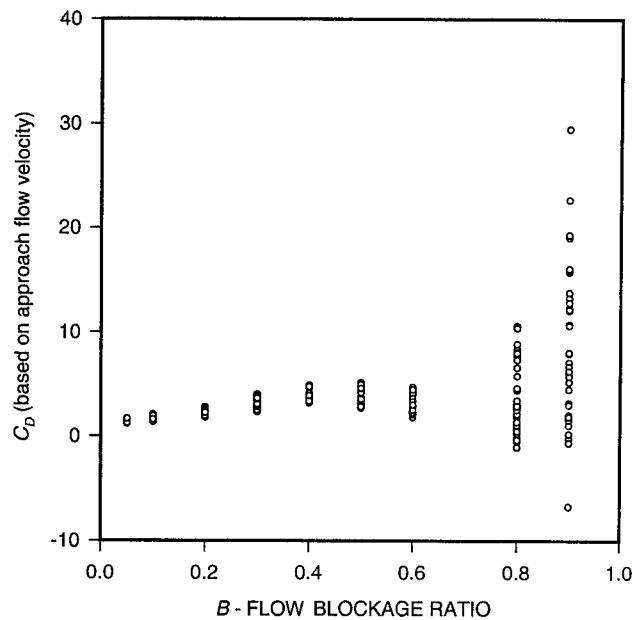


Figure A32. Method 4 variation of drag coefficient with blockage ratio.

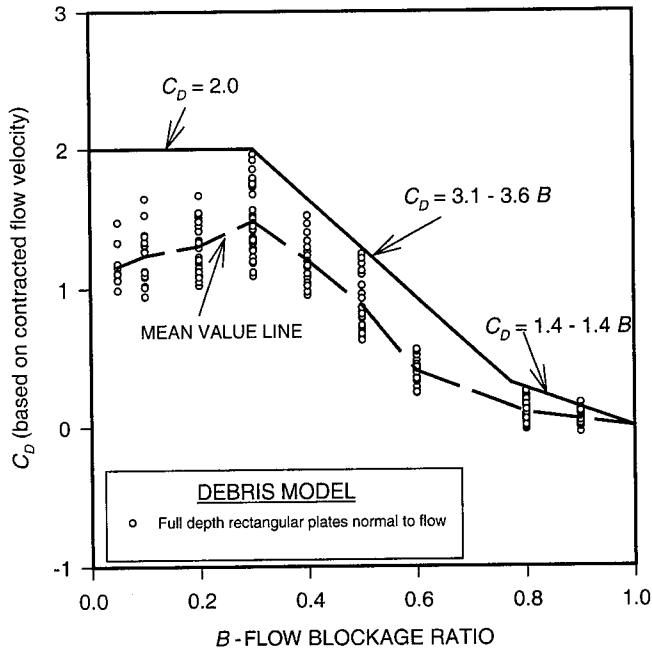


Figure A33. Method 3 variation of drag coefficient with blockage ratio, mean value, and envelope curves.

a mean value line. Table A10 shows equations for the line segments and limits for the equations.

**FORCE-PREDICTION MODEL BASED ON DEBRIS MODELS: WES AND UNIVERSITY OF QUEENSLAND DATA SETS**

Method 3 was used to compute drag coefficients for the simulated debris-accumulation conditions developed under the medium-scale testing at WES and for the idealized debris-modeling conditions at the University of Queensland. Figures A34 and A35 show the drag coefficients, computed using Method 3, for piers and superstructures, respectively.

**TABLE A10 Envelope line segments for full-depth-plate drag coefficients**

B - Range	Fr - Range	C <sub>D</sub>
B < 0.3	Fr < 0.4	C <sub>D</sub> = 2
B < 0.4	0.4 < Fr < 0.8	C <sub>D</sub> = 3 - 2.5 Fr
0.3 < B < 0.77	Fr < 1	C <sub>D</sub> = 3.1 - 3.6 B
B > 0.77	Fr < 1	C <sub>D</sub> = 1.4 - 1.4 B

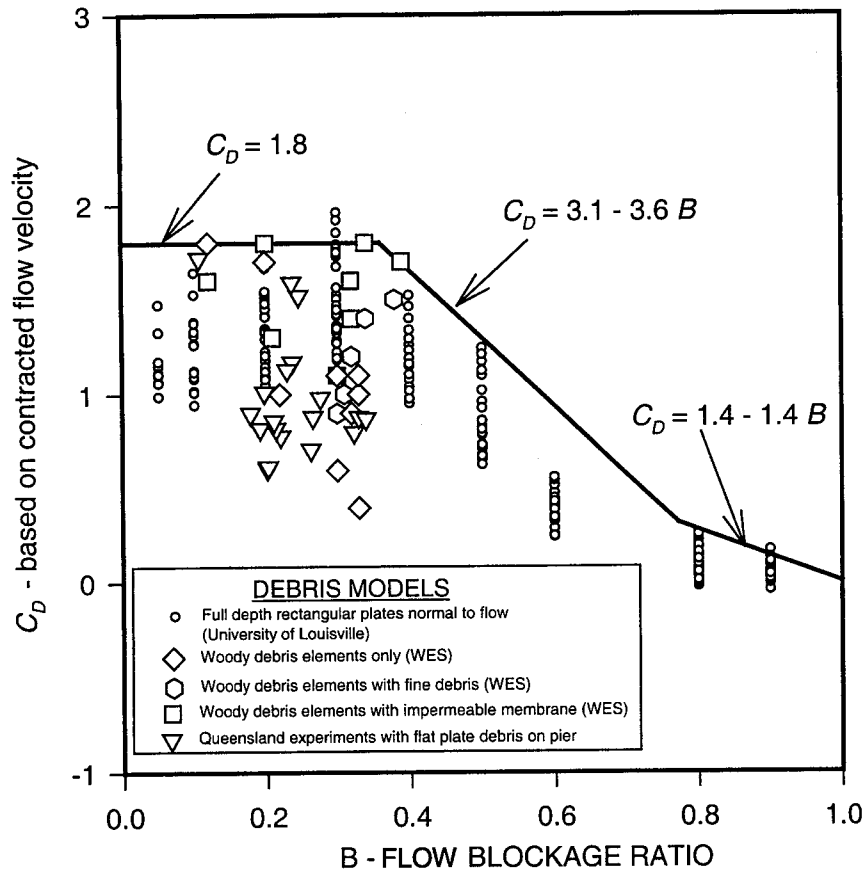


Figure A34. Method 3 variation of drag coefficient with blockage ratio for vertical plates, simulated debris, and idealized debris on piers.

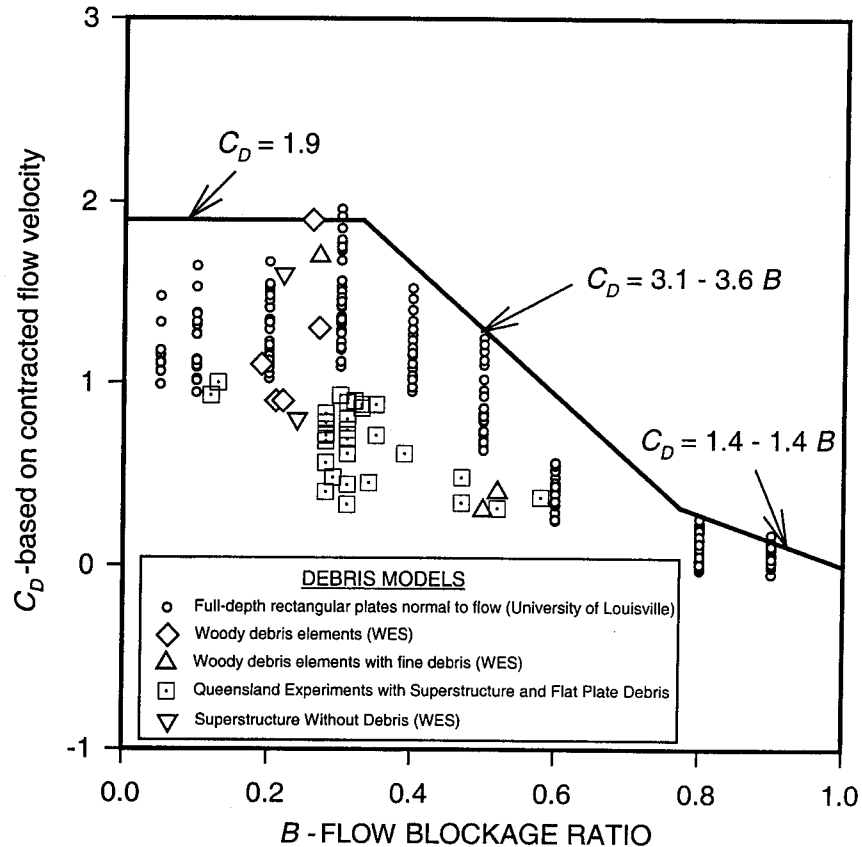


Figure A35. Method 3 variation of drag coefficient with blockage ratio for vertical plates, simulated debris, and idealized debris on superstructures.

### Debris on Piers

The data collected under WES medium-scale conditions for piers and under the University of Queensland idealized debris tests for piers fall within or slightly below the range of flat-plate data for both the debris on piers and the debris on superstructure. Lower drag coefficients can be attributed partly to the transfer of a portion of the debris load to the streambed that occurred in the WES tests because of debris accumulations that extended to the streambed. As anticipated, the highest drag coefficients in the WES data set corresponded to conditions in which the debris matrix was completely blocked by an impervious membrane. The coefficients of drag relations in Table A9 can be adjusted to reflect the information in Figure A34 for piers. Table A11 provides a conservative design set of relations for drag coefficients for debris on piers.

TABLE A11 Envelope line segments for drag coefficients for debris on piers

B - Range	Fr - Range	$C_D$
$B < 0.36$	$Fr < 0.4$	$C_D = 1.8$
$B < 0.36$	$0.4 < Fr < 0.8$	$C_D = 2.6 - 2.0 Fr$
$0.36 < B < 0.77$	$Fr < 1$	$C_D = 3.1 - 3.6 B$
$B > 0.77$	$Fr < 1$	$C_D = 1.4 - 1.4 B$

### Debris on Superstructures

Drag coefficients computed from the WES model debris on superstructures are in the range computed for plate experiments in which  $B < 0.3$ , as shown in Figure A35. Drag coefficients computed from the idealized debris experiments conducted at the University of Queensland provide much lower drag coefficients. The WES data and the University of Queensland data cover different ranges of flow blockage, with the exception of four overlapping data points. Given the discrepancy between data sets, a conservative envelope line with a maximum drag coefficient of 1.9, as provided in Figure A35, is recommended for design. As in the case for piers, an adjustment is provided for Froude numbers in the range of 0.4–0.8 (see Table A12).

TABLE A12 Envelope line segments for drag coefficients for debris on superstructures

B - Range	Fr - Range	$C_D$
$B < 0.33$	$Fr < 0.4$	$C_D = 1.9$
$B < 0.33$	$0.4 < Fr < 0.8$	$C_D = 2.8 - 2.25 Fr$
$0.33 < B < 0.77$	$Fr < 1$	$C_D = 3.1 - 3.6 B$
$B > 0.77$	$Fr < 1$	$C_D = 1.4 - 1.4 B$

## SUMMARY OF EXPERIMENTAL RESULTS

The force model in Method 3, which is based on a partitioning of the total force into hydrostatic and drag forces and on the use of a drag coefficient based on the contracted-flow velocity, provides a rational model for computing forces through the complete range of blockage ratios. In the other methods investigated, use of the approach velocity for the reference velocity caused large variations in the drag coefficient, especially at high blockage ratios. Using the total horizontal force to compute drag coefficients rather than partitioning the force into dynamic and hydrostatic forces caused large variations in drag coefficient at high blockage ratios. Froude numbers in the range of 0.4–0.8 (that is, the range

tested) significantly influenced drag coefficients. The effect of Froude number may be substantial outside the range tested in these experiments. The Reynolds number appeared not to affect Method 3 drag coefficients in the range of data examined.

Method 3 drag coefficients from the simulated debris on piers for the WES and University of Queensland data sets showed good agreement with the plate data. Conservative envelope relations for drag coefficient as a function of blockage width and Froude number were developed.

The WES data and the University of Queensland data provide substantially different values for Method 3 drag coefficient. Conservative envelope relations for drag coefficient, similar to those for debris on piers, were developed.

---

## PART 4: DRAFT SPECIFICATION FOR AND COMMENTARY ON DEBRIS ACCUMULATION FORCES

### SPECIFICATION FOR DEBRIS ACCUMULATION FORCES (GENERAL)

Water pressures on debris accumulations and the resulting debris forces transmitted to bridge piers and superstructures shall be considered in addition to the direct water pressure forces. Such pressures and forces shall be determined with consideration of site conditions and of expected modes of debris accumulation and debris interaction with streambeds and banks. The water forces include both

- Drag forces caused by debris that have accumulated on piers and superstructures and
- Hydrostatic forces caused by the effects of flow contraction.

### COMMENTARY ON DEBRIS ACCUMULATION FORCES (GENERAL)

Debris is considered buoyant or neutrally buoyant material that is transported by flow during flood events. Woody vegetation has been the primary cause of documented debris accumulation problems (Diehl 1997). The following modes of failure have been caused by debris forces in conjunction with forces, caused by the effects of flowing water, on submerged parts of the structure that are unencumbered with debris (Parola et al. 1998a):

- Substructure buckling,
- Shearing of the deck from the substructure, and
- Overturning of the structure.

The overall dimensions of debris accumulations depend on pier locations, geometry, and alignment to flow; shape, alignment, and position of the superstructure; stream channel flow velocity, planform, and cross-section geometry; and debris supply. In addition to increasing lateral loads, debris also increase floodwater elevations, stream velocities, and the potential for scour. Where foundation soils and sediments are susceptible to scour, resistance to lateral loads may be reduced by exposure, undermining of foundation elements by scour, or both. Scour also may increase the area of pier that is subject to the pressure forces of flowing water and debris. The combination of debris forces, increased area of pier that is subject to pressure, and reduced foundation resistance under conditions where maximum debris loads are likely may affect the stability of the structure.

Determining debris forces requires the following procedures:

- Estimate the geometry of debris accumulation on the structure,

- Compute flow hydraulics for situations changed by debris accumulations, and
- Compute hydrodynamic loads from the flow that is altered by the presence of debris.

On piers and superstructure components that have a high potential for debris delivery during design flow events and a high potential for debris accumulation, the maximum debris size should be used to compute debris loads. The elements of the bridge likely to accumulate debris include piers, superstructure beams, and any areas between bracing members, truss members, or both.

Streams typically shift over the design life of a structure. Piers on the floodplain, especially those near the channel, may become exposed to main-channel flow and debris transport conditions over time. At many sites, the shift can be rapid, while at other sites, significant migration of the channel may take decades. The susceptibility of floodplain piers to debris accumulation and the resulting forces should be considered where channel shift is possible.

The information on debris geometry is based on the field research by Diehl (1997) and on the suggestions of Wellwood and Fenwick (1989). The design log length that was provided by Diehl's observations (1997) is based on the stream's ability to transport trees to the bridge and on the capacity of tree trunks and limbs to support debris accumulation forces. Although many factors may contribute to the size of a design log, Diehl simplified the evaluation of a log sufficiently sturdy to lodge and transmit forces and recommended a design length of log.

Table A13 provides guidelines for determining the maximum extent of a debris accumulation lodged on piers, superstructures, or both. The "gap" referred to in the table corresponds to unobstructed distance between bridge elements or between bridge elements and streambed or banks.

If the distance between two piers is shorter than the design log length, then the region between the piers is considered a horizontal gap. If the distance from the bottom of the superstructure to the streambed or floodplain is shorter than the length of the design log, then the area between the streambed and superstructure is considered a vertical gap.

Although many factors are involved in determining the design log length, Diehl (1997) simplified the determination to the shortest of the following:

- The width of the channel upstream from the site,
- The maximum length of sturdy logs, and
- (In much of the United States) 9 m plus one-quarter of the width of the channel upstream from the site.

**TABLE A13** Maximum extent of debris accumulation

Accumulation Type	Width	Height
Pier	L	Y
Superstructure	S	H + 1.2 m below superstructure
Vertical Gap	W	D
Horizontal Gap	W	Smaller of D or Y

L = design length of log, S = span, Y = flow depth, H = vertical height of superstructure, D = vertical extent of gap, W = width of gap.

The maximum "sturdy-log" length is the length of log that can withstand the hydrodynamic forces on the debris accumulation. It is not the maximum length of mature riparian and floodplain trees. The maximum sturdy-log length that was suggested ranged from 24 m (in the Eastern U.S.) to 45 m (in California and in the Pacific Northwest). The information provided by Diehl (1997) should be used as a guide. The actual potential for debris accumulation on the structure depends on many factors, including site location, surrounding land use, and debris history. Field evidence may justify using design log lengths different from those given above.

In deep-flow conditions (that is, flow depths greater than 6 m) and under low-velocity conditions (that is, 1–2 m/s), debris accumulations may not extend to the streambed. Unfortunately, general information on the depth of debris accumulations is not available. Data specific to physiographic and ecological regions of each state are needed to develop more realistic debris accumulation depths and widths applicable to those regions. Engineering judgment that is based on the collection and analysis of debris' geometric characteristics should be used to limit both the width and depth of debris accumulations. Where deep scour is anticipated, the estimated debris accumulation may need to be increased to the depth of scour. For the deep-flow conditions described above, the extension of the debris into the scour hole may lead to unrealistically large estimates of debris accumulations.

The maximum vertical extent of a design debris accumulation on piers is given as the flow depth. This maximum extent recommendation is supported by some of Diehl's field observations (1997). However, under many deep-water conditions, adhering to the recommendation yields an unreasonably deep accumulation. Field evidence may justify using smaller design vertical extents of debris accumulations on piers.

### SPECIFICATION FOR DRAG FORCE ON DEBRIS

The pressure on the submerged profile area of the debris differs from the pressure on the structure perpendicular to the flow direction. The following formula quantifies this difference:

$$p_D = C_D w \frac{(V_r)^2}{2g} \quad (\text{A30})$$

where

$p_D$  = component of average stream pressure on debris due to stream flow, N/m<sup>2</sup>;

$w$  = specific weight of water (9,810 N/m<sup>3</sup>);

$g$  = gravitational acceleration constant (9.81 m/s<sup>2</sup>);

$V_r$  = reference velocity, m/s; and

$C_D$  = drag coefficient.

The drag coefficient values are provided for piers in Table A14 and for superstructures in Table A15. These values depend on the blockage ratio and on the flow Froude number.

Blockage ratio is defined as

$$B = \frac{A_b}{A_b + A_c} \quad (\text{A31})$$

where

$B$  = flow-blockage ratio;

$A_b$  = area of flow blocked by debris in the contracted bridge section, m<sup>2</sup>; and

$A_c$  = area of unobstructed cross-sectional flow in the contracted section, m<sup>2</sup>.

The Froude number is defined as

$$Fr = \frac{V_r}{\sqrt{gY_c}} \quad (\text{A32})$$

where

$Fr$  = Froude number;

$Y_c$  = average flow depth in the flow contraction, m;

$g$  = gravitational acceleration constant (9.81 m/s<sup>2</sup>); and

$V_r$  = reference velocity, m/s.

**TABLE A14** Drag pressure coefficient for debris on piers as a function of blockage ratio and flow Froude number

B - Range	Fr - Range	$C_D$
B < 0.36	Fr < 0.4	$C_D = 1.8$
B < 0.36	0.4 < Fr < 0.8	$C_D = 2.6 - 2.0 Fr$
0.36 < B < 0.77	Fr < 1	$C_D = 3.1 - 3.6 B$
B > 0.77	Fr < 1	$C_D = 1.4 - 1.4 B$

**TABLE A15 Drag pressure coefficient for debris on superstructures as a function of blockage ratio**

B - Range	Fr - Range	$C_D$
$B < 0.33$	$Fr < 0.4$	$C_D = 1.9$
$B < 0.33$	$0.4 < Fr < 0.8$	$C_D = 2.8 - 2.25 Fr$
$0.33 < B < 0.77$	$Fr < 1$	$C_D = 3.1 - 3.6 B$
$B > 0.77$	$Fr < 1$	$C_D = 1.4 - 1.4 B$

The reference velocity shall be determined by the following criteria:

- If the reduction in the waterway opening by debris and other bridge components is anticipated to be greater than 30 percent of the wetted cross-sectional flow area in the bridge opening, then the reference velocity is to be taken as the average velocity in the contracted section of the bridge opening.
- If the reduction in the waterway opening by debris and other bridge components is anticipated to be less than 30 percent of the wetted cross-sectional flow area, then the reference velocity is to be taken as the maximum local average velocity just outside the influence of the pier, the associated debris for piers, and the full-depth blockages by the superstructure. For floating debris accumulations on superstructures, the restricted-flow velocity under the superstructure should be used as the reference velocity.

#### COMMENTARY ON DRAG FORCE ON DEBRIS

The drag pressure is the average pressure difference from the upstream side to the downstream side of the debris. It produces a force in the direction of the approaching flow. The actual local pressure on debris will be highly nonuniform, with the highest local pressure on the upstream side of the debris and the lowest local pressure somewhere near the upstream edge of the downstream wakes. The drag pressure coefficients in Tables A14 and A15 are approximations derived from measurements of total drag force (see Chapter 2) and from the assumption that pressure distributions are uniform. The total drag force, as developed from the research studies, is computed as

$$F_D = C_D w A_D \frac{(V_r)^2}{2g} \quad (A33)$$

where

$F_D$  = drag force, N;

$C_D$  = drag coefficient (see Table A14 for piers and Table A15 for superstructures);

$w$  = specific weight of water (9,810 N/m<sup>3</sup>);

$g$  = gravitational acceleration constant (9.81 m/s<sup>2</sup>);

$A_D$  = area of wetted debris based on the upstream water surface elevation projected normal to flow direction, m<sup>2</sup>; and

$V_r$  = reference velocity, m/s.

For debris accumulations supported by a single pier and not aligned with the principal axis of the pier, the direction of drag force should be taken as the direction of the flow approaching the pier, with appropriate consideration for the uncertainty associated with predicting the local-flow direction.

The drag coefficients were developed from tests in which the Froude number was usually less than 0.8 (see Chapter 2). There is some evidence that, for higher Froude numbers, drag coefficients may be lower than those in Tables A14 and A15 (Hsieh 1964). For blockage ratios lower than 0.36, a reasonable assumption is that if  $Fr \geq 0.8$ , then  $C_D = 1.0$ .

#### SPECIFICATION FOR HYDROSTATIC FORCE ON DEBRIS

The following formula computes the horizontal component of hydrostatic pressure applied to the combined vertical profile area of the submerged structure and debris accumulation:

$$p_h = w h \quad (A34)$$

where

$p_h$  = hydrostatic pressure, N/m<sup>2</sup>;

$h$  = distance from the water surface elevation to the point of pressure computation, m; and

$w$  = specific weight of water (9,810 N/m<sup>3</sup>).

The reference water surface elevation on the upstream side of the debris accumulation and of the superstructure should be upstream of the region of flow contraction affected by the debris. The reference water surface elevation on the downstream side of the debris accumulation and the superstructure should be where the flow has expanded completely from the effects of the contraction at the debris.

#### COMMENTARY ON HYDROSTATIC FORCE ON DEBRIS

The variation in water surface elevation and the associated pressures near submerged structures is highly nonuniform. Hydrostatic pressure variation has been used to account for the forces caused by pressure variation from the upstream to the downstream side of the bridge. Changes in average flow depth cause these assumed hydrostatic pressure variations. On the structure, the total force that is associated with the hydrostatic pressure difference is approximated as

$$F_h = w(h_{cu} A_{hu} - h_{cd} A_{hd}) \quad (A35)$$

where

$F_h$  = horizontal hydrostatic force on area  $A_h$ , N;

$w$  = specific weight of water (9,810 N/m<sup>3</sup>);

$A_{hu}$  = area of the vertically projected, submerged portion of the debris accumulation below the upstream water surface, m<sup>2</sup>;

$h_{cu}$  = vertical distance from the upstream water surface to the centroid of area  $A_{hu}$ , m;

$A_{hd}$  = area of the vertically projected, submerged portion of the debris accumulation below the downstream water surface, m<sup>2</sup>; and

$h_{cd}$  = vertical distance from the downstream water surface to the centroid of area  $A_{hd}$ , m.

#### COMMENTARY ON LOCATION AND DIRECTION OF RESULTANT FORCES

The resultant drag force is through the centroid of the projected profile area. For an assumed rectangular profile area, the resultant force acts through the center of the accumulation. The location of the resultant hydrostatic force can be calculated by adding moments created by the upstream and downstream hydrostatic forces about a convenient axis, such as the water surface or streambed. For an assumed rectangular profile area, the resultant hydrostatic force on the upstream side of the accumulation would occur at a distance of two-thirds the depth of the accumulation measured from the upstream water surface. Similarly, the elevation of the downstream hydrostatic force may be obtained. The total force loca-

tion can be calculated by dividing the sum of the moments, which are created by the resultant drag and hydrostatic forces acting about a convenient horizontal axis, by the sum of the drag and hydrostatic forces.

The loads computed correspond to the pressure forces of the water on the debris. Transfer of the loads from the debris to the structure depends on many factors, including the characteristics of the debris accumulation and the degree to which streambed and banks support the debris accumulation. A few large debris elements may transfer large portions of the loads to a few points on the structure or to points on the streambed or banks. The researchers of this project recommend that the resultant force be applied as a point load. Less conservative distribution of the load to the structure may be warranted for situations in which more information is available on the debris configuration and structural susceptibility.

Debris accumulations on piers seem to align themselves with the flow direction. Because of the uncertainty associated with debris accumulation geometry and flood-flow direction, the resultant force should be applied with consideration of the anticipated range of possible flow directions and with consideration of the structure's susceptibility to the resultant forces over the range of flow directions that are possible over the structure's life. For superstructures and debris accumulations that span adjacent piers, the forces should be applied in at least two directions: (1) perpendicular to the face of the bridge and (2) in the direction of flow. Again, structure susceptibility and the possible variation of flow direction should be considered in selecting the appropriate design angle for applying the resultant forces.

## PART 5: BIBLIOGRAPHY

- American Association of State Highway and Transportation Officials, *AASHTO LRFD Bridge Design Specifications—Customary U.S. Units*, first edition, 1994, Washington, D.C.
- American Association of State Highway and Transportation Officials, *AASHTO LRFD Bridge Design Specifications—SI*, second edition, 1998, Washington, D.C.
- American Association of State Highway and Transportation Officials, *Standard Specifications for Highway Bridges*, fifteenth edition, 1992, Washington, D.C.
- American Association of State Highway and Transportation Officials, *Standard Specifications for Highway Bridges*, thirteenth edition, 1983, Washington, D.C.
- Apelt, C. J., "Flood Loads on Submerged Bridges," *Queensland Division Technical Papers*, Institution of Engineers Australia (Queensland Division), v. 27, no. 19, Publication No. QBG 1756, 1986a, pp. 17–23.
- Apelt, C. J., "Flood Forces on Bridges," *Conference Proceedings, 13th AARB—5th REAAA Combined Conference*, Adelaide, Australia, 25–29 August 1986b, v. 13, part 6, Bridges, pp. 40–46.
- Apelt, C. J., "Flow Loads on Bridge Piers," *The Journal of the Institution of Engineers, Australia*, July–Aug., 1965, pp. 185–191.
- Apelt, C. J. and L. T. Issac, "Bridge Piers—Hydrodynamic Force Coefficients," *ASCE Journal of Hydraulics Division*, 1968, pp. 17–30.
- Bacon, D., *Hydrodynamic Forces on Partially and Fully Submerged Bridges*, undergraduate thesis, University of Queensland, Australia, 1987.
- Bearman, P. W., "Some Effects of Free-Stream Turbulence and the Pressure of the Ground on the Flow Around Bluff Bodies," *Aerodynamic Drag Mechanisms*, Sovran, Morel and Mason (eds.). Plenum Press, 1978.
- Brunner, G. W., *HEC-RAS River Analysis System Hydraulic Reference Manual*, version 2.2, U.S. Army Corps of Engineers Hydrologic Engineering Center, Davis, C.A., 1998.
- Chang, F. F. M. and H. W. Shen, "Debris Problems in the River Environment," *Federal Highway Administration Report No. FHWA-RD-79-62*, 1979, 67 p.
- Cheung, J. C. K. and W. H. Melbourne, "Turbulence Effects on Some Aerodynamic Parameters of a Circular Cylinder at Supercritical Reynolds Number," *Journal of Wind Engineering and Industrial Aerodynamics*, vol. 14, 1983, p. 339.
- Courchesne, J. and A. Laneville, "An Experimental Evaluation of Drag Coefficient for Rectangular Cylinders Exposed to Grid Turbulence," *ASME Journal of Fluids Engineering*, vol. 104, 1982, p. 523.
- Denson, K. H., *Steady-State Drag, Lift and Rolling Moment Coefficients for Inundated Inland Bridges*, Mississippi Water Resources Research Institute, Mississippi State University, 1982, pp. 1–22.
- Diehl, T. H., "Potential Drift Accumulation at Bridges," *Federal Highway Administration Report No. FHWA-RD-97-028*, 1997.
- Eichert, B. S. and J. Peters, "Computer Determination of Flow Through Bridges," *ASCE Journal of Hydraulics Division*, vol. 96, no. HY7, 1970, pp. 1455–1468.
- El-Sherbiny, S., "Side Walls in Constrained Flow," *Conference Proceedings, 4th. Colloquium Industrial Aerodynamics*, Germany, 1980.
- FLOW-3D User's Manual*, version 7.1, Flow Science, Inc., Los Alamos, N.M., 1997.
- Froehlich, D. C., *Finite Element Surface-Water Modeling System: Two-Dimensional Flow in a Horizontal Plane* (Version 2 draft user's manual), Turner-Fairbank Highway Research Center, McLean, V.A., (in press).
- Hoerner, S. F., *Fluid-Dynamic Drag*, published by the author, 148 Busted Drive, Midland Park, N.J. 07432, 1965, pp. 3–11.
- Hsieh, T., "Resistance of Cylindrical Piers in Open-Channel Flow," *ASCE Journal of the Hydraulics Division*, vol. 90, no. HY 1, 1964.
- Hydrologic Engineering Center, *HEC-2 Water Surface Profiles Hydraulic Reference Manual*, version 2.2, U.S. Army Corps of Engineers, Davis, C.A., 1998.
- Jempson, M. A. and C. J. Apelt, "Hydrodynamic Forces on Partially and Fully Submerged Bridge Superstructures," *Conference Proceedings, 16th ARRB Conference, Part 3*, Australian Road Research Board, Perth, Western Australia, 1992.
- Koch, A., M. Carstenjen, and L. Hainz, *Von Der Bewegung Des Wassers Und Den Dabei Auftretenden Kraeften* ("Of the Movement of Water and the Power It Produces"), Springer (publisher), Berlin, Germany, 1926.
- Masch, F. D. and W. L. Moore, "Drag Forces in Velocity Gradient Flow," *ASCE Journal of the Hydraulics Division*, vol. 86, no. HY7, 1960.
- Mirajgaoker, A. G., discussion of T. Hsieh's "Resistance of Cylindrical Piers in Open Channel Flow," *ASCE Journal of the Hydraulics Division*, vol. 90, no. HY5, 1964.
- Montgomery, C. T., R. Gerard, W. J. Huiskamp, and R. W. Kornglsen, "Application of Ice Engineering to Bridge Design Standards," *Conference Proceedings, Cold Regions Engineering Specialty Conference*, Canadian Society for Civil Engineering, Montreal, Quebec, Canada, 1984, pp. 795–810.
- Mueller, D. S. and A. C. Parola, "Detailed Scour Measurements Around a Debris Accumulation," *ASCE Water Resources Engineering*, 1998, p. 234.
- Munson, B. R., D. F. Young, and T. H. Okiishi, *Fundamentals of Fluid Mechanics*, John Wiley & Sons, New York, 1990.
- National Association of Australian State Road Authorities, *NAASRA Bridge Design Specification*, Sydney, Australia, 1976.
- National Transportation Safety Board, *Highway Accident Report—Collapse of the Harrison Road Bridge Spans, Miamitown, Ohio, May 26, 1989*, Washington, D.C., 1990, 45 p.
- Naudascher, E., *Hydrodynamic Forces*, A. A. Balkema, Brookfield, V.T., 1991.
- Naudascher, E. and H. J. Medlarz, "Hydrodynamic Loading and Backwater Effect of Partially Submerged Bridges," *Journal of Hydraulic Research*, vol. 21, no. 3, 1983, pp. 213–232.
- O'Donnell, C. L., "Observation on the Causes of Bridge Damage in Pennsylvania and New York Due to Hurricane Agnes," *Highway Research Record, No. 479*, Highway Research Board, National Research Council, Washington, D.C., 1973, pp. 20–36.

- Parola, A. C., D. J. Hagerty, and S. Kamojjala, *NCHRP Report 417*, "Highway Infrastructure Damage Caused by the 1993 Upper Mississippi River Basin Flooding," Transportation Research Board, National Research Council, Washington, D.C., 1998a, pp. 1-195.
- Parola, A. C., S. Kamojjala, J. Richardson, and M. Kirby, "Numerical Simulation of Flow Patterns at a Bridge with Debris," *Conference Proceedings, ASCE Water Resources Engineering*, Memphis, T.N., 1998b.
- Ranga Raju, K. G., J. Loeser, and E. J. Plate, "Velocity Profiles and Fence Drag for a Turbulent Boundary Layer Along Smooth and Rough Flat Plates," *Journal Fluid Mechanics*, vol. 76, part 2, 1976, pp. 383-399.
- Richter, A. and E. Naudascher, "Fluctuating Forces on a Right Circular Cylinder in Confined Flow," *Journal Fluid Mechanics*, vol. 78, part 3, 1976, pp. 561-576.
- Rouse, H., "Critical Analysis of Open-Channel Resistance," *ASCE Journal Hydraulics Division*, vol. 91, no. HY 4 (Kobus and Newsham), 1965.
- Sakamoto, H., M. Moriya, and M. Arie, "A Study on the Flow Around Bluff Bodies Immersed in Turbulent Boundary Layers" (part 1, on the form drag of a normal plate), *Bulletin of the JSME*, vol. 18, no. 124, 1975, pp. 1126-1133.
- Sakamoto, H., M. Moriya, and M. Arie, "A Study on the Flow Around Bluff Bodies Immersed in Turbulent Boundary Layers" (part 2, the pressure forces acting on inclined plates), *Bulletin of the JSME*, vol. 20, no. 139, 1977, pp. 71-78.
- Schlichting, H., *Boundary-Layer Theory*, seventh edition, McGraw-Hill, New York, 1979.
- Vickery, B. J., "Fluctuating Lift and Drag on a Long Cylinder of Square Cross-Section in a Smooth and a Turbulent Stream," *Journal Fluid Mechanics*, vol. 25, part 3, 1966, pp. 481-494.
- Vose, A., *Hydrodynamic Forces on Fully and Partially Submerged Bridges*, undergraduate thesis, University of Queensland, Australia, 1985.
- Wellwood, N. and J. Fenwick, "A Flood Loading Methodology for Bridges," *Conference Proceedings, 15th ARRB Conference*, part 3, 1989, pp. 315-341.
- White, F. M., *Fluid Mechanics*, third edition, McGraw-Hill, New York, 1994.
-

The **Transportation Research Board** is a unit of the National Research Council, which serves the National Academy of Sciences and the National Academy of Engineering. The Board's mission is to promote innovation and progress in transportation by stimulating and conducting research, facilitating the dissemination of information, and encouraging the implementation of research results. The Board's varied activities annually draw on approximately 4,000 engineers, scientists, and other transportation researchers and practitioners from the public and private sectors and academia, all of whom contribute their expertise in the public interest. The program is supported by state transportation departments, federal agencies including the component administrations of the U.S. Department of Transportation, and other organizations and individuals interested in the development of transportation.

The National Academy of Sciences is a private, nonprofit, self-perpetuating society of distinguished scholars engaged in scientific and engineering research, dedicated to the furtherance of science and technology and to their use for the general welfare. Upon the authority of the charter granted to it by the Congress in 1863, the Academy has a mandate that requires it to advise the federal government on scientific and technical matters. Dr. Bruce M. Alberts is president of the National Academy of Sciences.

The National Academy of Engineering was established in 1964, under the charter of the National Academy of Sciences, as a parallel organization of outstanding engineers. It is autonomous in its administration and in the selection of its members, sharing with the National Academy of Sciences the responsibility for advising the federal government. The National Academy of Engineering also sponsors engineering programs aimed at meeting national needs, encourages education and research, and recognizes the superior achievements of engineers. Dr. William A. Wulf is president of the National Academy of Engineering.

The Institute of Medicine was established in 1970 by the National Academy of Sciences to secure the services of eminent members of appropriate professions in the examination of policy matters pertaining to the health of the public. The Institute acts under the responsibility given to the National Academy of Sciences by its congressional charter to be an adviser to the federal government and, upon its own initiative, to identify issues of medical care, research, and education. Dr. Kenneth I. Shine is president of the Institute of Medicine.

The National Research Council was organized by the National Academy of Sciences in 1916 to associate the broad community of science and technology with the Academy's purpose of furthering knowledge and advising the federal government. Functioning in accordance with general policies determined by the Academy, the Council has become the principal operating agency of both the National Academy of Sciences and the National Academy of Engineering in providing services to the government, the public, and the scientific and engineering communities. The Council is administered jointly by both the Academies and the Institute of Medicine. Dr. Bruce M. Alberts and Dr. William A. Wulf are chairman and vice chairman, respectively, of the National Research Council.

Abbreviations used without definitions in TRB publications:

AASHO	American Association of State Highway Officials
AASHTO	American Association of State Highway and Transportation Officials
ASCE	American Society of Civil Engineers
ASME	American Society of Mechanical Engineers
ASTM	American Society for Testing and Materials
FAA	Federal Aviation Administration
FHWA	Federal Highway Administration
FRA	Federal Railroad Administration
FTA	Federal Transit Administration
IEEE	Institute of Electrical and Electronics Engineers
ITE	Institute of Transportation Engineers
NCHRP	National Cooperative Highway Research Program
NCTRP	National Cooperative Transit Research and Development Program
NHTSA	National Highway Traffic Safety Administration
SAE	Society of Automotive Engineers
TCRP	Transit Cooperative Research Program
TRB	Transportation Research Board
U.S.DOT	United States Department of Transportation

## THE NATIONAL ACADEMIES

*Advisers to the Nation on Science, Engineering, and Medicine*

National Academy of Sciences  
 National Academy of Engineering  
 Institute of Medicine  
 National Research Council

**TRANSPORTATION RESEARCH BOARD**  
National Research Council  
2101 Constitution Avenue, N.W.  
Washington, D.C. 20418

**ADDRESS CORRECTION REQUESTED**

---

